Tobias Spitaler, BSc

Coherent Transport from Molecular Dynamics

MASTER'S THESIS

to achieve the university degree of

Diplom-Ingenieur

Master's degree programme: Technical Physics

submitted to

Graz University of Technology

Supervisors

Univ.-Prof. Ph.D, Peter Hadley

Institute of Solid State Physics

Dr. Olga Natalia Bedoya-Martínez

Dr. René Hammer

Materials Center Leoben Forschung GmbH

Graz, July 2020

AFFIDAVIT

I declare that I have authored this thesis independently, that I have not used other than the declared sources/resources, and that I have explicitly indicated all material which has been quoted either literally or by content from the sources used. The text document uploaded to TUGRAZonline is identical to the present master's thesis.

Date, Signature

Acknowledgements

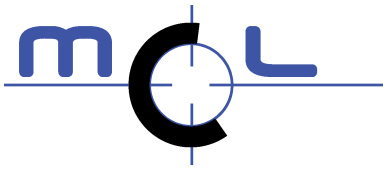

The author gratefully acknowledges the financial support under the scope of the COMET program within the K2 Center “Integrated Computational Material, Process and Product Engineering (IC-MPPE)” (Project No 859480). This program is supported by the Austrian Federal Ministries for Climate Action, Environment, Energy, Mobility, Innovation and Technology (BMK) and for Digital and Economic Affairs (BMDW), represented by the Austrian research funding association (FFG), and the federal states of Styria, Upper Austria and Tyrol.

Abstract

Phonons are quasiparticles describing the lattice vibrations in a crystal, and they are responsible of transporting heat and sound. Phonon transport in bulk materials is usually described by a diffusive picture. At nanoscale lengths, however, boundaries and interfaces play an important role. At this scale, when the phonon mean free path is larger than the length a phonon can travels before meeting a boundary, transport becomes 'ballistic'. In the ballistic regime phonons can be scattered diffusively or be reflected specularly (coherently) at interfaces. Phonons with a wavelength in the order of the structure sizes are scattered coherently, which is a manifestation of the wave-like nature of the phonons. This phonon coherence creates phonon band gaps and alters the phonon dispersion relation. Materials which show coherence effects, have potential applications in thermo-optics, thermoelectrics, as phonon sources, filters, and detectors, heat-waveguides and more.

In this work, computer simulations are used to design potential superlattices that feature significant phonon coherence. The dynamics of the atoms within the superlattices is simulated using classical molecular dynamics. The fluctuations of the atomic velocities are tracked throughout the simulation, and their correlations are used to calculate the coherence length. The method is initially tested for two test-superlattices (one-dimensional and bulk superlattices interacting by means of a Lennard-Jones potential). Then, the coherence lengths of GaN/InN superlattices, as well as structures made of monolayers of InN in a GaN matrix, are investigated. It is shown that acoustic modes feature high phonon coherence lengths (up to a few 100 nm), and that superlattices with low period feature higher phonon coherence lengths than superlattice with long period. Drawbacks and possible improvements of the used method are discussed.

Kurzfassung

Phononen sind Quasiteilchen, welche die Gitterschwingungen in einem Kristall beschreiben. In Isolatoren und Halbleitern sind Phononen maßgeblich verantwortlich für den Transport von Schall und Wärme. Der Phononentransport in Volumen-materialien wird üblicherweise diffus beschrieben. Im Nanometer-Bereich spielen die Grenzen und Grenzflächen eine wichtige Rolle. In diesem Längenbereich, wenn die mittlere freie Weglänge der Phononen größer ist, als die Strecke, welche ein Phonon zurücklegen kann bis es auf eine Grenzfläche trifft, wird der Phononentransport ‚ballistisch'. Im ballistischen Bereich können die Phononen an den Grenzflächen diffus oder gespiegelt (kohärent) reflektiert werden. Phononen mit einer Wellenlänge im Bereich der typischen Strukturgrößen werden kohärent gestreut, was eine Manifestation der Wellennatur der Phononen ist. Die Kohärenz der Phononen führt zu phononischen Bandlücken und ändert die Phononen Dispersionsrelation. Materialien, welche Kohärenzeffekte zeigen haben mögliche Anwendungen im Bereich Thermooptik, Thermoelektrik, als Quellen, Filter und Detektoren für Phononen, als Wärme-Wellenleiter und weitere Anwendungen.

In dieser Arbeit werden mit Computer-Simulationen Superlattices entworfen, welche signifikante Phononen-Kohärenz zeigen. Die Dynamik der Atome innerhalb der Superlattices wird mit klassischer Moleküldynamik simuliert. Die Fluktuationen der atomaren Geschwindigkeit werden während der Simulation aufgezeichnet und aus den Korrelationen der Geschwindigkeiten wird die Kohärenzlänge berechnet. Die Methode wird zunächst an zwei Testsystemen getestet (ein- und drei-dimensionale Superlattices mit einem Lennard-Jones Potential). Anschließend wird die Kohärenzlänge von GaN/InN Superlattices und von Strukturen mit einer Monolage von InN in einer GaN-Matrix untersucht. Es wird gezeigt, dass die akustischen Phononen eine hohe Kohärenzlange zeigen (bis zu einigen

100 nm) und dass Superlattices mit kleiner Superlattice-Periode eine höhere Kohärenzlange zeigen als Superlattices mit einer langen Periode. Nachteile und mögliche Verbesserungen der Methode werden diskutiert.

Contents

1. Introduction

Phonons are the quanta describing the lattice vibrations of a crystal. Understanding the vibrations in solids is of fundamental interest and becomes more and more important in application [1, 2, 3]. Sound and heat are carried by lattice vibrations through a solid. By understanding the lattice vibrations, materials with desired phonon properties can be engineered for applications as thermoelectric energy conversion [4], thermal engineering [5, 6] and thermal diodes [1].
Phonons are described as quasiparticles of collective movements of atoms, carrying one energy quantum $\hbar\omega$, traveling with a propagation speed according to their group velocity, and having a finite lifetime determined by scattering mechanisms. Possible scattering mechanisms are phonon-phonon scattering, scattering of phonons with other quasiparticles like electrons, scattering at defects and crystal imperfections, and scattering at interfaces and boundaries.
The average distance a phonon travels before a scattering event takes place is the phonon mean free path (MFP). At nanoscale lengths, the scattering at interfaces becomes more and more important as the interface density gets higher. At this scale, the phonons mean free path exceeds the characteristic length of the material, and the diffusive transport picture has to be replaced by the ballistic one, as phonons will scatter at the interfaces and not in the bulk. Phonons can be scattered diffusely (incoherent) or be reflected specularly (coherent) at the interfaces [7, 8, 9]. If the typical structure size is in the order of the wavelength of the phonons, the phonons will be coherent as the wave-like nature of the phonons appears. Coherent phonons are in-phase oscillations of neighboring atoms that keep the phase information when they are scattered coherently. The coherence of phonons leads to a change in the dispersion relation, to the appearing of phononic band gaps, and can influence the thermal conductivity [10]. The phonon coherence can be used to engineer materials with desired phonon properties.

Materials which are promising candidates to show coherent phonon transport are superlattices [2, 8]. Superlattices are periodic arrangements of layers of two ore more materials. They are ideal systems to study the coherence of phonons, because of their typical structure sizes. Their lattice period is in the order of the nanometers, thus feature structure sizes in the order of the wavelengths of the phonons. Moreover, it is easy to vary the typical structure size by changing the thickness of the layers, resulting ideal to study the struture size dependence of the phonon coherence. Possible applications of superlattices showing coherent phonons are in thermo-optics, thermoelectrics [4], as sources, filters and detectors of coherent phonons, heat-waveguides and more.

The engineering of materials with desired phonon properties can lead to many possible applications. Superlattices with short structure sizes show wave interference effects, but are often difficult to fabricate experimentally, involving demanding thin film techniques that are not always well established. Computer simulations allows to investigate the physical behavior of different structures without the need of experimentally fabricating them, accelerating the process of finding and developing new materials. The goal of this thesis is to use molecular dynamics simulations to simulate and obtain superlattices that feature phonon coherence. A recently reported methodology based on molecular dynamics [11, 12] is implemented and used to extract a phonon-frequency dependent coherence length. The implemented code is tested on two toy systems. The code is then used to study gallium nitride / indium nitride (GaN/InN) superlattices. The piezoelectricity [13] of the GaN/InN systems could be used to generate coherence phonons. These phonons, as long as they keep their coherence, can propagate in the superlattice, which would serve then as a source of coherent phonons.

The thesis is structured as follow: In the next chapter, some theoretical background is described. Lattice dynamics and molecular dynamics are described, which are the simulation methods used in this thesis. Then the methodology to calculate the phonon coherence length [11, 12] is presented. This methodology estimates the coherence lengths from molecular dynamics trajectories, by calculating the cross correlations of the atomic velocities. In other words, from these calculations one can calculate upto which separation-distance the motion of atoms is still correlated.

In the third chapter, the computational details and the used software packages are described. The force field potentials describing the interactions between the atoms in the crystal are also introduced. A Lennard Jones potential is used to describe one dimensional superlattices (linear chains of atoms) and crystalline argon (FCC-crystals). Gallium nitride/indium nitride superlattices are described with a modified Stillinger Weber potential. The details of the lattice dynamics and molecular dynamics are presented. Furthermore, the code and the post-processing tools to analyze the data are explained.
The results of the simulated superlattices are presented in the fourth chapter. The density of states and the frequency dependent coherence length is calculated for various superlattice periods for the same system to analyze the influence of the superlattice period on the phonon coherence. The implemented code for calculating the phonon coherence length, was tested on one dimensional and bulk superlattices. The results of this two systems are discussed and compared to results previously reported in the literature. These calculations have provided a better understanding of the microscopic picture of the phonon coherence.
For the gallium nitride/indium nitride system, superlattices with various layer thicknesses, and structures with monolayers of indium nitrite in a gallium nitride matrix are considered. The superlattices have periods of 1.06, 2.12, 6.36 and 10.6 nm. In the molecular dynamics simulations $3 \times 2 \times N$ supercells were initially considered. To better resolve the acoustic modes, and to better capture their long coherence lengths, $1 \times 1 \times N$ supercells were simulated. The coherence length of the longitudinal modes of these superlattices, and the method for calculating it are presented and discussed. GaN/InN superlattices have a large lattice mismatch, and a defect free growth of thick InN layers on GaN layers is difficult [14], but it is possible to grow monolayers of InN layers on GaN [15]. Thus, structures with monolayers of InN are simulated for various thicknesses of GaN in between. The coherence length of the longitudinal modes are calculated.

2. Theory

In this chapter some theoretical background important for this thesis is given. Lattice dynamics is described before briefly explaining molecular dynamics. The phonon density of states can be calculated from the velocity auto-correlation function. This latter is obtained from a molecular dynamics simulation. The methodology used to obtain the microscopic picture of the phonon´s coherence is presented [11, 12]. At the end of the chapter, the wurtzite crystal structure and its orthogonal representation are shortly presented.

2.1. Phonons and Lattice Dynamics

Atoms in a crystal are not fixed at their equilibrium position but vibrate around it. In the harmonic approximation the potential between two atoms is expanded around the equilibrium position, and truncated after the harmonic term. In this simple picture, the atoms in a crystal can be thought of as connected by stronger and weaker springs. Lattice Dynamics is the study of the vibrations in a crystal. With a plane wave Ansatz, the equations of motions of the atoms in the system can be solved. The solutions are normal modes of vibration with a certain wave vector $\boldsymbol{k}$ and frequency ω. In this section, Lattice Dynamics is presented, and it mostly follows the review of Dove [16].

Lets consider an atomic chain of atoms connected by springs of constant K. There are two different atoms in the unit cell of this system, with different masses m_1 and m_2. The equilibrium distance of the atoms is $a/2$ (Figure 2.1). Periodic boundary conditions are applied, and the system consists of N unit cells ($2N$ atoms). The displacement of atom j ($j = 1, 2$) in unit cell

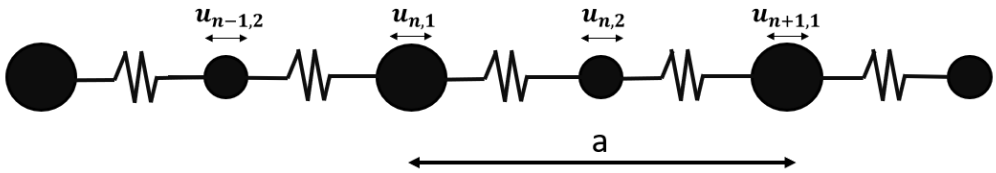

Figure 2.1.: Diatomic chain of equidistant atoms with two different masses. The length of the unit cell is a, the atoms are connected by springs with spring constant K. $u_{n,1}$ is the displacement of atom 1 in unit cell n from the equilibrium position.

n $(n = 1, 2, ..., N)$ is denoted as $u_{n,j}$. The equations of motion can be written as:

$$m_1 \ddot{u}_{n,1} = -K(u_{n,1} - u_{n-1,2}) + K(u_{n,2} - u_{n,1}) \tag{2.1}$$

$$m_2 \ddot{u}_{n,2} = -K(u_{n,2} - u_{n,1}) + K(u_{n+1,1} - u_{n,2}) \tag{2.2}$$

As we have periodic boundary conditions we use, according to Bloch's theorem, a plane wave Ansatz:

$$u_{n,j} = u_j^0 e^{i(kna - \omega t)}, \tag{2.3}$$

where u_j^0 is the amplitude, and k has the allowed values:

$$k = k_m = \frac{2\pi m}{Na} \quad \text{for } m = 0, \pm 1, \pm 2, ... \pm \frac{N}{2}. \tag{2.4}$$

Putting the Ansatz (2.3) into the equations of motion, one gets by dividing through the common exponential in each term and using $u_{n\pm1,j} = u_{n,j}\, exp(\pm ika)$:

$$m_1 \omega^2 u_1^0 = K\left(2u_1^0 - (1 + e^{-ika})u_2^0\right) \tag{2.5}$$

$$m_2 \omega^2 u_2^0 = K\left(2u_2^0 - (1 + e^{ika})u_1^0\right) \tag{2.6}$$

Equations (2.5) and (2.6) can be written as a matrix equation.

$$\begin{bmatrix} m_1\omega^2 - 2K & K(1+e^{-ika}) \\ K(1+e^{ika}) & m_2\omega^2 - 2K \end{bmatrix} \begin{bmatrix} u_1^0 \\ u_2^0 \end{bmatrix} = \begin{bmatrix} 0 \\ 0 \end{bmatrix}. \tag{2.7}$$

The solutions of these set equation are the modes of vibrations and are obtained by setting the determinant of the matrix equation equal to zero. There are two solutions for the frequency ω for every allowed k:

$$\omega_{1,2}^2 = \frac{K}{m_1 m_2}\left(m_1 + m_2 \pm \sqrt{m_1^2 + m_2^2 + 2m_1 m_2 cos(ka)}\right). \tag{2.8}$$

Eq. (2.8) relates the frequency to the wave vector and is called the dispersion relation. In Figure 2.2 the dispersion relation for the two atomic chain is plotted for different mass ratios m_1/m_2. If the masses are not equal, a gap appears in the dispersion relation, which grows larger with larger mass ratio. For every allowed wave vector k there are two solutions and two branches appear in the dispersion relation. The lower branch is called the acoustic branch. For low k, the acoustic modes correspond to in-phase motion of neighboring atoms, similar as sound waves and, thus, the origin of their name. For the optical modes, the neighboring modes move out of phase. They are called optical as in some materials these modes can be excited optically.

To calculate the phonon modes in three dimensions, the above statements need to be generalized, and the Newton's equations of motion need to be solved to calculate the phonon frequencies. The energy of the system is at the minimum, when the atoms are at their equilibrium positions. The total energy can be expanded in a Taylor series for small displacements of the atoms around their equilibrium positions:

$$E(\boldsymbol{r}+\boldsymbol{u}) = E(\boldsymbol{r}) + \sum_{j,j'}\sum_{a,b}\sum_{n,n'} \left.\frac{\partial^2 E}{\partial u_{j;a}^{n}\partial u_{j';b}^{n'}}\right|_{\boldsymbol{r}} u_{j,a}^{n} u_{j',b}^{n'}, \tag{2.9}$$

Here the atoms in the unit cell are denoted as j and j', the unit cells are labeled as n, n' and a, b label the Cartesian coordinates.

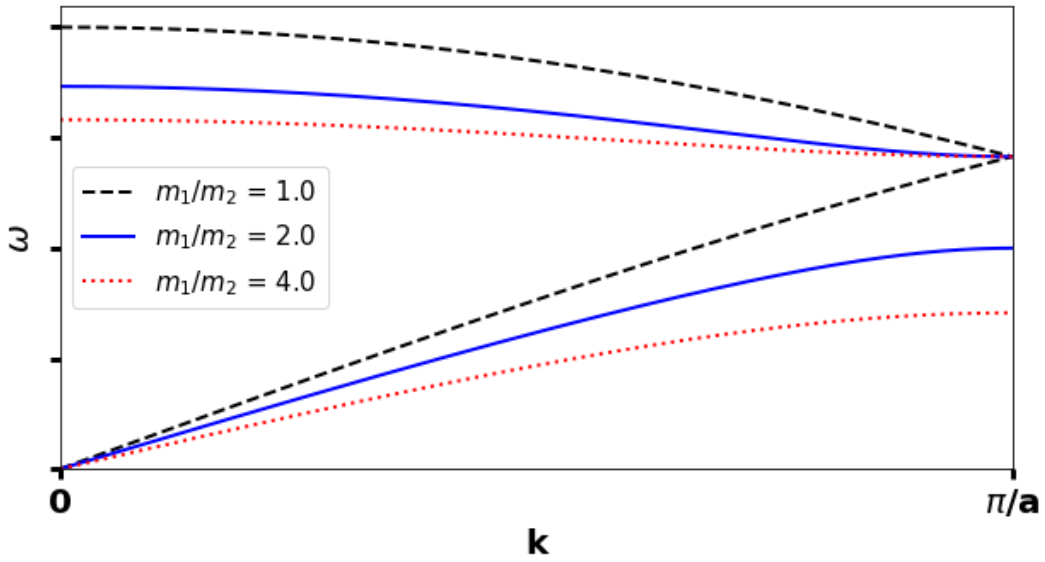

Figure 2.2.: Dispersion relation of a two-atomic chain with different mass ratios m_1/m_2. The larger the mass ratio, the larger the gap in the dispersion becomes. There are two atoms in the unit cell leading to one acoustic and one optical branch.

The linear term in Eq. (2.9) vanishes as the energy is at a minimum at $\boldsymbol{r}$, and the series is truncated after the quadratic term (harmonic approximation). The second derivatives are the force constants, which describe how the force on an atom j' in the unit cell n' changes, when the atom j in unit cell n is displaced in the direction a.

$$\Phi^{n,n'}_{j,j';a,b} = \frac{\partial^2 E}{\partial u^n_{j;a} \partial u^{n'}_{j';b}} = -\frac{\partial F^{n'}_{j';b}}{\partial u^n_{j;a}} \tag{2.10}$$

The displacement of atom j in unit cell n is described with a plane wave Ansatz:

$$\boldsymbol{u}^n_j(t) = \tilde{\boldsymbol{u}}_j e^{i(\boldsymbol{k}\boldsymbol{R}_n - \omega t)} \tag{2.11}$$

$\tilde{\boldsymbol{u}}_j$ is the amplitude, $\boldsymbol{R}_n$ the position of unit cell n. One defines $e_j = \tilde{u}_j/m_j$, with m_j the mass of atom j and inserts this Ansatz (2.11) into the equations of motion. This leads to a matrix equation and the matrix is called the dynamical matrix. The dynamical matrix needs to be diagonalized to obtain the solutions (for simplicity, the Cartesian indexes are omitted):

$$\boldsymbol{D}_{j,j'}(\boldsymbol{k}) = \frac{1}{\sqrt{m_j m_{j'}}} \sum_{n'} \Phi_{j,j'}^{n,n'} e^{i\boldsymbol{k}(\boldsymbol{R}_0 - \boldsymbol{R}_{n'})}. \tag{2.12}$$

The sum in Eq. (2.12) would go over all pairs of unit cells (n, n'), but it is sufficient to just look at the pairs of the first unit cell at $R = 0$ with all the other unit cells. The eigenvalues of the dynamical matrix are the squared phonon frequencies,

$$\omega^2(\boldsymbol{k})\boldsymbol{e} = \boldsymbol{D}(\boldsymbol{k})\boldsymbol{e}, \tag{2.13}$$

while the eigenvectors describe the relative amplitudes of the atoms in a phonon mode:

$$\boldsymbol{e} = (\ldots\ \tilde{u}_j/m_j \ldots\ ) \tag{2.14}$$

The eigenvectors contains dN_{uc} entries, where N_{uc} is the number of atoms in the unit cell and d is the dimension of the system. With the method of calculating the phonons established, one needs to calculate the force constant matrix (equation 2.10) from an inter atomic potential to describe the vibrations of a crystal. The harmonic approximation is useful to describe the vibrations of atoms in a system. It is, however only valid when the displacements from the equilibrium positions are small. The harmonic lattice dynamics does not include temperature effects and anharmonic effects like thermal expansion. Anharmonic lattice dynamics can be used to investigate thermal expansion by using the Grüneisen parameters.

In quantum mechanics, the energy of a harmonic oscillator is quantized. The quanta of the lattice vibrations are called phonons, and the energy of a single oscillator can be written as:

$$E_n = \left(n + \frac{1}{2}\right)\hbar\omega, \tag{2.15}$$

with n the number of excited phonons. The phonons are bosons and follow a Bose-Einstein distribution. The average occupation number of a mode with frequency $\omega_{\boldsymbol{k},\lambda}$ is:

$$\langle n(\omega_{\boldsymbol{k},\lambda})\rangle = \frac{1}{e^{\left(\hbar\omega_{\boldsymbol{k},\lambda}/k_bT\right)}-1} \tag{2.16}$$

In lattice dynamics, the phonon modes are calculated from the classical Newton's equations of motion and the bosonic nature of the phonons is taken into account by imposing the Bose-Einstein distribution. Molecular dynamics is a purely classical method and the bosonic nature of the phonons is not captured and all modes are occupied uniformly (equipartition theorem).

2.2. Superlattices and phonon coherence

Superlattices are periodic arrangements of layers of two or more crystalline materials with periods in the order of nanometers. Due to the periodic arrangement of the layers in the superlattices, phonon confinements are reached, and an additional translational symmetry is introduced. This leads to Brillouin-zone-folding and to a change in the phonon density of states. Superlattices have a high interface density. In the limit in which the phonon's mean free path exceeds the typical structure size of the system, and the crystal is of high quality that scattering from defects plays a minor role, phonons are scattered at the interface or at a boundary, before another type of scattering takes place (e.g. phonon-phonon). In this limit transport is ballistic rather than diffusive.

In the diffusive regime, the phase relation between the phonons is random and phonons are not coherent (i.e. incoherent). Coherent phonons are collective motions of atoms, where the phase relation between the vibrations is not random. Coherent phonons can be excited by outer stimuli (e.g. light, mechanic stimuli). A coherent wave packet moves through the crystal without losing the phase relationship between the vibrations. The questions that arise in the case of superlattices are, what is the coherence phonon

length, and whether the scattered phonons at the interfaces are transmitted coherently or incoherently.

Superlattices have been addressed to show coherent phonon transport in theoretical and experimental studies [10, 9]. Often the coherence of longitudinal acoustic phonons is studied [17, 18, 19, 20], involving just a small part of the whole phonon spectrum. The longitudinal acoustic phonons are generated by a short laser pump pulse and then detected with another pulse in a pump probe technique.

The phonon modes contribute differently to the thermal conductivity, depending on the occupation number a smaller or larger part of the phonon spectrum is involved in the heat conduction. A minimum in the thermal conductivity as a function of the superlattice period (usually with atomically flat interfaces) have been reported in experiments and simulations [21, 22, 23, 8, 24]. Interfaces are barriers for phonon and hence heat transport, and a higher interface density should lead to a lower thermal conductivity. The minimum of the thermal conductivity is explained by a transition from a phonon diffusive interface scattering to a phonon ballistic coherent transport through the interfaces. A recent study of the thermal conductivity in superlattices, using the Boltzmann transport equation [25], showed that the Boltzmann equation is not able to predict the experimental trends of thermal conductivity in superlattices, leading to the conclusion, that phonon interference and coherence plays an important role. Another study, based on a Boltzmann transport model, uses different transport models for short and long wavelength modes. They showed that thermal transport of Si/Ge superlattices can be explained by an interplay of coherent and incoherent phonon transport [26].
In summary, phonon coherence has been shown to be present in superlattices. Moreover, they are ideal systems to study phonon coherence, as the superlattice period and the total thickness of the superlattice can be varied systematically.

2.3. Molecular Dynamics

Molecular dynamics (MD) is a method to study the dynamics of a system composed of atoms. Only a short introduction to the method is given here based on [27, 28], where further information can be found. MD is based on integrating the classical equations of motions for all the particles in a system. The force F on the particle of mass m in the potential energy surface U is $\boldsymbol{F} = -\nabla U$. According to Newton's second law, the acceleration of the particle is $m\ddot{\boldsymbol{x}}(t) = \boldsymbol{F}(t)$. Assuming a constant force in the short time interval Δt, the position $\boldsymbol{x}$ and velocity $\dot{\boldsymbol{x}}$ are:

$$\boldsymbol{x}(t + \Delta t) = \boldsymbol{x}(t) + \dot{\boldsymbol{x}}(t)\Delta t + \frac{1}{2m}\boldsymbol{F}(t)(\Delta t)^2 \tag{2.17}$$

$$\dot{\boldsymbol{x}}(t + \Delta t) = \dot{\boldsymbol{x}}(t) + \frac{1}{m}\boldsymbol{F}(t)\Delta t \tag{2.18}$$

In an MD simulation, a large number of particles N is simulated. These particles interact by means of a potential energy $U(\boldsymbol{X})$, that depends on the relative positions among the particles. Here $\boldsymbol{X}$ stands for all particle positions $x_1, x_2, ..., x_N$.

The workflow of an MD simulation is presented in Figure 2.3. To start an MD simulation, the initial positions $\boldsymbol{x}_0$ and initial velocities $\boldsymbol{v}_0$ of the particles are set. For a crystalline system, the atoms are placed at their equilibrium positions in the crystal. The forces on all particles are calculated according to the potential energy $U(\boldsymbol{X_0})$. Then the equations of motions (2.17,2.18) are integrated leading to new positions $\boldsymbol{X}(t_0 + dt)$ and velocities $\dot{\boldsymbol{X}}(t_0 + dt)$, with dt being the time-step of the simulation. New forces are calculated according to the new positions, which then are used to integrate the equations of motion again. In this way, the time evolution of the system is simulated. The time-step dt of the simulation needs to be sufficiently small, so that the total energy of the system is conserved, and that atoms do not move too far in one simulation step.

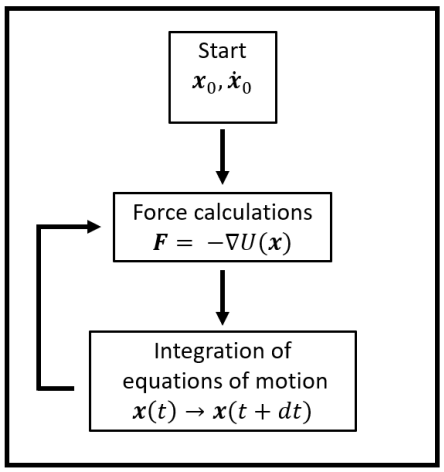

Figure 2.3.: Workflow of a simple molecular dynamics simulation

2.4. Vibrational density of states from the velocity auto-correlation function

In this work, molecular dynamics simulations are done to learn about the phonons in a crystal. In this section the relationship between the Fourier transform of the velocity auto-correlation function (VACF), calculated from the trajectories of an MD simulation, and the vibrational density of states (DOS) [29, 30] is shown.

The vibrational density of states $\rho(\omega)$ is a function of the angular frequency ω. The density of states expresses how many vibrational states are in the interval between ω and $\omega + d\omega$. The density of states can be calculated either from a phonon band dispersion using lattice dynamics, or from the velocity auto correlation function using molecular dynamics.

The auto-correlation function $C(\tau)$ of a time signal $x(t)$ is a measure of how strongly the signal at time t is correlated to itself at time $t + \tau$. The auto-correlation is defined as:

$$C(\tau) = \lim_{T \to \infty} \frac{1}{T} \int_0^T x(t_0)x(t_0 + \tau)\, dt_0 \tag{2.19}$$

The integral is an average over different time origins t_0. If the system is at equilibrium, and the signal stationary, the auto-correlation function does not depend on the origin t_0. Then the auto-correlation function is often denoted as:

$$C(\tau) = \langle x(t_0)x(t_0 + \tau) \rangle, \tag{2.20}$$

The velocity auto-correlation function (for one atom j) is:

$$\mathrm{VACF}_j(\tau) = \langle v_j(t_0)v_j(t_0 + \tau) \rangle, \tag{2.21}$$

where $\boldsymbol{v}_j(t)$ is the velocity of the atom j in the system, and it is assumed that its Fourier transform exists.

$$\boldsymbol{v}_j(\omega) = \int_{-\infty}^{\infty} \boldsymbol{v}_j(t) e^{i\omega t} dt. \tag{2.22}$$

The power spectrum of the velocity (2.22) is:

$$|\boldsymbol{v}_j(\omega)|^2 = \int_{-\infty}^{\infty} \int_{-\infty}^{\infty} \boldsymbol{v}_j(t)\boldsymbol{v}_j(t') e^{i\omega(t-t')} dt dt'. \tag{2.23}$$

If the physical system is in equilibrium, the power spectrum only depends on the difference between times, $t'' = t - t'$:

$$|\boldsymbol{v}_j(\omega)|^2 = \int_{-\infty}^{\infty} \int_{-\infty}^{\infty} \boldsymbol{v}_j(t'' + t')\boldsymbol{v}_j(t') e^{i\omega t''} dt'' dt' \tag{2.24}$$

Within the harmonic approximation, the coordinates $u_\alpha(t)$ (α labels the $3N$ atomic coordinates, i.e. in all three dimensions of all atoms j) can be written in terms of the modes of vibrations in the system:

$$u_\alpha(t) = \frac{1}{\sqrt{m_j}} \sum_{\boldsymbol{k},p} \boldsymbol{e}(\boldsymbol{k}, p; \alpha) e^{i\boldsymbol{k}\boldsymbol{R}_j}\, q(\boldsymbol{k}, p) e^{-i\omega_{(\boldsymbol{k},p)}t} \tag{2.25}$$

The normal modes are labeled with the wave vector k and the branch p, $\boldsymbol{e}(\boldsymbol{k}, p; \alpha)$ is the component of the mode eigenvector regarding the coordinate α, $\boldsymbol{R}_j$ is the position and m_j the mass of the atom j to which belongs the coordinate α. $q(\boldsymbol{k}, p)$ are called the normal mode coordinates and $e^{-i\omega_{(\boldsymbol{k},p)}t}$ is the time dependence of the normal mode coordinate. For a simpler notation, the normal modes are labelled with s instead of $(\boldsymbol{k}, p)$ and the quantity $Q_{s\alpha} = \boldsymbol{e}(\boldsymbol{k}, p; \alpha)e^{i\boldsymbol{k}\boldsymbol{R}_j}q(\boldsymbol{k}, p)$ is used:

$$u_\alpha(t) = \frac{1}{\sqrt{m_j}} \sum_s Q_{s\alpha} e^{-i\omega_s t} \tag{2.26}$$

The sum goes over all normal modes s of the system. The velocity is the time derivative of Eq. (2.26):

$$\dot{u}_\alpha(t) = v_\alpha(t) = \frac{1}{\sqrt{m_j}} \sum_s Q_{s\alpha}(-i\omega_s) e^{-i\omega_s t} \tag{2.27}$$

Putting (2.27) into equation (2.24), and summing over all N atoms in the system, and $3N$ coordinates respectively, we obtain:

$$\frac{1}{N}\sum_{i=j}^{N} m_j |\boldsymbol{v}_j(\omega)|^2 = \frac{1}{N}\sum_{s,s'}\sum_{\alpha=1}^{3N} \int_{-\infty}^{\infty} Q_{s\alpha} Q^*_{s'\alpha}(i\omega_s)(i\omega'_s) e^{i(\omega+\omega_s)t''} dt'' \times \int_{-\infty}^{\infty} e^{i(\omega'_s-\omega_s)t'} dt' \tag{2.28}$$

As $\int_{-\infty}^{\infty} e^{i(\omega'_s-\omega_s)t'} dt' = \delta_{s,s'}$, we can simplify (2.28):

$$\sum_{j=1}^{N} m_j |\boldsymbol{v}_j(\omega)|^2 = \sum_s \sum_{\alpha=1}^{3N} \int_{-\infty}^{\infty} |Q_{s\alpha}|^2 \omega_s^2 e^{i(\omega+\omega_s)t''} dt'' \tag{2.29}$$

If the system is in thermal equilibrium, the equipartition theorem applies and $|Q_{s\alpha}|^2\omega_s^2 = k_b T$:

$$\sum_{j=1}^{N} m_j |\boldsymbol{v}_j(\omega)|^2 = \sum_s \int_{-\infty}^{\infty} 3Nk_bTe^{i(\omega+\omega_s)t''}dt'' = 3Nk_bT\sum_s \delta(\omega+\omega_s) \quad (2.30)$$

In the harmonic approximation, the density of states is a sum of delta functions and can be written as $\rho(\omega) = \sum_s \delta(\omega + \omega_S)$. From Eq. (2.30) we can get the following expression for the density of states:

$$\rho(\omega) = \frac{1}{3Nk_bT}\sum_{j=1}^{N} m_j |\boldsymbol{v}_j(\omega)|^2 \quad (2.31)$$

If we look at the expression (2.24) for the power spectrum $|\boldsymbol{v}_j(\omega)|^2$, we can identify the integral over t' as an average over different origins of time t'. Setting $t' = 0$ and $t'' = t$, the equation (2.24) is identified as the velocity auto-correlation function. Fourier-transform of the velocity auto-correlation function equals the power spectrum.

$$|\boldsymbol{v}_j(\omega)|^2 = \int_{-\infty}^{\infty} \langle \boldsymbol{v}_j(t)\boldsymbol{v}_j(0)\rangle e^{i\omega(t)}dt \quad (2.32)$$

Using (2.32), the vibrational density of states is proportional to the Fourier transform of the velocity auto-correlation function [29, 30].

$$\rho(\omega) = \frac{1}{3Nk_bT}\int_{-\infty}^{\infty}\sum_{j=1}^{N} m_j \langle v_j(t)v_j(0)\rangle e^{i\omega t}dt \quad (2.33)$$

2.5. Microscopic picture of phonon coherence

In order to calculate the phonon coherence length from molecular dynamics simulations, we need a microscopic picture of the phonon coherence. This microscopic picture is obtained from a methodology reported in the literature [11, 12]. The following chapter is based on these works. The methodology is explained in detail, as a big part of this thesis is based on it. The methodology makes use of the second order coherence theory, that states that any coherence phenomena can be formalized as a correlation [31]. For example, the spatial correlations of electromagnetic fields leads to spatial coherence of electromagnetic light [32]. The spatial coherence of wave-functions leads also to spatial coherence of Bose-Einstein condensates [33]. In analogy, for phonons this would mean that the phonon coherence corresponds to the spatial correlation of atomic displacements.

If two atoms in the crystal, which are separated by a certain distance l vibrate in phase, their motion will be correlated. This correlated motion comes from phonon-wave-packets moving through the crystal. Atoms within the wave-packet move non-randomly, featuring a phase relationship and, thus, are correlated. Atoms separated by a larger distance $l + \Delta l$ might not show a correlated motion as the phase-information is lost for a long distance. In the microscopic picture provided by the methodology proposed by [11] and [12], the distance over which atoms show a correlated motion corresponds to the spatial coherence length l_c.

For the formalization, let us consider a crystal whose unit cell has n_{uc} atoms. The primitive vectors of the Bravais lattice are $\boldsymbol{a}_i$. The (equilibrium) position of the cell labeled k in the d-dimensional system is denoted as $\boldsymbol{R}_k^0 = \sum_i^d c_i^k \boldsymbol{a_i}$, with $c_i^k \in \mathbb{Z}$. The velocity of the atom b, in the unit cell k, is $\boldsymbol{v}(t, \boldsymbol{R}_k^0, b)$.
The cross correlation function $\langle v_a(t) v_b(t+\tau) \rangle_t$ between two velocities (the indices a and b label different atoms) is (2.34):

$$\langle v_a(t) v_b(t+\tau) \rangle_t = \lim_{T \to \infty} \frac{1}{T} \int_0^T v_a(t_0) v_b(t_0+\tau)\, dt_0. \tag{2.34}$$

As the times from the MD simulation are discrete, the integral becomes a sum. Thus, Eq. (2.34) can be written as:

$$\langle \boldsymbol{v}_a(t)\boldsymbol{v}_b(t+\tau)\rangle_t = \frac{1}{N_t}\sum_{t_0}\boldsymbol{v}_a(t_0)\boldsymbol{v}_b(t_0+\tau) \tag{2.35}$$

As the system is in equilibrium, and the velocity field is stationary, the correlation function just depends on the time difference $\tau = t_2 - t_1$. For improving the statistics, the correlation in equation (2.35) is calculated as an average over all N_t possible origins t_0.

If the system is in equilibrium, and assuming a stationary velocity field, the mutual coherence function $T(\tau, \boldsymbol{R}_k^0, \boldsymbol{R}_l^0)$ is calculated. The mutual coherence function is the mass-weighted time cross-correlation function between the velocities of an atom in unit cell k with the corresponding atom in unit cell l. The summation goes over the n_{uc} atoms in the unit cell.

$$T(\tau, \boldsymbol{R}_k^0, \boldsymbol{R}_l^0) = \frac{1}{2}\sum_{b=1}^{n_{uc}} m_b \langle \boldsymbol{v}(t, \boldsymbol{R}_k^0, b)\boldsymbol{v}(t+\tau, \boldsymbol{R}_l^0, b)\rangle_t \tag{2.36}$$

Taking the time Fourier transform of equation (2.36), leads to the spatial cross spectral density function $T(\omega, \boldsymbol{R}_k^0, \boldsymbol{R}_l^0)$.

$$T(\omega, \boldsymbol{R}_k^0, \boldsymbol{R}_l^0) = \frac{1}{2}\sum_{b=1}^{n_{uc}} m_b\ \boldsymbol{v}^*(\omega, \boldsymbol{R}_k^0, b) \times \boldsymbol{v}(\omega, \boldsymbol{R}_l^0, b), \tag{2.37}$$

where $\boldsymbol{v}(\omega, \boldsymbol{R}_l^0, b)$ is the Fourier transform of the velocity $\boldsymbol{v}(t, \boldsymbol{R}_k^0, b)$, and $\boldsymbol{v}^*(\omega, \boldsymbol{R}_l^0, b)$ its complex conjugate. The cross spectral density function will in general be complex, because $\boldsymbol{v}^*(\omega, \boldsymbol{R}_k^0, b)$ and $\boldsymbol{v}(\omega, \boldsymbol{R}_l^0, b)$ are velocities of different atoms (in unit cell at position $\boldsymbol{R}_k^0$ and $\boldsymbol{R}_l^0$). The trajectories of different atoms are different and $\boldsymbol{v}^*(\omega, \boldsymbol{R}_k^0, b)$ is not simply the complex conjugate of the velocity $\boldsymbol{v}(\omega, \boldsymbol{R}_l^0, b)$ of the other atom (as it is the case for auto-correlations).
To go from Eq. (2.36) to Eq. (2.37), we used the Wiener-Khinchin and the cross correlation theorems. The theorems are explained in the appendix A.1.

In the following, next to a stationarity in time, a discrete translation symmetry is assumed. Therefore, in the next step spatial correlations (aside of time correlations) are calculated from the cross spectral density function (2.37).

$$T(\omega, \boldsymbol{R}) = \frac{1}{2} \sum_{b=1}^{n_u c} m_b \langle \boldsymbol{v}^*(\omega, \boldsymbol{R}^0, b) \boldsymbol{v}(\omega, \boldsymbol{R}^0 + \boldsymbol{R}, b) \rangle_{\boldsymbol{R}^0}. \tag{2.38}$$

Here $\langle \dots \rangle_{\boldsymbol{R}^0}$ denotes the spatial cross correlation. The vector $\boldsymbol{R}$ belongs to the Bravais lattice, and $\hat{\boldsymbol{R}} = \frac{\boldsymbol{R}}{|\boldsymbol{R}|}$ is the spatial correlation direction, along which the correlations are calculated. In the above equation, the translational symmetry is assumed for distances corresponding to the materials' unit cells. In essence, this means that all unit cells separated by the same distance vector $\boldsymbol{R}$ should show similar coherence and, hence, are summed up. Strictly speaking, the translational symmetry holds only for distances corresponding to the superlattice periodicity, and is broken for other distances as the material changes according to the superlattice period.

Eq. (2.38) is the sum of the correlations of all atoms in the system which are separated by the same distance vector $\boldsymbol{R}$:

$$T(\omega, \boldsymbol{R}) = \sum_{\boldsymbol{R}_i^0} T(\omega, \boldsymbol{R}_i^0, \boldsymbol{R}_i^0 + \boldsymbol{R}). \tag{2.39}$$

It contains the space dependent correlation information as a function of frequency. The larger the distance $R = |\boldsymbol{R}|$, the lower the correlated signal will be, as atoms further away will show less correlated motion.

Choosing a single frequency ω_0, the ideal functional behavior is an attenuated wave:

$$\frac{T(\omega_0, R)}{T(\omega_0, R = 0)} = \cos\left(\frac{2\pi R}{\lambda_0}\right) * e^{-\frac{R}{l_c}} \tag{2.40}$$

The decay of the attenuated wave is determined by the frequency dependent coherence length $l_c(\omega_0)$. Here, λ_0 is the wavelength of the phonon-mode with frequency ω_0. If there are two or more modes at the same frequency

ω_0, the calculated spatial cross correlation from a simulation will be a sum of two or more attenuated waves (2.40) with different decay rates l_c and different λ_0.

As shown in this section, it is possible to extract frequency dependent coherence properties from the velocity field of the atoms in the system. Molecular Dynamics is a good method to simulate the velocity field of a system over time to capture the statistical fluctuations of the velocity-field, and allows for relatively large simulations. Molecular Dynamics naturally includes all anharmonicities of the potential between the atoms. The anharmonic part of the potential is important to describe the phonon scattering. Using the microscopic picture described in this section, it is possible to extract the frequency dependent coherence length. A drawback of the method is that although it is frequency dependent, it does not resolve the coherence length depending on the wave-vector. If there are two different modes with the same frequency along a certain symmetry direction, it is not possible to distinguish them with the presented method, and calculate a coherence length for each individual mode.

2.6. Spectral energy density

Latour et al [12, 34] have shown that the spectral energy density $T(\omega, \boldsymbol{k})$ can be obtained from the cross spectral density function by Fourier transform in space:

$$T(\omega, \boldsymbol{R}) = \sum_{\boldsymbol{k}} \left(\sum_{p} \frac{1}{2} |\dot{q}(\omega, \boldsymbol{k}, p)|^2 \right) e^{-i\boldsymbol{k}\boldsymbol{R}}. \tag{2.41}$$

The spectral energy density is given as:

$$T(\omega, \boldsymbol{k}) = \sum_{p} \frac{1}{2} |\dot{q}(\omega, \boldsymbol{k}, p)|^2, \tag{2.42}$$

where $\dot{q}(\omega, \boldsymbol{k}, p)$ is the time Fourier transform of the time derivative of the normal mode coordinate (see Eq. 2.26) of the mode $(\boldsymbol{k}, p)$. The sum goes over all branches p of the dispersion relation. The spectral energy density (2.42) tells for each wave-vector $\boldsymbol{k}$, among which frequencies the energy of

the vibrations is distributed in the system. The spectral energy density can be calculated from the velocities of an MD simulation, if the eigenmodes of the system are known (for example by doing LD). Using the spectral energy density, the coherence length could possibly be resolved wave-vector dependent, next to a frequency dependent resolution.

2.7. Wurtzite crystal structure

Gallium nitrite and indium nitride have a wurtzite crystal structure at room temperature. Here, the lattice vectors of the wurtzite crystal structure and their equivalent orthogonal representation are presented. The orthogonal representation is used for building the simulation cells of gallium nitride / indium nitride superlattices. The wurtzite crystal structure is a hexagonal crystal system with four atoms in the conventional unit cell. The wurtzite unit cell is shown in Figure 2.4. The primitive vectors are the following:

$$\begin{aligned} \boldsymbol{A}_1 &= \frac{1}{2}a\hat{\boldsymbol{x}} - \frac{\sqrt{3}}{2}a\hat{\boldsymbol{y}} \\ \boldsymbol{A}_2 &= \frac{1}{2}a\hat{\boldsymbol{x}} + \frac{\sqrt{3}}{2}a\hat{\boldsymbol{y}} \\ \boldsymbol{A}_3 &= c\hat{\boldsymbol{z}} \end{aligned} \tag{2.43}$$

The basis vectors, describing the positions of the atoms in the cell, are:

$$\begin{aligned} \boldsymbol{B}_1 &= \frac{1}{3}\boldsymbol{A}_1 + \frac{2}{3}\boldsymbol{A}_2 \\ \boldsymbol{B}_2 &= \frac{2}{3}\boldsymbol{A}_1 + \frac{1}{3}\boldsymbol{A}_2 + \frac{1}{2}\boldsymbol{A}_3 \\ \boldsymbol{B}_3 &= \frac{1}{3}\boldsymbol{A}_1 + \frac{2}{3}\boldsymbol{A}_2 + u\boldsymbol{A}_3 \\ \boldsymbol{B}_4 &= \frac{2}{3}\boldsymbol{A}_1 + \frac{1}{3}\boldsymbol{A}_2 + (\frac{1}{2} + u)\boldsymbol{A}_3 \end{aligned} \tag{2.44}$$

In this thesis, an orthogonal representation of the wurtzite unit cell is used to construct the supercells for the molecular dynamics simulations. The

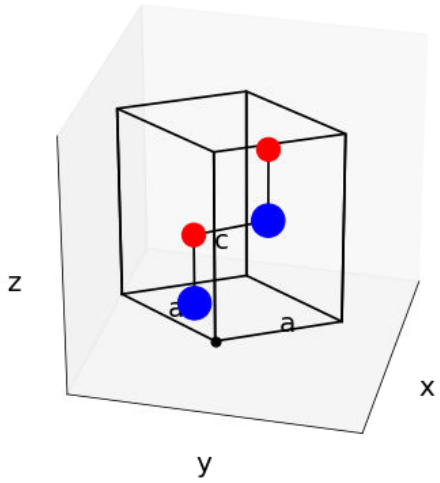

Figure 2.4.: Wurtzite crystal structure with 4 atoms in the basis.

change in basis can be described by a matrix $\boldsymbol{M}$ [35]:

$$(\boldsymbol{A}_1', \boldsymbol{A}_2', \boldsymbol{A}_3') = (\boldsymbol{A}_1, \boldsymbol{A}_2, \boldsymbol{A}_3)\boldsymbol{M} \tag{2.45}$$

where $\boldsymbol{A}_i'$ are the new lattice vectors, $\boldsymbol{A}_i$ the old lattice vectors. The lattice vectors are column-vectors and $\boldsymbol{A}_1$ is the first column of the matrix $(\boldsymbol{A}_1, \boldsymbol{A}_2, \boldsymbol{A}_3)$. The matrix for the transformation from the wurtzite basis to the orthogonal representation is:

$$\begin{bmatrix} 1 & -1 & 0 \\ 1 & 1 & 0 \\ 0 & 0 & 1 \end{bmatrix} \tag{2.46}$$

and Eq. (2.45) reads for the case of the transformation of the wurtzite structure to the orthogonal representation:

$$\begin{pmatrix} \frac{1}{2}a & -\frac{\sqrt{3}}{2}a & 0 \\ \frac{1}{2}a & \frac{\sqrt{3}}{2}a & 0 \\ 0 & 0 & 1c \end{pmatrix} \begin{bmatrix} 1 & -1 & 0 \\ 1 & 1 & 0 \\ 0 & 0 & 1 \end{bmatrix} = \begin{pmatrix} a & 0 & 0 \\ 0 & \sqrt{3}a & 0 \\ 0 & 0 & c \end{pmatrix} \tag{2.47}$$

The resulting lattice vectors are:

$$\begin{aligned} \boldsymbol{A}_1' &= a\hat{\boldsymbol{x}} \\ \boldsymbol{A}_2' &= \sqrt{3}a\hat{\boldsymbol{y}} \\ \boldsymbol{A}_3' &= c\hat{\boldsymbol{z}} \end{aligned} \tag{2.48}$$

In Figure 2.5 the hexagonal character of the wurtzite crystal structure can be seen in a cross section of the x-y plane. Moreover, the lattice vectors in the first two dimensions of wurtzite unit cell and the orthogonal representation of it are shown. The determinant of the transfer matrix $\boldsymbol{M}$ gives the ratio of the volumes of the old and new unit cells. The determinant of the transfer matrix (2.46) is 2. The orthogonal representation has the double volume and has eight atoms in its basis, which can also be seen in Figure 2.5. There are two points within the red cell, four points at the faces (which are counted half) and each point counts for two atoms, as two atoms are above each other at the same x-y coordinates.

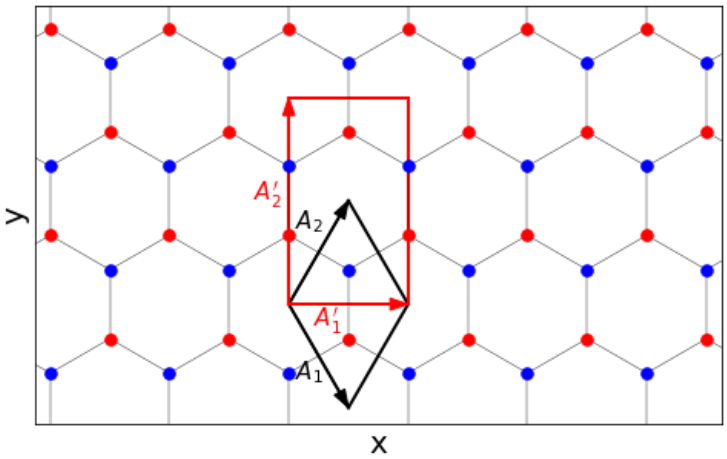

Figure 2.5.: Cross section of a wurtzite crystal (for instance GaN or InN). The c-direction is perpendicular to the paper. The black lines are the edges of the wurtzite unit cell and the red dashed lines the edges of the orthogonal representation.

A point in the unit cell can be written as a column vector who's entries are fractional values with respect to the lengths of the lattice vectors.

$$\boldsymbol{x}^T = (x_1, x_2, x_3); \quad 0 \leq x_i < 1 \tag{2.49}$$

The atoms position (basis vectors (2.44)) can be written as

$$B = \sum_i x_i \boldsymbol{A_i}. \tag{2.50}$$

The presentation of an atom as a vector with fractional values of the lattice vectors (Eq. 2.49) changes with the change of basis as well [35]

$$\boldsymbol{x'} = \boldsymbol{M}^{-1}\boldsymbol{x} + \boldsymbol{t}. \tag{2.51}$$

$\boldsymbol{t}$ is a translation-vector, which is needed so that the atom is in the new unit cell. The translation-vector is chosen here so that one atom sits at $(0,0,0)^T$. The eight basis vectors b_i for the orthogonal representation are the following:

$$\begin{aligned}
\boldsymbol{b}_1 &= \vec{0} \\
\boldsymbol{b}_2 &= u\boldsymbol{A}'_3 \\
\boldsymbol{b}_3 &= \frac{1}{2}\boldsymbol{A}'_1 + \frac{1}{6}\boldsymbol{A}'_2 + \frac{1}{2}\boldsymbol{A}'_3 \\
\boldsymbol{b}_4 &= \frac{1}{2}\boldsymbol{A}'_1 + \frac{1}{6}\boldsymbol{A}'_2 + (u + \frac{1}{2})\boldsymbol{A}'_3 \\
\boldsymbol{b}_5 &= \frac{1}{2}\boldsymbol{A}'_1 + \frac{1}{2}\boldsymbol{A}'_2 \\
\boldsymbol{b}_6 &= \frac{1}{2}\boldsymbol{A}'_1 + \frac{1}{2}\boldsymbol{A}'_2 + u\boldsymbol{A}'_3 \\
\boldsymbol{b}_7 &= \frac{2}{3}\boldsymbol{A}'_2 + \frac{1}{2}\boldsymbol{A}'_3 \\
\boldsymbol{b}_8 &= \frac{2}{3}\boldsymbol{A}'_2 + (u + \frac{1}{2})\boldsymbol{A}'_3
\end{aligned} \tag{2.52}$$

3. Computation

In the following sections details about the computation and the used programs are given. First, the force field potentials are presented: To simulate a one-dimensional superlattice and a three-dimensional FCC superlattice, a Lennard-Jones potential is used, while for GaN/InN superlattices, a three-body potential is needed. The choice of the potential is also discussed. The used programs and software packages for lattice dynamics and molecular dynamics are presented. Details about the MD simulations are given. Moreover, the thermostats and barostat used during the molecular dynamics are described. They are used to simulate a system at a desired temperature and pressure, respectively. At the end of the chapter some details about the post-processing of the MD simulations to calculate the cross spectral density function and the coherence length are given.

3.1. Force Field Potentials

In a molecular dynamics simulation the dynamics or time evolution of the system is determined by the masses of the particles and the potential energy between the particles, from which the forces are calculated. The reliability of the properties calculated out of an MD simulation depends on the reliability of the potential. Therefore, it is crucial to have a good potential, which describes the real system as close as possible. The lack of a satisfactory empirical potential can be overcome by doing ab-initio molecular dynamics. Accurate results can be obtained from ab-initio MD, but with far higher computational costs. In this thesis, systems with up to a few ten-thousand particles are simulated for time scales up to nanoseconds, involving million integration time-steps. Such large simulations can not be performed in the framework of ab-initio techniques in reasonable time. With classical force

field potentials, it is possible to simulate such large systems over longer time-scales. Growing computational power and massively parallelized MD packages allow for simulations of larger and larger systems.
The classical force fields are a sum of different contributions (two-body interactions, three-body interactions, long and short-range interactions) to the potential, and each contribution is described with an analytical functions. The analytical functions have parameters, which can be adjusted. Thus, a potential with the same analytical functions can describe different systems. The parameters are determined by a fitting procedure, in which the parameters are adjusted so that the potential reproduces desired properties of the material. For example, the equilibrium phase at a given temperature, crystal structure, elastic properties. During the fitting procedure, the parameters of the potential are changed so that the difference between the physical quantities resulting from the potential and the experimental values or ab-initio data becomes a minimum. As mentioned above all the 'physics' relies in the potential, therefore it is crucial to use a potential which accurately describes the properties of interest.

3.1.1. Lennard Jones potential

A simple classical potential is the Lennard-Jones (LJ) potential. It consists of a two-body potential which depends just on the distance r between the two interacting particles:

$$E = 4\epsilon \left(\left(\frac{\sigma}{r}\right)^{12} - \left(\frac{\sigma}{r}\right)^{6} \right). \tag{3.1}$$

The depth of the potential is given by ϵ, σ is the distance for which the potential has a zero-crossing. The equilibrium distance between the two particles is given by $r_0 = 2^{1/6}\sigma$.

The Lennard-Jones potential (see Figure 3.1) goes towards zero for large distances, and hence the interactions between distant particles can be neglected. To reduce computational time, the potential is set to zero for a certain cutoff distance r_c. For the Lennard-Jones potential this distance is usually around $r_c = 3\sigma$. In this work, the LJ-potential is used as a toy model for method development.

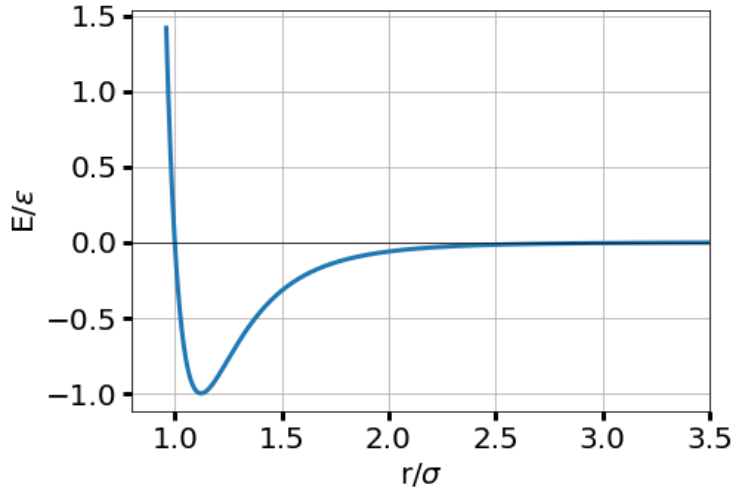

Figure 3.1.: Lennard-Jones potential (equiation (3.1)) as a function of reduced distance r/σ

3.1.2. Many-body potential for GaN/InN

Many semiconductor materials form covalent bonds, which are difficult to describe with two-body potentials, as the interaction strength depends on the local environment. Gallium nitrite, for example, has a wurtzite crystal structure at room temperature. The potential energy in this cases does not depend only on the distance between two particles, but also on the local environment, through the angle between atomic bonds. Three-body potential terms are needed to describe the potential change due to bond bending in the system, for example by punishing a deviation from the equilibrium angle. The Stillinger-Weber potential [36] and the Tersoff potential [37] are examples for many body potentials.

Gallium-Nitrite and Indium-Nitrite both have a wurtzite crystal structure as the equilibrium crystal structure at room temperature. For simulations of superlattices, consisting of two materials A and B, the potential needs to accurately describe both materials independently. Moreover, as both materials will be in contact at the interfaces of the superlattice, the potential also needs to accurately describe the interactions between all the atoms of material A with all the atoms of material B. This is a further difficulty in developing a feasible force field potential or finding it in literature. For

	modified SW potential	[39]
a	3.173 Å	3.190 Å
c	5.171 Å	5.189 Å

Table 3.1.: Lattice parameters of GaN at 300 K compared to experimental values [39].

superlattices of GaN/InN, a Stillinger-Weber potential from the literature is used which has been modified by the authors [38] such that both GaN and InN are stable in wurtzite and zinc blende structure, but with the wurtzite structure as the equilibrium phase having a slightly lower energy as the zinc blende phase. Zhou et al. [38] parametrized the potential by fitting to the bond-lengths, lattice constants, cohesive energies and bulk modulus. They conducted as well growth-MD simulations of GaN and InN on a substrate of the same material and the opposite material to benchmark the potential.

Usually, the parametrization of potentials for crystals does not account for phonon properties like the band structure and DOS during the fitting procedure. The potential mentioned above was created to simulate the growth of InGaN thin films, and to reproduce stacking fault energies. No phonon properties were taken into account during the fitting of the potential by the creators of the potential [38]. Therefore, a bench-marking of the potential and investigation of phonon properties was done in this work. The lattice parameters, and the phonon dispersion for GaN and InN resulting from the modified Stillinger Weber potential are presented here, while the results of further bench marking (elastic constants, thermal conductivity of GaN and InN) are presented in the Appendix A.2 and A.3. The lattice parameters of GaN with the modified Stillinger-Weber potential are in good agreement with the experimental values (Table 3.1), while the lattice parameters of InN are slightly lower than the experimental values (Table 3.2).

The dispersion relation of wurtzite GaN can be found in Figure 3.2. The dispersion relation is compared to a first principle calculation. To calculate the ab-initio data, force constants from the **almaBTE** database were used [41]. Already, at the Γ point, it can be seen that the modified Stillinger-Weber potential partially deviates from the ab-initio calculation. The phonon

	modified SW potential	[40]
a	3.499 Å	3.5340 Å
c	5.683 Å	5.7088 Å

Table 3.2.: Lattice parameters of InN at 300 K compared to experimental values [40].

frequencies are overestimated by the Stillinger-Weber potential. This can be seen in the deviation with respect to the DFT results for instance at 5 THz. The transverse acoustic branches are steeper leading to a higher group velocity of the acoustics phonons. The optical bands below the large gap tend to be flatter with the Stillinger-Weber potential, leading to a lower group velocity of these modes. The frequencies above the band-gap are higher as the ab-initio frequencies.

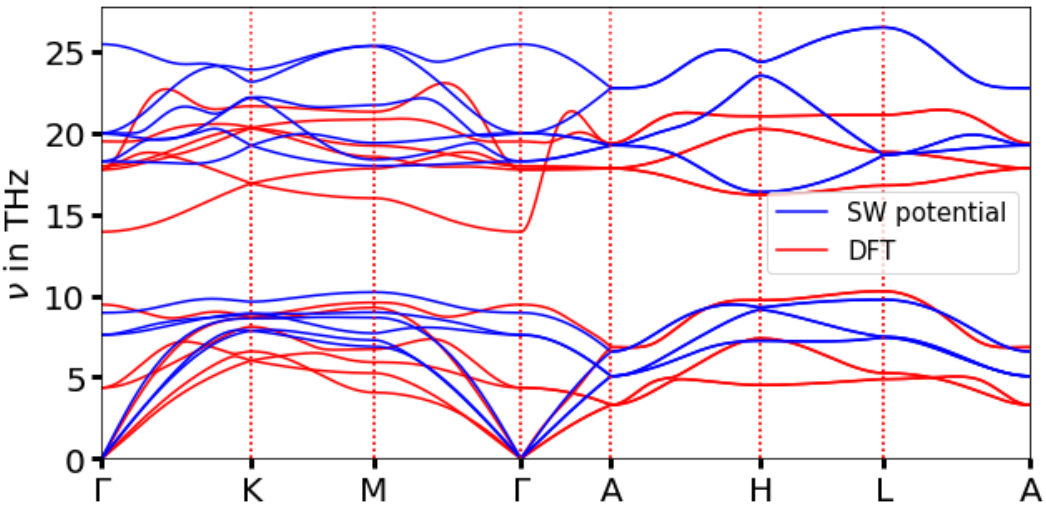

Figure 3.2.: Phonon dispersion relation from LD of wurtzite GaN with the modified Stillinger-Weber potential (SW) [38] compared to the dispersion relation calculated with ab-initio force constants (DFT). The ab-initio force constants are taken from the **almaBTE** database [41].

The dispersion relation obtained from lattice dynamics of the wurtzite InN (for 0 K) is depicted in Figure 3.3 (blue lines). Compared to the dispersion relation from DFT of Ref. [42], the phonon frequencies of InN are underestimated by the modified Stillinger-Weber potential of [38]. This is prominent

for modes below the band gap, where the Stillinger-Weber potential gives frequencies up to 5 THz, while the frequencies of the DFT data reach above 7 THz. A large deviation is at the Γ point where the frequencies from DFT data are nearly three times higher.
A dispersion relation at T = 300 K is obtained from a renormalization of the force constants using **DynaPhoPy** [43], which is a program that includes anharmonic effects at finite temperature. **DynaPhoPy** does a normal mode decomposition by projecting the velocities of an MD simulation onto the harmonic phonon modes calculated by **phonopy**. The power spectrum is calculated, and anharmonic properties are extracted by fitting the power spectrum to Lorentzian functions. Anharmonic properties like the phonon life-times and the frequency shift at finite temperature can be calculated. The dispersion relation at T = 0 K is shown in red in Figure 3.3. The modes below the band gap show a strong anharmonic frequency shift, with the frequencies at the Γ point being almost twice as high than at 0 K. The dispersion relation at 300 K shows a better agreement to the calculated dispersion relation from DFT from Ref. [42]. We have seen that while at Γ-point the frequency at $\nu = 3.8$ THz is overestimated, the frequency at $\nu = 5.8$ THz is slightly underestimated.

The potential does not perfectly reproduce the ab-inito phonon properties. Unfortunately, we have not found better force fields. Moreover, parametrizing our own potential is beyond the scope of the thesis. We expect, however, that the SW potential is still able to provide good trends for the phonon coherence of GaN/InN superlattices.

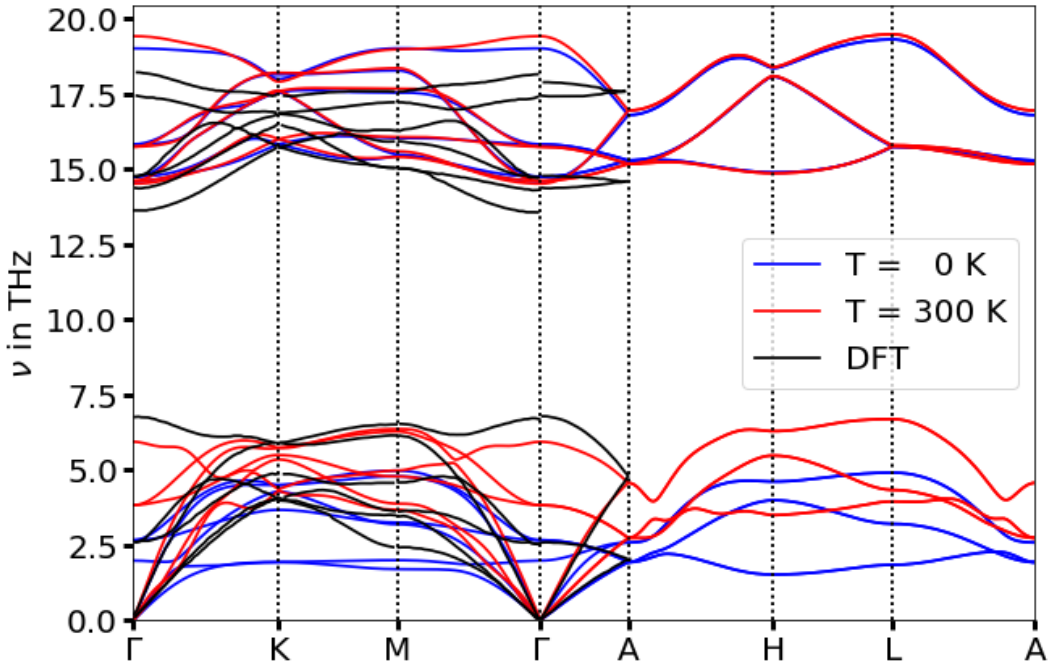

Figure 3.3.: Phonon dispersion relation from LD of wurtzite InN with the modified Stillinger-Weber potential. The band structure at $T = 300\,\mathrm{K}$ was calculated using the renormalized force constants resulting from a **DynaPhoPy** calculation, which uses an MD trajectory to include anharmonic effects. The anharmonic frequency shift is strong for the modes below the band gap. The phonon dispersion from DFT is taken from Ref. [42].

3.2. Lattice Dynamics

In this section it is shortly mentioned the software packages used for the lattice dynamics calculations. The force constants (equation 2.10) are calculated by using a finite difference scheme. A supercell of the crystal structure to investigate is created. Using the **Python** software **phonoLAMMPS** [44], the forces due to a small displacement of an atom are calculated and the force constant matrix is created. The supercell needs to be large enough so that an atom far away of the displaced atom does not feel a force. The lattice dynamics calculations are done with the open source package **phonopy** [45]. Anharmonic phonon properties at finite temperature are calculated with

the software package **DynaPhoPy** [43]. **DynaPhoPy** is used to calculate dispersion relations at finite temperature, phonon lifetimes, mean free paths and thermal conductivity.

3.3. Molecular Dynamics

Molecular dynamics simulations are performed with the open source MD-code **LAMMPS** (Large-scale Atomic/Molecular Massively Parallel Simulator) [46, 47]. The code is optimized to calculate the forces between particles in parallel, allowing long simulation times and large simulation cells.

For initializing a molecular dynamics simulation, the initial coordinates of the atoms in a supercell are submitted to **LAMMPS**. The supercell is created by integer replications of the crystal unit cell along its primitive lattice vectors. The MD-simulations are run at finite temperature T. The temperature in **LAMMPS** is calculated from the average kinetic energy of the N atoms in the system according to Eq. (3.2), where d is the dimension of the system, k_B is the Boltzmann constant, and $m_i|\boldsymbol{v}_i|^2$ is the kinetic energy of a particle i.

$$\frac{d}{2}k_bT = \frac{N}{2}\sum_{i=1}^{N} m_i|\boldsymbol{v}_i|^2 \tag{3.2}$$

For initialization, the velocities of the particles in each dimension are set according to a Gaussian distribution with a mean value at zero, and a width such that the total kinetic energies of the particles corresponds to the desired temperature. The velocities of the system can be set in a way that the total momentum and angular momentum of the system is zero, to avoid translation or rotation of the whole system.

Periodic boundaries are applied to the system. In each direction, there is a periodic replication of the simulation box. The particles interact with their periodic images across the boundaries of the box. Moreover, the particles can cross the boundary of the box and reenter at the other side. In section 2.1, it was mentioned that a one-dimensional system with periodic boundaries has only certain allowed discrete wave-vectors for the vibrational modes, which depend on the number of unit-cells in each direction. In general, the

total number of modes in a system is dN, with N the number of atoms and d the dimension of the system.

After the simulation box is set up, the integration of the Newton's equations of motion is performed, and the dynamics of the system is simulated. The standard integrator in LAMMPS is a velocity-Verlet integrator, which is also used for this work. An explanation of the velocity-Verlet algorithm can be found in [48]. The time step of integration needs to be chosen sufficiently small such that the particles do not move to far in one time step, and that the total energy of the system is conserved.

The velocity fields for calculating the coherence length have to be sampled at equilibrium; therefore, we choose a micro-canonical ensemble, at a finite temperature T. In the micro-canonical ensemble the particles number N, the volume of the system, and the total energy E are kept constant. Such a type of simulation will be called in the following as NVE-simulation. Before an NVE-simulation, therefore, one needs the equilibrium volume (V) of a given system at a desired temperature. The equilibrium volume is calculated out of an NPT-simulation, i.e. from running an MD-simulation at a desired temperature (T) and pressure (P). In practice, in an NPT-simulation, the particles equations of motions are altered so that the system is driven towards the desired temperature and pressure.

In our simulations, one of the thermostats used is the Langevin. The system temperature is controlled by random collisions of the system particles with a background solvent. The virtual background solvent acts as a heat bath, which is at the desired temperature. The random collisions and a a frictional drag, which is proportional to the particles velocity, drives the system towards the desired temperature. A description of the thermostat can be found in [49].
Nose-Hoover style thermostats and barostats, also used in this thesis, use non-Hamiltonian equations of motions [50]. The thermostatting and barostatting is done by coupling the velocities and the domain extensions to dynamical variables. The equations of motions are designed in a way, that the velocities and positions are sampled from a canonical (NVT) or isothermal-isobaric (NPT) ensemble [47]. The Langevin is used sometimes for the NVT-equilibration, which is done before an NPT simulation. In the NPT

simulations a Nose-Hoover is used. For the NVT-equilibrations before an NVE run, the Nose-Hoover thermostat is used.

To extract the equilibrium volume of a system of interest at given finite temperature, first a supercell is created. A supercell is an integer replication of a crystal unit cell in all directions. An energy minimization at zero Kelvin, using **LAMMPS**, is performed. In the next step, velocities are assigned to the atoms according to the desired temperature. A thermostat is then applied to the system, and the system is equilibrated in a short NVT-run. The barostat is switched on, allowing the supercell to adjust its volume, and the lattice constants of the simulation cell are recorded in regular time intervals during the NPT-run. As the simulation box is allowed to extend and contract, the system will reach the equilibrium volume after some time, but the volume will still fluctuate around its equilibrium. By doing a time average over the recorded lattice constants, once equilibrium is reached, the equilibrium volume is calculated.

For the NVE-run, the super-cell volume is updated to the value calculated during the NPT-run, and velocities are assigned according to the desired temperature. The random assignment of the velocities according to a Gaussian distribution does not represent the equilibrium state of the system.Therefore, the system needs to be equilibrated in an NVT-run at the desired temperature. The NVT-run should be sufficiently long, such that the system reaches an equilibrium and one gets a collection of equilibrium configurations, belonging to the configurational space of the system at a given temperature. After the equilibration, the thermostat is switched off, and the system is simulated in the NVE-ensemble to sample the equilibrium velocity field. As the thermostat in the NVT-run changes the Newton's equations of motions, this change of the equations of motions might lead to a deviation from the real equilibrium of the system. Therefore it is good practice to let the system equilibrate for some time in the NVE-ensemble, and not to start sampling the velocity field at the beginning of the NVE-run. The velocities of all the atoms in the supercell are sampled at a constant time interval. The size of the needed sampling time interval Δt depends on the vibrational spectrum of the system. The maximum frequency ν_{max} from a discrete Fourier transform of discrete data depends on the time step of Δt (Eq. 3.3). For systems with high phonon frequencies, the velocities need to

be sampled at shorter time intervals.

$$\nu_{max} = \frac{1}{2\Delta t}; \qquad \omega_{max} = \frac{\pi}{\Delta t} \tag{3.3}$$

These velocities, which are the main ingredient for our coherence length calculations, are saved for a few thousand or ten-thousand of atoms, and for many time steps. As the saved files become very large for long simulations, the sampling step Δt is kept as small as possible. This save the computational effort in the post-processing step. Nonetheless, the sampling step needs to be chosen such that ν_{max} is larger than all the relevant vibrational frequencies in the system.

3.4. Post-processing of the velocity field and calculation of the cross spectral density function

During the NVE-Simulations, the velocity of each atom is saved every certain time step (i.e. every sampling time step Δt). To post-process the velocities and to calculate the coherence lengths, a **Python** code was written. The code can be found in the Appendix B.1. For calculating the cross spectral density function (Eq. 2.39), we need to correlate the atoms of one unit cell with the corresponding atoms of the unit cell a distance R away in the correlation direction $\hat{\boldsymbol{R}}$. To achieve this, one needs to identify which atom sits at which position. Every particle in a **LAMMPS** simulation has a unique integer number as an identifier, which allows to unambiguously identify the particle throughout the whole simulation. Additionally, each unit cell in the simulations super-cell is labeled and assigned an integer number as identifier. Then, it is identified which atom belongs to which unit cell.

In the next step, the unit cells which need to be correlated are identified. Only cells along the correlation direction $\hat{\boldsymbol{R}}$ are correlated. To explain this better, let's consider the superlattice in Figure 3.4, with four atoms in the (pure materials) unit cell. The supercell is extended 4 unit cells in the vertical

direction. Only cells along the correlation direction $\hat{R}$ are correlated with each other. For example, the unit cells within the yellow frame, for different distances between the cells. Likewise, the frame is moved up and down to correlate the other cells along the correlation direction. The correlations for same distances of different frames are summed up to achieve better statistics. (This is equivalent to correlating the atoms of planes (perpendicular to the correlation direction) of unit-cells to the corresponding atoms of planes at a certain distance).

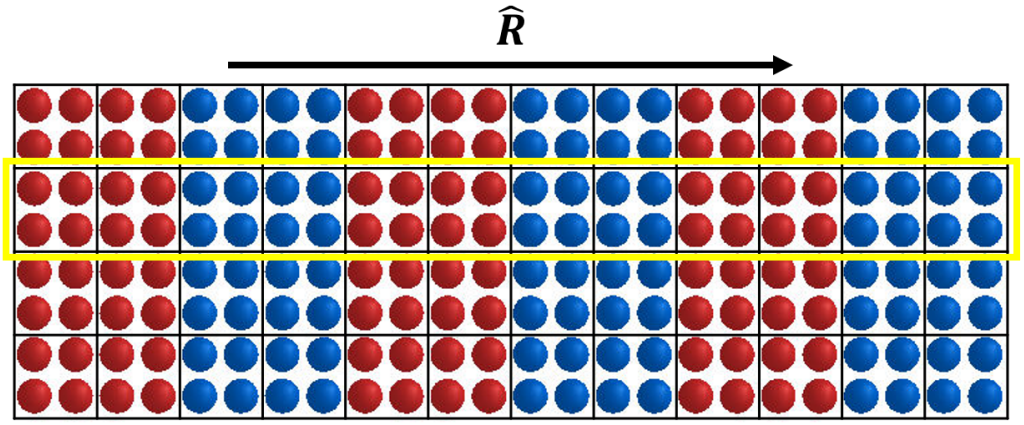

Figure 3.4.: Only cells along the correlation direction $\hat{R}$ are correlated.

Periodic boundary conditions are applied to the supercell. In Figure 3.5, the (one-dimensional) simulation box with unit cells A-G, has periodic images on both sides. The simulation box in this example has a length of 7. The maximum distance between two unit cells along the correlation direction, is half the simulation box size. For example, the unit cell E is a distance of 4 away from A, but the periodic image E* is a distance 3 away from A, resulting closer than E. Thus, only distances up to one half of the simulation box size are considered when calculating the cross spectral density function.

The Fast-Fourier-Transforms of the velocities are calculated with the `numpy.fft` package. The maximum frequency is, as stated in equation (3.3), $\nu_{max} = \frac{1}{2\Delta t}$. The resolution, ν_R, in frequency of the Fourier-transformed

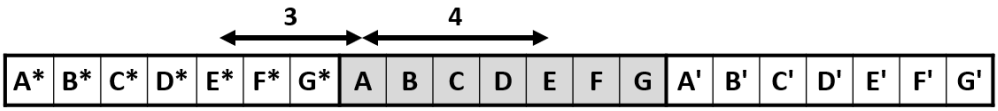

Figure 3.5.: The periodic image E* is closer to A than E, because of periodic boundary conditions. The maximum distance considered for calculating the cross spectral density function is half the simulation box size.

signal depends on the length, N_t, of the input signal for the discrete Fourier transform.

$$\nu_R = \frac{1}{N_t \Delta t} \tag{3.4}$$

N_t is the number of discrete time points at which the velocity was sampled. The longer the time series, the higher the resolution in frequency is, and the statistics of the correlations gets better. As the velocities in time are a real signal, the positive frequencies already contain all the information in the frequency domain.

Following the example in Figure 3.5, the cross spectral density function (Eq. 2.38) is calculated for each distance R like follows. For distance $R = 0$ each unit cell is correlated with itself, and the auto-correlations are summed up. $T(R = 0)$ corresponds to the DOS. For distance $R = 1$, unit cell A is correlated with B, B with C, ... and G with the periodic image A', and all the correlations are summed up for $T(R = 1)$. For distance $R = 2$: A-C,B-D,C-E, ..., G-B'. This is repeated for every possible distance until the maximum distance, which is 3 in this example: A-D,B-E,...,G-C'. After the cross spectral density function is calculated, the coherence length for every frequency can be calculated by fitting an attenuated wave (Eq. 2.40) to the cross spectral density function.

4. Results

After having presented the microscopical picture of the phonon coherence length, and the details about the molecular dynamics simulation, the results are presented in this chapter. First, the coherence length of superlattices of a one-dimensional chain of atoms is presented. Then, a FCC crystal interacting with a Lennard-Jones potential is discussed. These two systems are simulated to test the post-processing code, and to better understand the microscopical picture. The post-processing code can be found in the Appendix B.1. The coherence length is extracted by fitting the cross spectral density function (Eq. 2.37) to an attenuated wave (Eq. 2.40). As the fitting procedure is not always successful, another approach for extracting the coherence length from the cross spectral density function is adopted, which is based on the idea of treating the spectral density function as a probability density function.
After the test systems, GaN/InN superlattices are discussed. These systems are realistic and of interest because GaN/InN structures show piezoelectric effects, which could be harnessed for generating coherent phonons. This would allow to use GaN/InN superlattices as a source of coherent phonons. The phonon density of states and phonon coherence length of GaN/InN superlattices of various superlattice periods are presented. Two different supercells have been used for this superlattices: $3 \times 2 \times N$ and $1 \times 1 \times N$. The latter supercells allow for a better resolution of the acoustic phonons.
Structures of a monolayer of InN in a GaN matrix are simulated and discussed. The creation of superlattices of GaN/InN is experimentally limited due to the large lattice mismatch among the systems, which leads to the introduction of dislocations. Monolayers of InN on a GaN matrix have, nonetheless, been created experimentally [15].

4.1. One-dimensional Lennard Jones superlattice

Part of the master thesis was to develop the code for post-processing the velocities obtained from a molecular dynamics simulation. This code allows to calculate the velocity correlation functions, the cross spectral density function, and from that the phonon coherence length. The methodology to estimate the phonon coherence was adapted from Ref. [11, 12]. For validation of the code the same one-dimensional system as in Ref. [12] is simulated. This helps to better understand the method, the microscopic picture of the phonon coherence, and the phonon coherence length. Moreover, it allows to compare the results from the written code to the results reported in Ref. [12].

The atoms in the one-dimensional system interact by means of a Lennard-Jones potential (3.1). The system consists of two materials M1 and M2. Each material contains two atoms in the unit cell (Figure 4.1). The four atoms differ in mass but interact via the same Lennard-Jones potential. In M1, atom A has the mass of Argon $m_{1,A} = m_{Ar} = 39.948\,\mathrm{u}$, while atom B has $m_{1,B} = 2M_{Ar}$, the corresponding atoms in M2 have masses $m_{2,A} = \frac{3}{2}m_{Ar}$ and $m_{2,B} = 3m_{Ar}$. The σ parameter of the Lennard-Jones potential is that of argon, $\sigma = \sigma_{Ar} = 3.405\,\text{Å}$, while the depth of the potential is 5 times deeper, $\epsilon = 5\epsilon_{Ar} = 1.19\,\mathrm{kcal/mol}$. The NPT simulation of this system results in an equilibrium distance between the atoms of 3.82 Å. Three different kind of superlattices were created, with a superlattice period of $d_{SL} = 1.53$, 6.11 and 24.5 nm. The superlattice with $d_{SL} = 1.53\,\mathrm{nm}$ corresponds to a stacking of M1-M2-M1-M2.

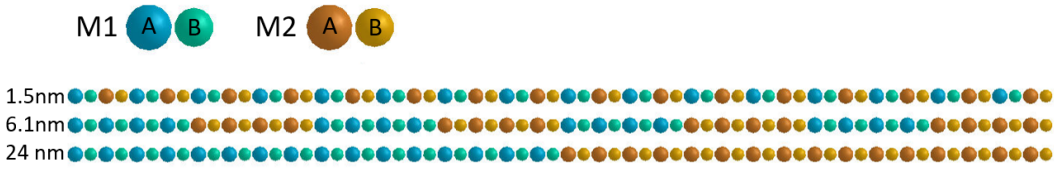

Figure 4.1.: One-dimensional superlattices made of two materials (M1 and M2) with each having two atoms (A,B) in the unit cell. Three different superlattices with periods of $d_{SL} = 1.53$, 6.11 and 24.5 nm were considered.

The number of atoms, N, in the simulation cell is 8000 as in Ref. [12], which corresponds to a cell length of 3056 nm. N is kept constant for the three superlattices, in order to keep the same number of modes in the system. The time step of the MD simulation is 1 fs. The system was first relaxed for 10^6 steps (= 1 ns) in the NVT ensemble at 10 K. The NVE ensemble is simulated for 6×10^6 steps (= 6 ns), and the velocities are sampled every 128 time-steps. A sampling step of 128 fs corresponds, according to Eq. (3.3), to a maximum frequency of $\nu_{max} = 3.9$ THz.

4.1.1. Lattice Dynamics

First the dispersion relation and the DOS from lattice dynamics for the two individual materials and the superlattice with the smallest period ($d_{SL} = 1.53$ nm) are compared (Figure 4.2). From lattice dynamics, one can already learn about the influence of the superlattice structure on the dispersion relation and the DOS. This will serve as well as a reference for molecular dynamics.
Material M1 and M2 have both a band gap of roughly 0.5 THz with material M1 having higher frequencies as M2 because of the lighter atoms. The superlattice has two more band gaps because of the Brillouin-zone folding. The combined DOS of M1 and M2 would leave only one gap below 1.5 THz with no states.

4.1.2. Density of states from Molecular Dynamics

From MD the density of states was calculated as described in chapter 2.4. For the superlattice with $d_{SL} = 1.53$ nm, the DOS is shown in Figure 4.3. Three band gaps appear in the DOS (0.7, 1.3 and 1.9 THz) as in the case of the lattice dynamics, although the DOS does not fall completely to 0. The DOS of the raw data is noisy. As it can be seen in the plot for the corresponding velocity auto-correlation function, Figure 4.4, the VACF decays to zero after a certain time. However, it will fluctuate around zero due to numerical noise, and because the time series to calculate the VACF are not infinitely long. In the lower part of figure, there is a cutout of the VACF for lower

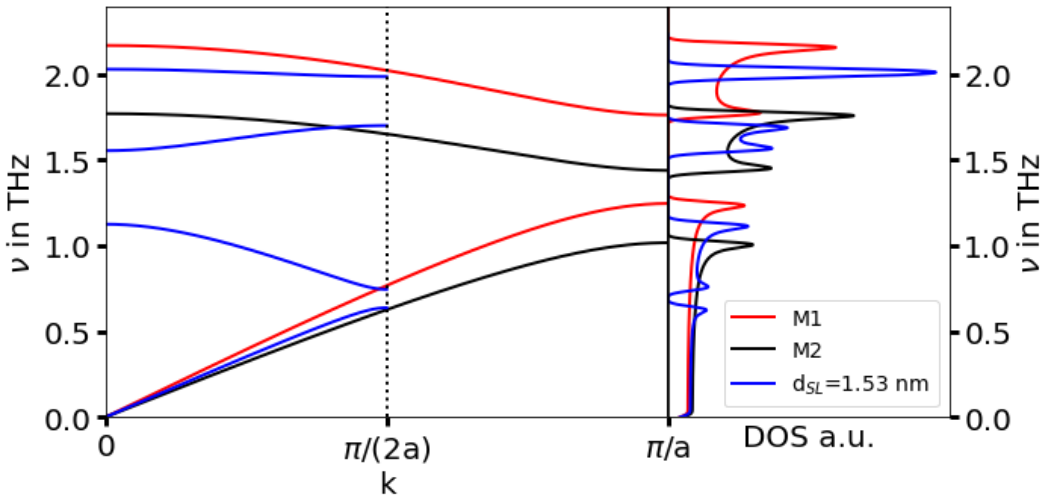

Figure 4.2.: Dispersion relation and DOS from LD of M1,M2 and superlattice with d_{SL} = 1.53 nm. a = 0.764 nm is the length of the unit cell of M1 and M2.

values. The orange curve displays the VACF, which is smoothed with a Gaussian function (Eq. 4.1). Calculating the DOS by Fourier transforming the smoothed VACF results in the smooth orange DOS shown in Figure 4.3. The plots of the DOS in this thesis always involve some degree of smoothing.

$$\mathrm{VACF}_{\mathrm{smooth}}(\tau) = \mathrm{VACF}(\tau) \times e^{-\left(\frac{\tau}{\sigma}\right)^2} \tag{4.1}$$

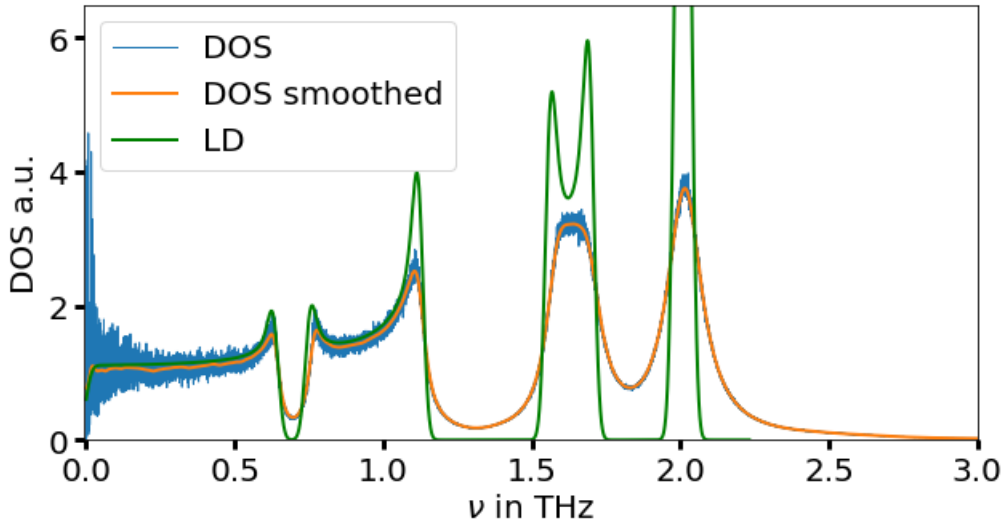

Figure 4.3.: Vibrational density of states from MD of the one-dimensional superlattice with $d_{SL} = 1.53\,\text{nm}$. The figure compares the DOS calculated from the raw data of the VACF to the DOS from the smoothed VACF. For comparison the DOS from LD is shown in green.

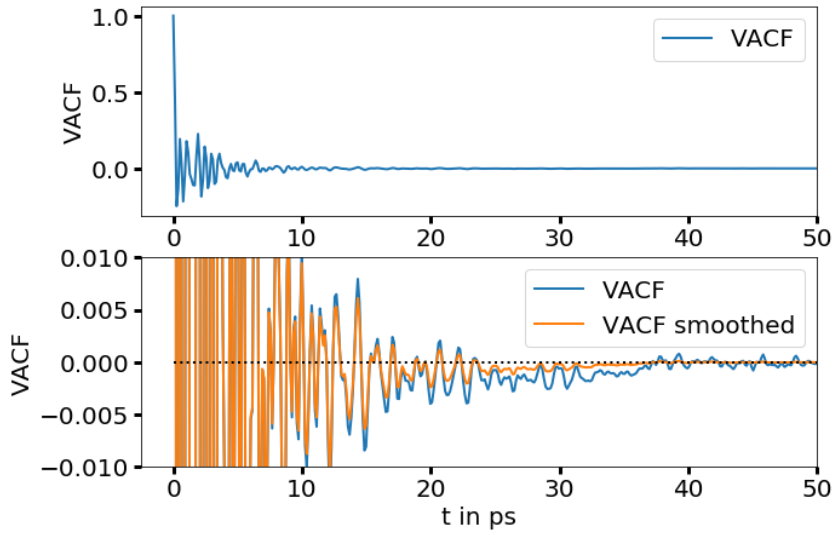

Figure 4.4.: The upper plot shows the velocity auto-correlation function of the 1-dimensional superlattice with $d_{SL} = 1.53\,\text{nm}$. The lower plot shows the smoothing of the VACF (equation 4.1) to bring it towards zero for long times τ.

4.1.3. Calculation of the coherence length

The coherence length for the superlattice with $d_{SL} = 1.53\,\text{nm}$ is calculated by fitting Eq. (2.40) to the calculated cross spectral density function $T(\nu, R)$ for different frequencies ν. As $T(\nu, R)$ is a complex quantity, the fit is done to the real part of $T(\nu, R)$. The parameters of the least squares fit for each frequency are the wavelength, λ, and the coherence length, l_c. The initial guess for the wavelength $\lambda(\nu)$, depending on the frequency, is done according to the linear dispersion relation ($\omega(k) = kv_g$) for the low frequency acoustic modes: $\lambda(\nu) = \frac{v_g}{2\nu}$. The group velocity, v_g, in this region is extracted from a lattice dynamics calculation. An example of the data used for the fitting and the resulting fitting, for one frequency ν of the spectrum, is shown in Figure 4.5. It can be seen that the data follows the attenuated wave closely.

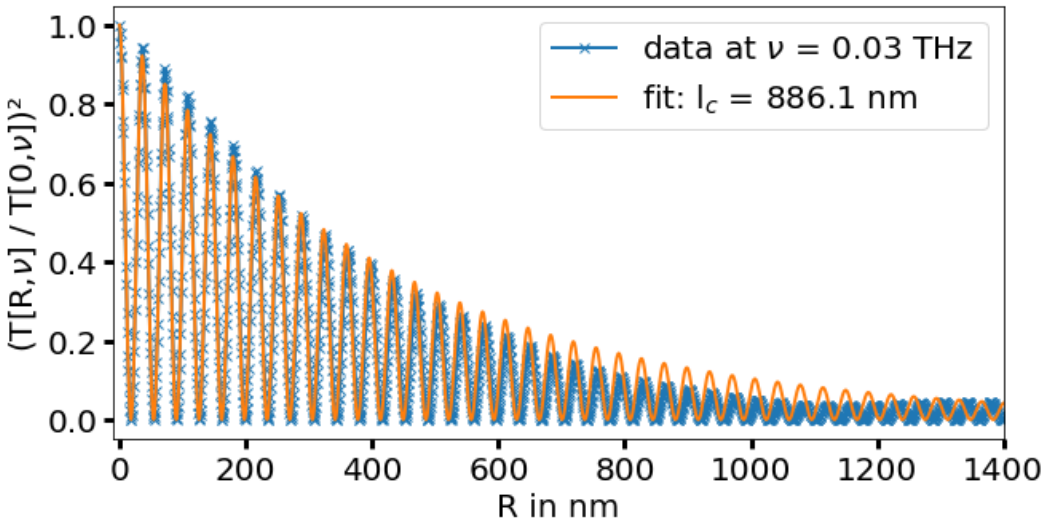

Figure 4.5.: Example for the fit to the cross spectral density function $T(\nu, R)$ to extract the coherence length for the 1-dimensional superlattice with $d_{SL} = 1.53\,\text{nm}$

Figure 4.6 shows the calculated coherence length for the phonons of the 1.53 nm-superlattice. A clear trend shows that lower frequencies have a higher coherence length. This is expected as the low frequency modes are acoustic modes with a long wavelength. A wave-packet consisting of modes with a large wavelength has a large spacial extension and will have a large

coherence length.
The coherence length is larger by a factor of roughly 2.5 compared to the values in Ref. [12]. This deviation stays the same for all coherence lengths calculated in for the one-dimensional test system. As the trend in coherence length is the same, a possible explanation of this deviation is a constant in the definition of the coherence length.

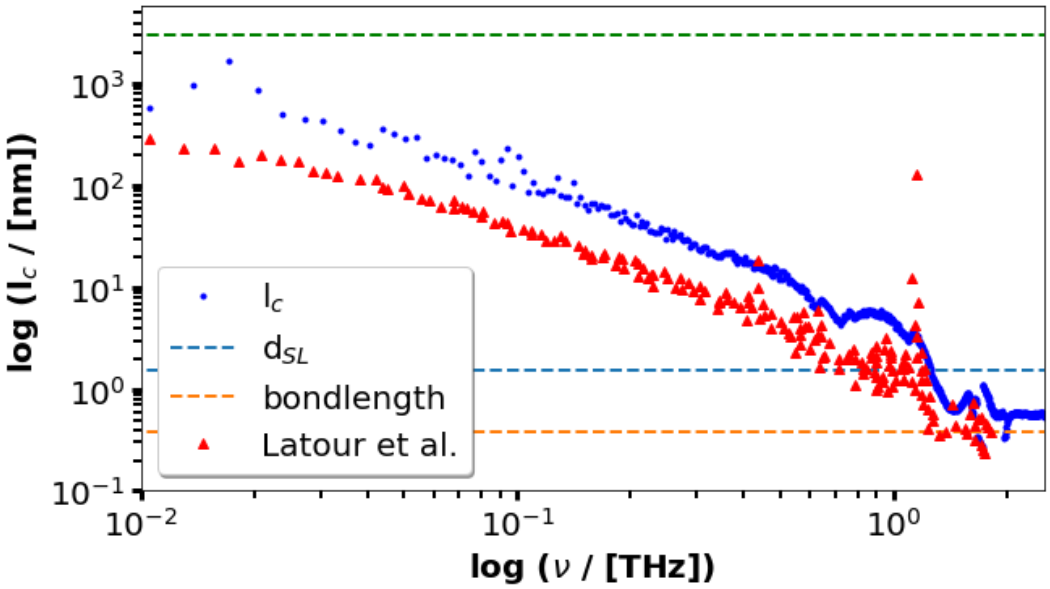

Figure 4.6.: Double logarithmic plot of the coherence lengths l_c for the one 1-D SL with SL-period $d_{SL} = 1.53\,\text{nm}$ as a function of frequency ν. The data in red is from Ref. [12].

The fitting procedure to the spatial cross correlation function is not always as reliable as in the case shown in Figure 4.5. In Figure 4.7 the data for three different frequencies for the $d_{SL} = 1.53\,\text{nm}$ superlattice is shown. To extract the coherence length, a fit is done to the squared real part of the spatial cross spectral density function. The higher the frequency, the less reliable this fit works in this case.

The fit usually works well for low frequencies (4.6 a). The frequency of 0.3 THz lies in the acoustic region. These low frequencies correspond to acoustic modes with long wavelengths. This means that the oscillations in R are slow and usually these modes have a high coherence length. In this

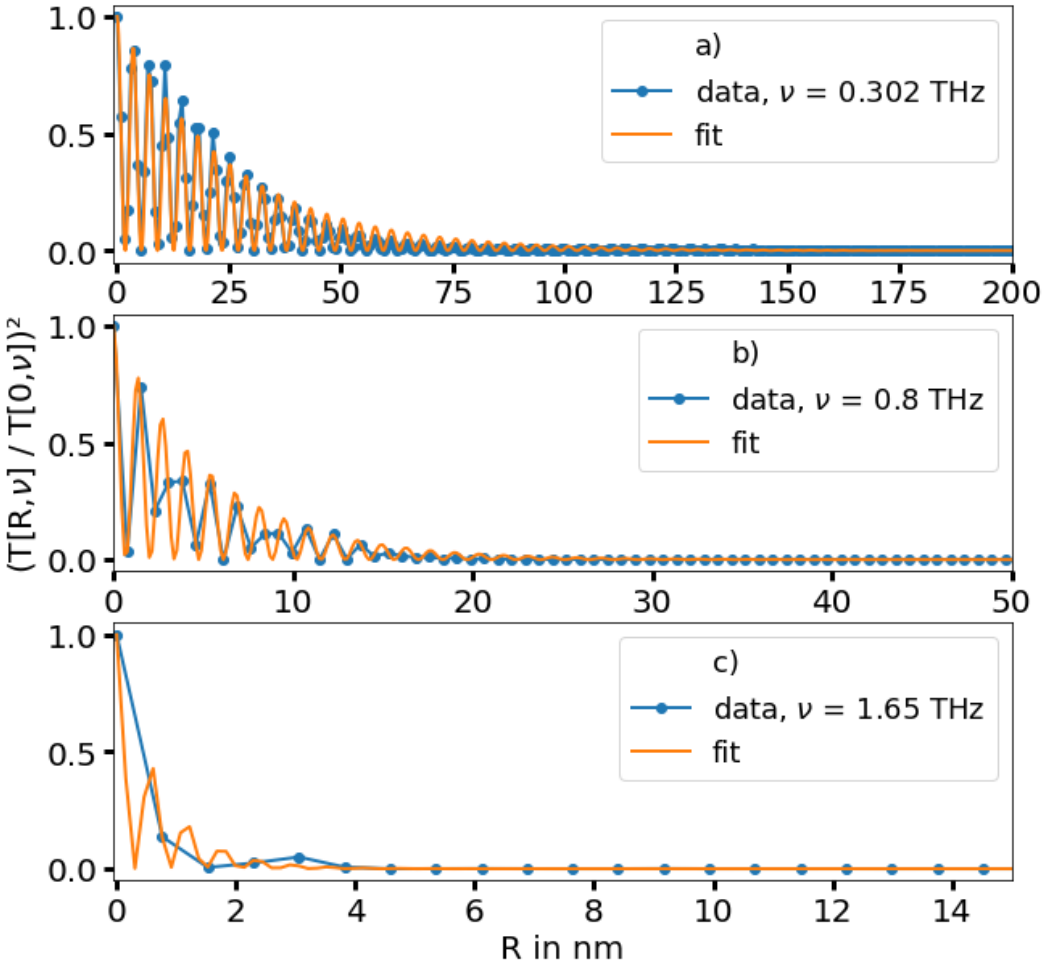

Figure 4.7.: Real part of the spatial cross spectral density function $T(R, \nu)$ over distance R for three different frequencies of the 1-D superlattice with a superlattice period of 1.53 nm. The fit to the square of equation (2.40) works well for the low frequencies like 0.3 THz. For higher frequencies the attenuated wave decays fast, and the resolution in R is not high enough to represent the oscillating part. The frequencies are not in a gap of the DOS (see Figure 4.3). Note the different scale of the abscissa in the three plots.

case the function does not decay to zero rapidly. Indeed the data decays to 0 after approximately 75 nm (The whole range of the distance R, which would go up to 1528 nm, corresponding to half the size of the simulation

cell, is not shown.). Often the function stays at zero, after it decays, but this is not always the case. This might be due to numerical noise or not enough statistics. For the lowest acoustic frequencies, the cross spectral density function does not decay to zero for the whole range of distances R. This modes have a very long wavelength, and have a coherence length larger than the simulated supercell.
For the upper frequencies of the acoustic region and optical modes, the fit does not work very well. (In the case of the $d_{SL} = 1.53\,\text{nm}$ superlattice, the fit works reasonably well up to 0.5 THz. This depends on the system and has to be checked for each simulated system separately). The data to fit is a discrete function of the distance R. The resolution in distance is given by the lattice constant of the (pure material) unit cell in the system, which for the given system is $\Delta R = 7.6\,\text{Å}$. If the wavelength λ is small, according to equation (2.40), the oscillations have a high frequency in distance R . At some point, the resolution in R is not high enough to resolve the oscillations, as seen in Figure 4.7b). This makes it difficult to fit the data. Additionally, the coherence length for high frequency and optical modes is usually low. This leads to a rapid decay of the attenuated wave (Figure 4.7c). Although the fitting procedure does not reproduce well the attenuated wave for high frequencies, the value for the exponential decay is still assumed to be a good estimator for the coherence length.

4.1.4. Results of the coherence lengths

As already mentioned, the coherence length is generally higher for modes with lower frequencies and higher wavelengths. It is also interesting to have a closer look at the band gaps of the DOS, and the coherence length in this region. At the edges of the band-gaps, peaks in the coherence length appear as can be seen in Figure 4.8, which is a cutout of Figure 4.6. Latour and coworkers [12] have found more prominent peaks at this positions and they associated these peaks to standing modes with large spatial extension. The gaps in the dispersion relation appear where the branches meet the Brillouin-zone boundary or the center of the Brillouin zone. The branches flatten out at these points, and the group velocity of the modes drops to zero. Thus, these modes correspond to standing modes with a large spatial

extension. The plot of the DOS, below the coherence length, shows that the peaks in the coherence length coincide with the peaks in the DOS next to the band gaps.

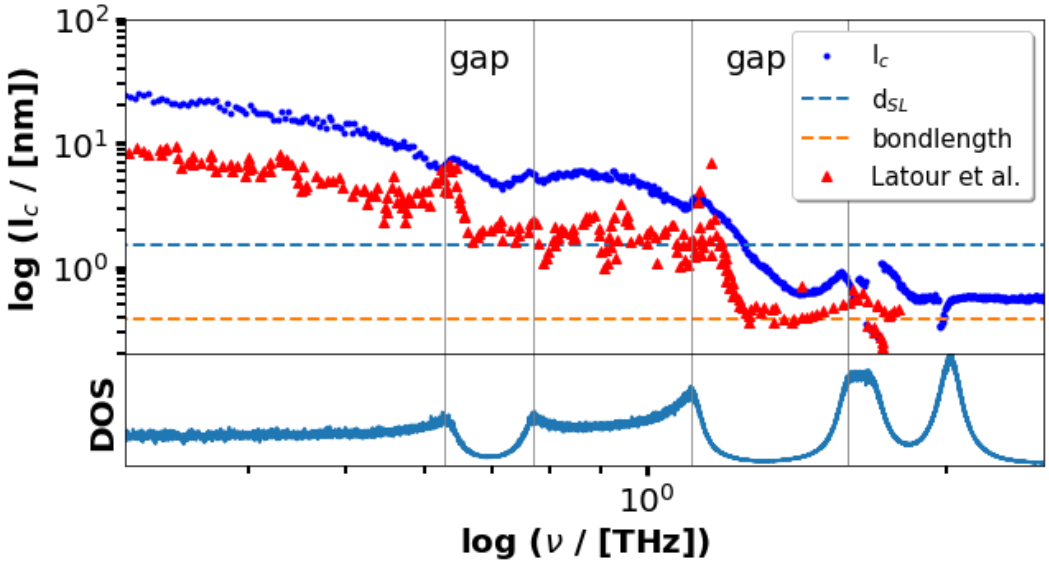

Figure 4.8.: Cutout of the plot for the coherence length in Figure 4.6. At the edges of the band gaps, peaks in the coherence length appear. These high coherence lengths correspond to standing modes with a large spatial extension. The reference data (red triangles) is from Ref. [12].

One would assume to have zero coherence length in between the band gaps, as there are no allowed modes at these frequencies. As there is still a signal in the cross spectral density function, the coherence length is not zero. The density of states is low in the regions of the band gaps, but it is not zero. A reason for this is that due to finite temperatures, the frequencies are not sharp but broadened. The non zero coherence length in the gaps suggests that still modes of the individual materials exist in the layers of the individual materials. Looking at the dispersion relations from lattice dynamics of the pure materials (Figure 4.2), one sees that at least one of the pure materials has modes at frequencies of 0.7 THz and 1.9 THz, where the superlattice has a band gap. Only at 1.3 THz neither of the pure materials has allowed modes. For the frequencies in the band-gap of the superlattice, one

would need to calculate the coherence lengths for the individual materials for the frequencies in the gaps [12].

For this one-dimensional system, the coherence lengths for the three different superlattice periods are similar, and they seem to not depend on the period, as can be seen in Figure 4.9. At least in the region where the coherence length is not determined by the band gaps of the band structure, the coherence lengths are similar. Above 0.1 THz the coherence lengths of the superlattice with $d_{SL} = 6.11$ nm is lower than the coherence length of the other two superlattices. In this region, the dispersion relations show many gaps due to Brillouin-zone folding, which makes it difficult to compare the coherence lengths directly. Latour et al. [12] also found the coherence length independent from the superlattice period.

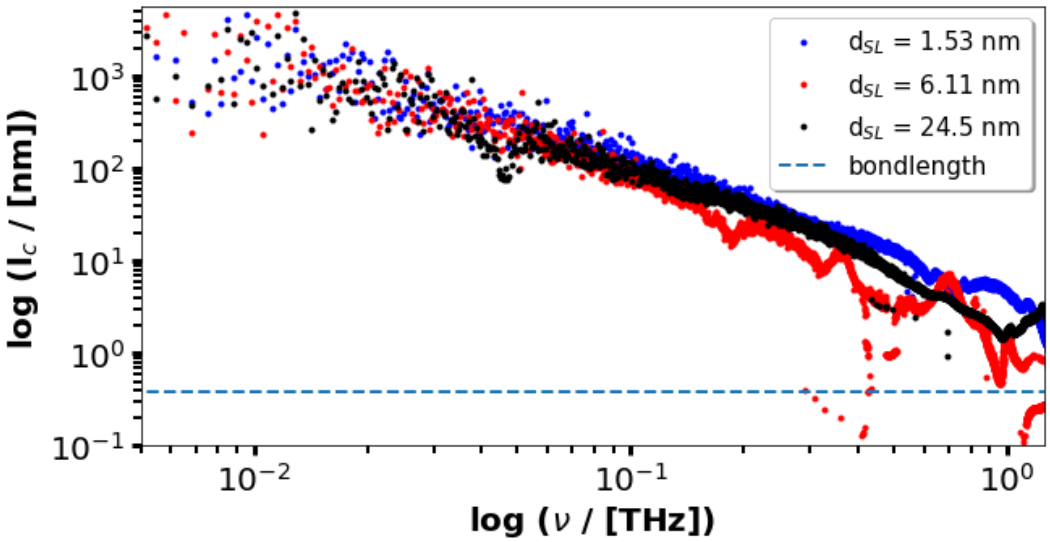

Figure 4.9.: Comparison of the coherence length for the one-dimensional LJ-superlattices with different superlattice periods d_{SL}. The coherence length of phonons of the same frequency does not depend on the superlattice period.

If the coherence length is independent of the superlattice period, it does not mean that a phonon mode of frequency ν with the same coherence length in all systems will show a ballistic transport behavior in all three systems. If the coherence length is larger than the superlattice period, the transport is considered to be ballistic/coherent. If the coherence length is

smaller than the superlattice period, the phonons will scatter diffusively at the interface, leading to an incoherent transport. (The coherence of the phonons can also be limited by phonon scattering of the bulk constituents). In Figure 4.10, the coherence length divided by the superlattice period is plotted to indicate which modes are coherent and which are incoherent. For the superlattice with the smallest period, the frequency range of coherent phonons encompasses most of the spectrum.
As the values of the coherence length in this work are larger by a factor of roughly 2.5 compared to the values reported in Ref. [12], a larger range of modes is considered to be coherent than in the reference. The trend in the coherence length is similar as in the reference; still the high deviation in the quantitative values of the coherence length can not be explained. In Ref. [12], an average over 20 independent simulations of the same system was used to calculate the cross spectral density function, while in this work only one simulation was used. For sure, the statistics is not as good as in the reference, leading to a larger error in the estimated coherence length, but it is not believed that this is the reason for the systematic offset.

In summary, the coherence length for the 1-D Lennard-Jones superlattices were calculated by fitting an attenuated wave to the cross spectral density function. The fitting works reasonably well for acoustic modes with long wavelengths and is not as reliable for modes with higher frequencies. The acoustic modes with lower frequencies show higher coherence lengths (Fig. 4.6). The coherence length was found to be largely independent of the superlattice period (Fig. 4.9). To define weather the phonons are coherent or not, the coherence length is compared to the superlattice period.

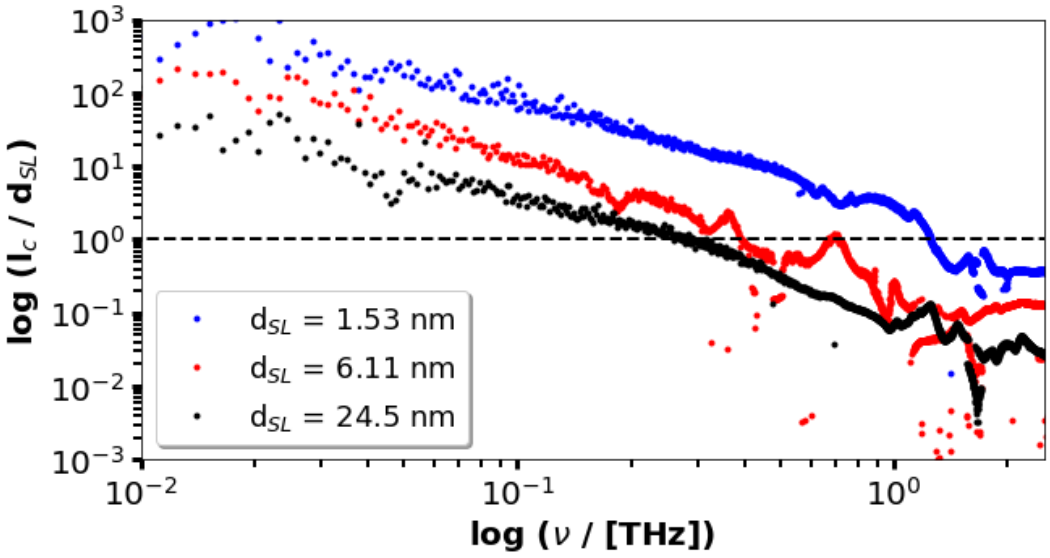

Figure 4.10.: Coherence length divided by the superlattice period d_{SL} for the one-dimensional LJ-superlattices. If the ratio $\frac{l_c}{d_{SL}}$ is larger than one (marked by the dashed line), the phonons are considered to be coherent. If the ratio is lower than one, the phonon scatter diffusively at the interfaces, and their transport is considered to be incoherent.

4.2. Three-dimensional Lennard Jones superlattice

After having studied the phonon coherence of the one-dimensional Lennard-Jones superlattices, a three-dimensional systems is investigated. As another test system, superlattices consisting of crystalline Argon, at a temperature of 40 K, are simulated. The superlattices are made of two different materials with a face centered cubic (FCC) crystal structure. The atoms interact by means of a LJ-potential (Eq. 3.1). All the atoms have the mass of Argon $m_{Ar} = 39.948\,\mathrm{u}$. The first material M1 interacts with a Lennard Jones potential with a depth twice that of Argon ($\epsilon_{M1} = 2\epsilon_{Ar} = 0.476\,\mathrm{kcal/mol}$). The potential depth of the second material is 2.5 times deeper than the depth of the first material. Atoms of the two different materials at the interfaces interact with an average potential depth. The other parameter of

the potential, defining the distance between the particles, is $\sigma = 3.405\,\text{Å}$. This system is suitable because there is no lattice mismatch at the interfaces, which could hinder phonon coherence. This system was studied in Ref. [11], but with smaller supercell-sizes. The system is simulated at a temperature of 40 K. The time step of the simulation is set to $\Delta t = 1\,\text{fs}$. For all systems, the equilibrium volume is calculated with an NPT simulation. The system is equilibrated in an NVT run for 5×10^5 steps (= 0.5 ns), and simulated in the NVE ensemble for 10^6 steps (= 1 ns). The velocities were sampled in the NVE ensemble every 80 steps, which, according to Eq. (3.3), leads to a maximum frequency of $\nu_{max} = 6.25\,\text{THz}$.

Superlattices with a period of $d_{SL} = 1, 2, 4, 8, 16\,\text{nm}$ are created. For clarification, the superlattice with 1 nm corresponds to a stacking of M1-M2-M1-M2 in z direction. The coherence length was calculated along the superlattice period. Therefore, the supercells have a structure of $3 \times 3 \times N$ repeat units, with the system periodic in z direction. N is chosen such that the number of atoms in the super-cell is 72000 or close to it. The dimensions of the simulated supercells are roughly $1.6 \times 1.6 \times 1050\,\text{nm}$.

4.2.1. Lattice Dynamics

Lattice dynamics calculations of the superlattices show the appearance of band gaps due to Brillouin-zone folding. In Figure 4.11, the dispersion relation in the superlattice direction is plotted (as a reduced zone scheme) for some of the superlattices and the pure materials of which the superlattices consist. The highest allowed wave-vector for the pure materials is $k_{max} = \pi/a$, where a is the lattice constant (of the cubic FCC unit cell). If one considers the superlattice unit cell as the new unit cell of the system, the lattice constant a gets larger with superlattice period and, thus, the maximum wave-vector becomes smaller. The branch of the 1 nm superlattice goes to the middle of the figure, where it gets folded back and a gap appears. The lattice parameter of the 2 nm superlattice is twice as large, and the allowed wave-vector is half the size. The first branch of this superlattice gets folded back at around 0.6 THz. The higher the superlattice period, the more often the branch gets folded back, leading to more band gaps, which are as well narrower. The dispersion relations of the superlattices are calculated

by viewing the superlattice as a new larger unit cell. As the unit cells have more atoms, more branches appear in the dispersion relation.

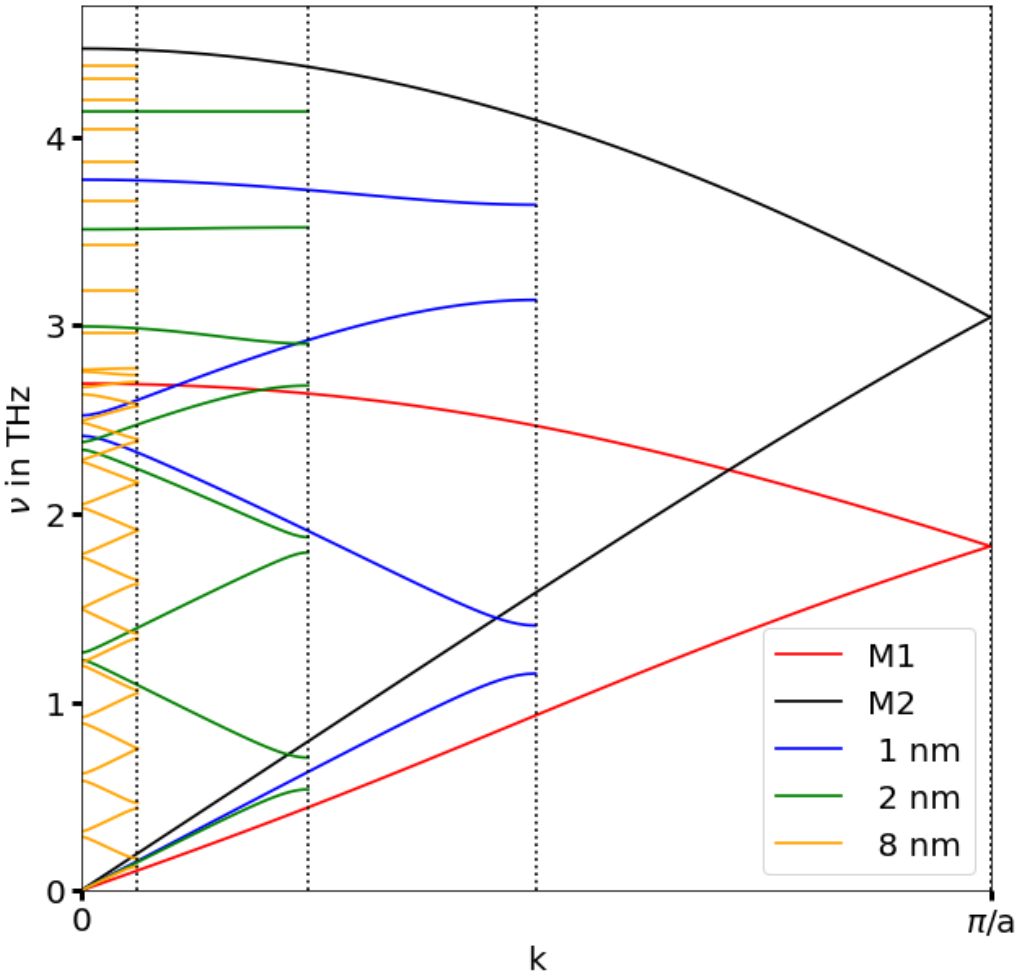

Figure 4.11.: Phonon dispersion relation in the superlattice direction for the three-dimensional Lennard Jones superlattices using LD. Only the longitudinal branches are shown.

In Figure 4.12 the full dispersion relation for the superlattice unit cell of the superlattice with period $d_{SL} = 1\,\text{nm}$. For completeness, the superlattice unit-cell and the Brillouin-zone are shown in the Appendix A.5. The superlattice direction is along Γ to Z. In Figure 4.11 the dispersion relation in the

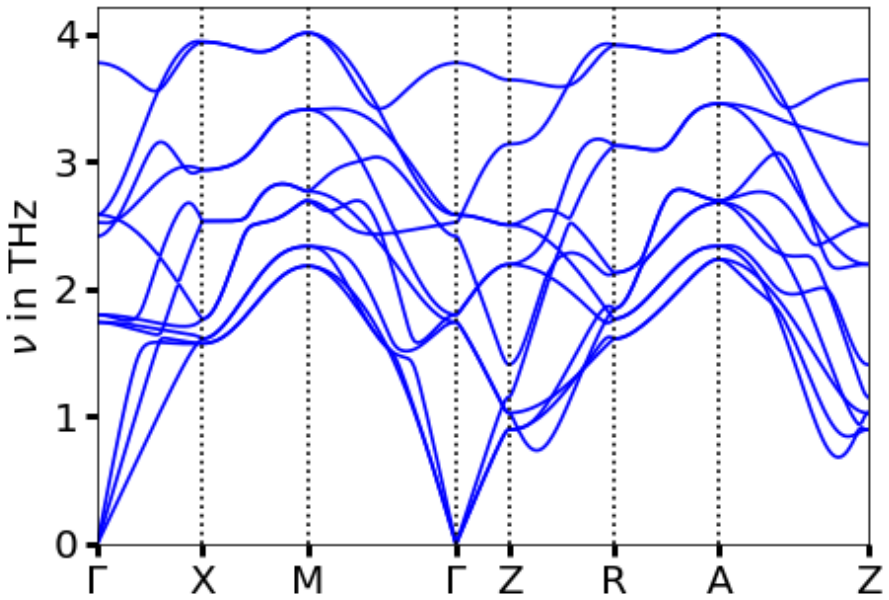

Figure 4.12.: Phonon dispersion relation of the superlattice with $d_{SL} = 1\,\text{nm}$. The superlattice unit-cell and the Brillouin-zone are shown in the Appendix A.5.

superlattice direction is plotted, only for the longitudinal modes.

4.2.2. DOS with Molecular Dynamics

The DOS of the superlattices is calculated from the velocities obtained during the molecular dynamics simulations. Comparing the DOS of superlattices with different superlattice periods already gives an insight into phonon coherence in these systems. The DOS is also useful to interpret the results for the coherence lengths.
In contrast to the one-dimensional system discussed before, the velocity of one atom has three components in all three dimensions of the system, and there are longitudinal and transverse vibrational modes in the system. The total density of states in the three-dimensional system is the sum of the DOS in all three dimensions. The density of states of velocities in z-direction is calculated by calculating the velocity auto-correlation function of the z-velocity component. In Figure 4.13 the DOS in z-direction from the MD simulations is shown for all the superlattices. The DOS of the superlattices with a period of 1 nm, 2 nm and 4 nm are clearly different from each other (Figure 4.13). For higher superlattice period (8 nm and above), the DOS does not depend on the superlattice period anymore. Their DOS resembles the combined density of states of the pure materials M1 and M2. The change in the DOS is a sign of the wave like nature of the phonons. The results in Figure 4.13 suggest that wave interference occurs, and that phonons are coherent in systems with a superlattice period of 4 nm and below.

The gaps due to the folding of the branches of the dispersion relation are clearly seen in the low frequency part of the DOS (Figure 4.14). For example a gap appears for the 2 nm-superlattice at 0.6 THz, which is also predicted by the lattice dynamics calculation. The gaps of the superlattices with higher period can also be seen. The folding does occur as well in the region with higher frequencies, but as there is not a single (acoustic) branch, and the DOS is smeared out over several branches, the appearing gaps due to the Brillouin zone folding are not clearly visible in Figure 4.13.

The appearance of gaps in the DOS along the z-direction does not guarantee that there will be a gap in the total density of states. The transverse acoustic phonons have different group velocities to that of the longitudinal modes, and gaps can appear at different frequencies. In Figure 4.15, the gaps of the transverse and the longitudinal modes appear at different frequencies,

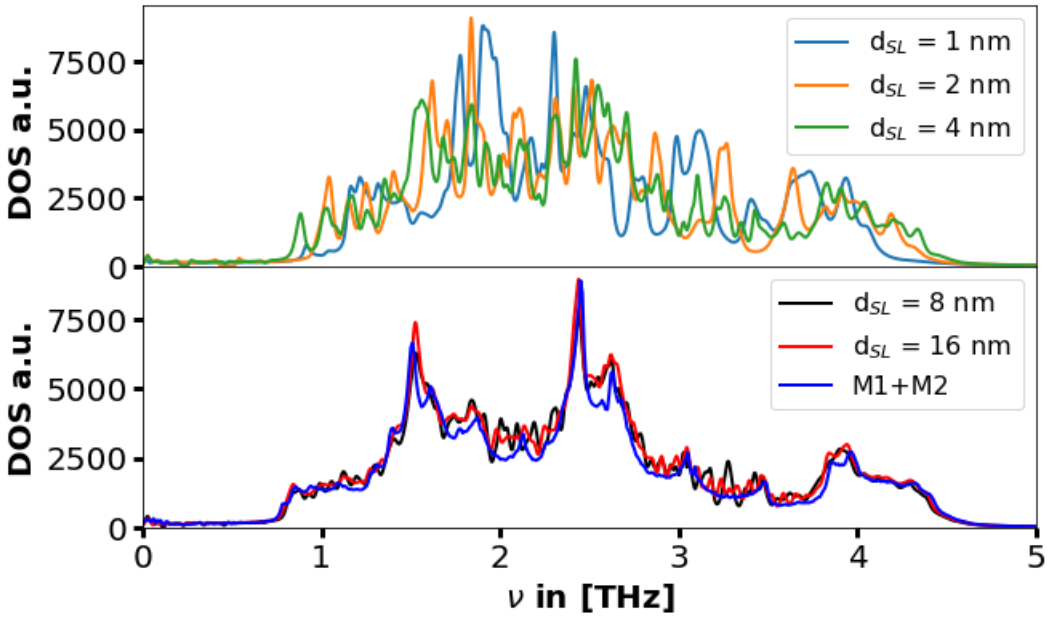

Figure 4.13.: Vibrational density of states (DOS) in z-direction of the LJ superlattices for different superlattice periods. In the lower plot, the combined DOS of the pure materials M1 and M2 is plotted.

leading to a non zero DOS for the whole frequency range.

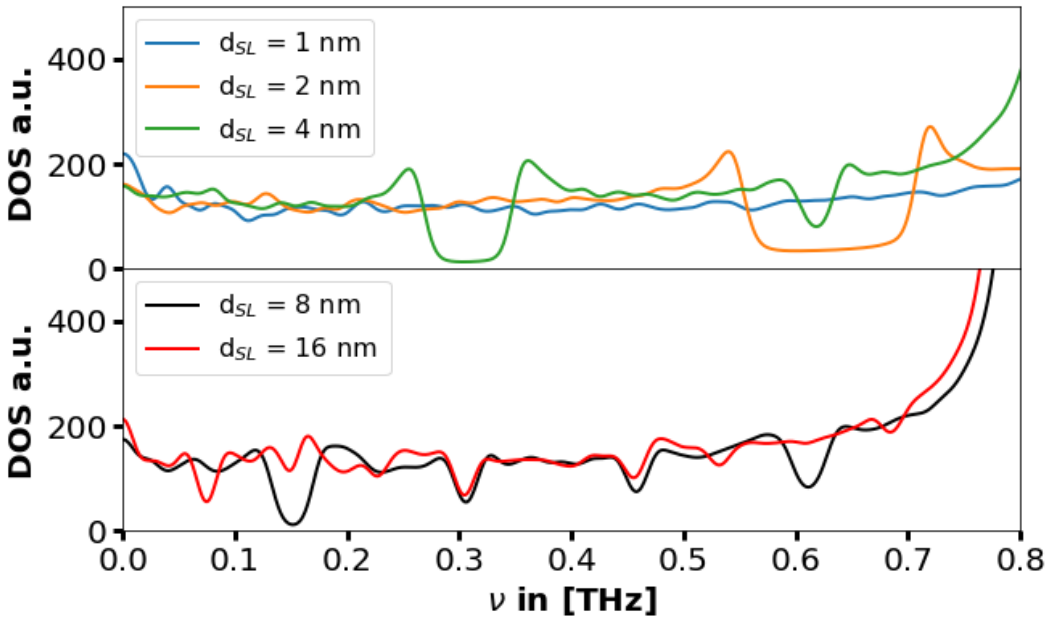

Figure 4.14.: Acoustic region of the DOS for the LJ-superlattices. Due to Brillouin-zone folding, phononic gaps appear in the bands.

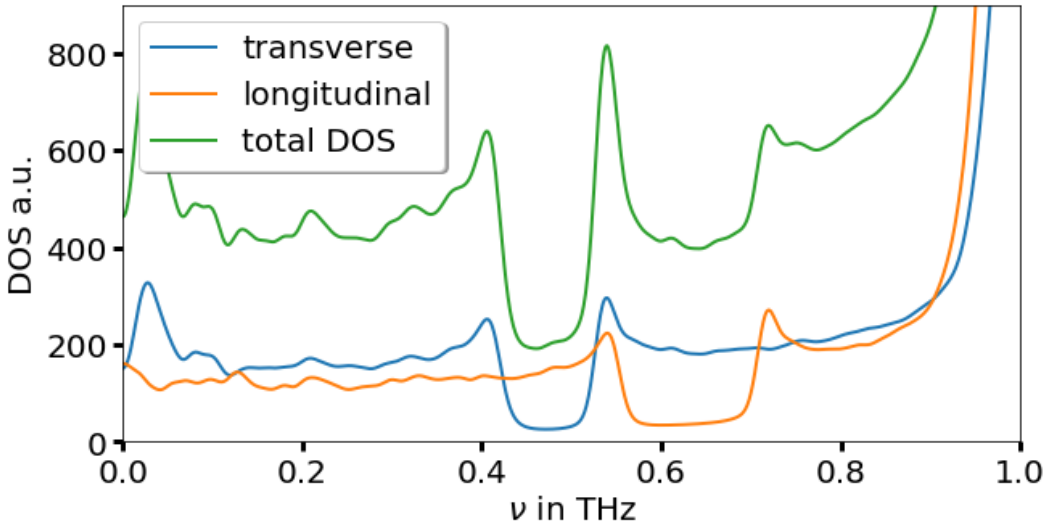

Figure 4.15.: DOS of the LJ-superlattice with $d_{SL} = 2\,\text{nm}$ in the acoustic region. The gaps due to Brillouin-zone folding appear at different frequencies for longitudinal and transverse modes; the total DOS does not drop to zero for the whole frequency range.

4.2.3. Coherence length calculations

In the case of three-dimensional systems, the cross spectral density function (Eq. 2.37) is calculated by treating the components of the velocity separately. This results in a separate cross spectral density for each Cartesian direction. The superlattice is extended in z-direction, and we calculate the coherence of phonons along the z-direction. A longitudinal wave with propagation direction along z deflects the atom in z-direction. Thus, the z velocity component corresponds to longitudinal phonon modes in this direction, while the components in x and y correspond to transverse phonon modes. All the following results refer to the longitudinal phonon modes if not stated otherwise, but similar results can be obtained for transverse modes.

To estimate the coherence length, the cross spectral density function needs to be fitted to Eq. (2.40) like for the one-dimensional case. The fit has presented some difficulties when doing the fit over the whole frequency spectrum. Already in the acoustic region, there is a fast drop in the cross spectral density function (see Figure 4.17). The first data point (i.e. at $R = 0$) is at 1, because the data is normalized to it. The following data points are too low to follow an exponential decaying trend including the data point at $R = 0$, but follow an exponential trend with a lower amplitude. Fitting to this exponential decay was not successful, as there is the amplitude A as a third parameter to fit ($Acos(2\pi R/\lambda)exp(-R/l_c)$). The first thought to explain this abrupt drop is that there are two or more modes at the same frequency, and that the cross spectral density function is the sum of two or more attenuated waves. But looking at the phonon dispersion in Figure 4.16,b) for wave-vectors pointing in z direction) at the frequency of 0.562 THz, there is only one allowed longitudinal mode. There are two transverse modes at this frequency, but the transverse modes are not leading to oscillations in z-direction, and the cross spectral density here was calculated from the velocities in z. Another explanation could be other modes with a wave vector not in the direction of the superlattice. As the supercell is extended 3 unit-cells in x and y, there are few modes with wave vectors perpendicular to the superlattice axis. This modes can lead to vibrations in z direction and affect the velocities in z-direction. The propagation direction of these perpendicular modes is not in the correlation direction, and they will not be coherent in the correlation direction. Still they can contribute to the cross

spectral density function and lower its value.

As the fitting procedure does not give satisfactory results for the coherence length, another estimator of the coherence length is used like in Ref. [11]. The idea is to treat the cross spectral density function as a probability density function. The probability density function $C(\nu, R)$ is constructed from the absolute square of the real part of the cross spectral density function:

$$C(\nu, R) = |Re(T(\nu, R))|^2. \tag{4.2}$$

For a certain frequency ν_0, the normalized cumulative distribution function $F(r, \nu_0)$ is calculated as:

$$F(r, \nu_0) = \frac{\sum_{R=0}^{r} C(\nu_0, R)}{\sum_{R=0}^{R_{max}} C(\nu_0, R)} \tag{4.3}$$

The coherence length is then estimated as the distance $l_c = r$, where the cumulative distribution function equals $F(r, \nu_0) = 95\%$. This means that up to this length, 95 % of the correlated signal is taken into account. In Figure 4.18 a comparison between the two estimators for l_c is shown assuming an ideal behavior of the cross spectral density function like in Eq. 2.40. The coherence length l_c is extracted from $|T(\nu, R)|^2$ by a fitting procedure (black dot in Fig. 2.40). The red dot marks the distance where the cumulative distribution function equals 95%, which corresponds to the coherence length $l_{c,2}$. The ratio $\frac{l_{c,2}}{l_c}$ = 1.42 in this example. The two estimators deviate from each other. The ratio between the two estimators depends on the wavelength of the attenuated wave and resolution in R (defines how good the data-points reproduce the attenuated wave). The ratio between l_c and the maximum R plays also a role. If the wave does not completely decay until R_{max}, the estimator $l_{c,2}$ is adulterated. A rapid decay and a lot of noise in the (long) tail of $T(\nu, R)$ can lead also to an overestimation of $l_{c,2}$. As the fitting procedure does not work, the cumulative distribution function is used to estimate the coherence lengths.

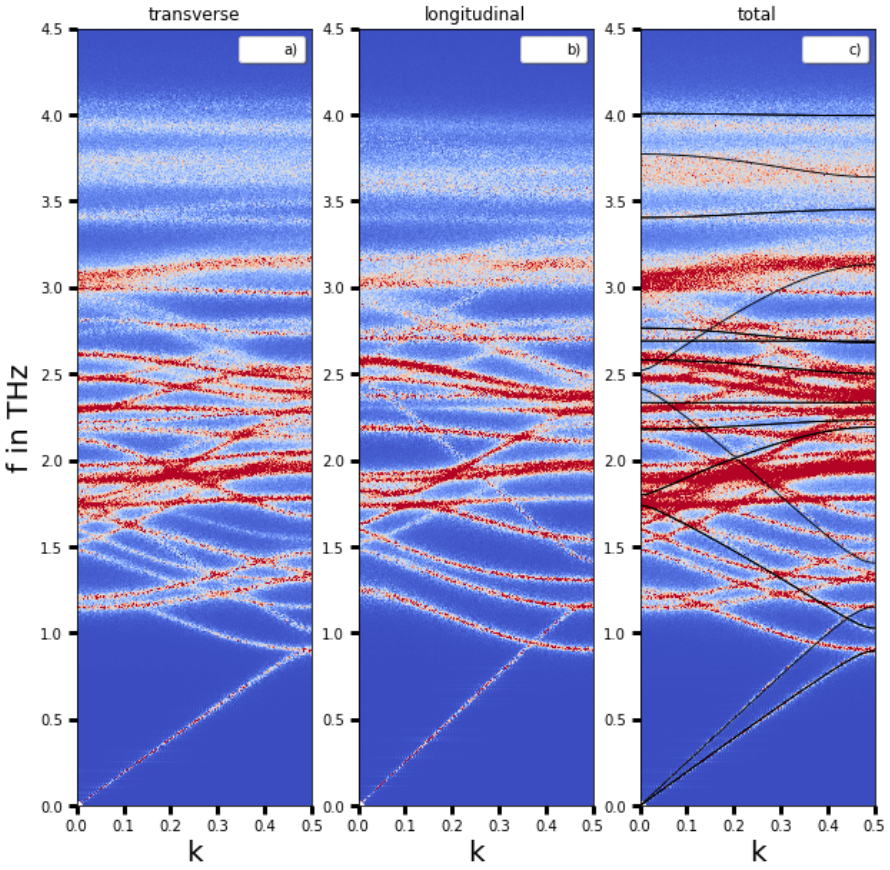

Figure 4.16.: 2D-representation of the spectral energy density for the LJ-superlattice with $d_{SL} = 1\,\text{nm}$. In practice it is given by the spatial Fourier transform of the cross spectral density function (Eq. 2.41). The colors give the magnitude of the spectral energy density, with dark blue being zero intensity and red being high intensity. The wave vector, k, points in the direction of the superlattice axis. Spectral densities a) from velocity components perpendicular to the superlattice axis (transverse modes), and b) from the velocity components along the superlattice axis (longitudinal modes). c) Total spectral energy density, along with the bands calculated by a LD simulation (black lines). In the spectral energy density appear more bands than from the LD simulation. When calculating the spectral energy density, the spatial Fourier transform was conducted as if the system was one-dimensional in the z direction, and it was assumed that there are no contributions to the velocity from modes with wave-vectors not pointing into the z direction. As they still are naturally present in the simulation, there are more branches in the spectral energy density than in the band structure from LD.
(For clarification only the values of $T(\nu, R)$ for which the distance R was part of the superlattice Bravais-lattice was used to calculate the spatial Fourier transform.)

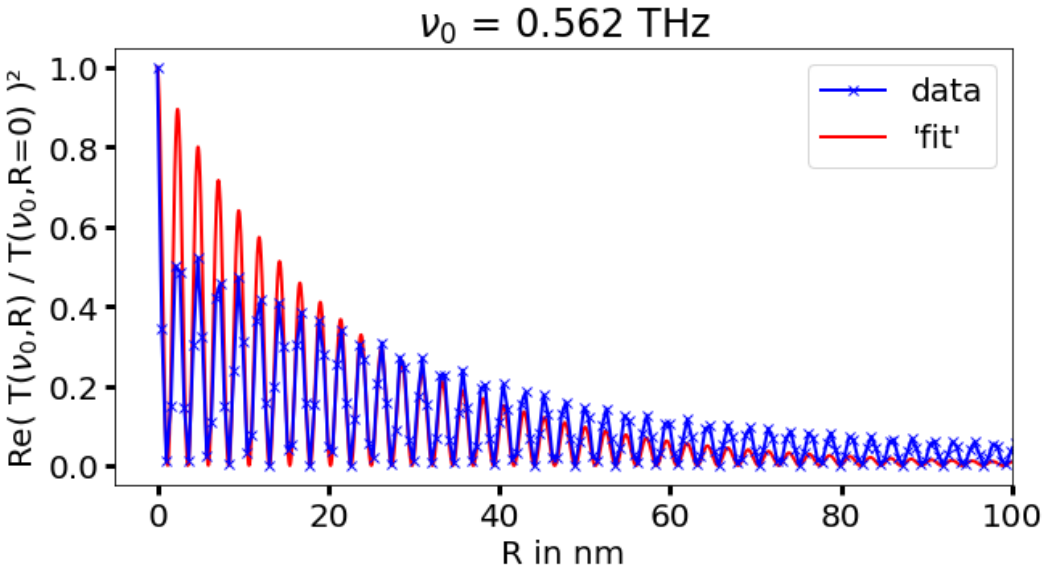

Figure 4.17.: The cross spectral density function $T(\nu, R)$ has a fast drop after the data point at $R = 0$, leading to a non-exponential behavior. This results in a wrong fit to equation (2.40). Example of $T(\nu, R)$ for the LJ-superlattice with $d_{SL} = 1\,\text{nm}$.

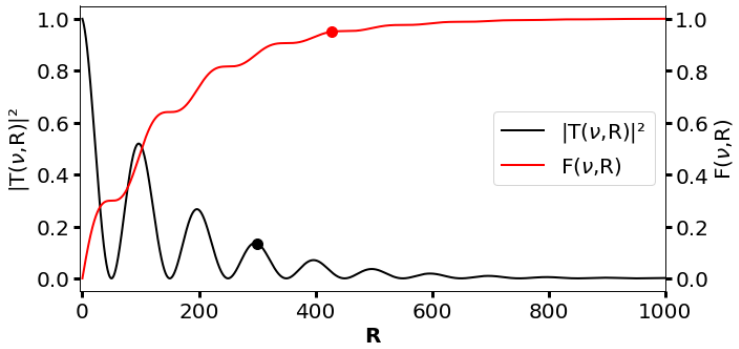

Figure 4.18.: The squared cross spectral density function $|T(\nu, R)|^2$ has the ideal behavior of an attenuated wave (Eq. 2.40). The red curve is the cumulative distribution function. The black dot marks coherence length from the cross spectral density function, while the red dot marks the distance where the cumulative distribution function is 95%. This distance is the second estimator of the coherence length.

4.2.4. Results of coherence lengths

The results for the coherence length for the Lennard-Jones superlattices, extracted with the above mentioned approach, are shown in Figure 4.19. All five superlattices with different period show a high phonon coherence in the acoustic region. As already mentioned, this is expected. Acoustic phonons have a large wavelength, and thus a large spatial extension.

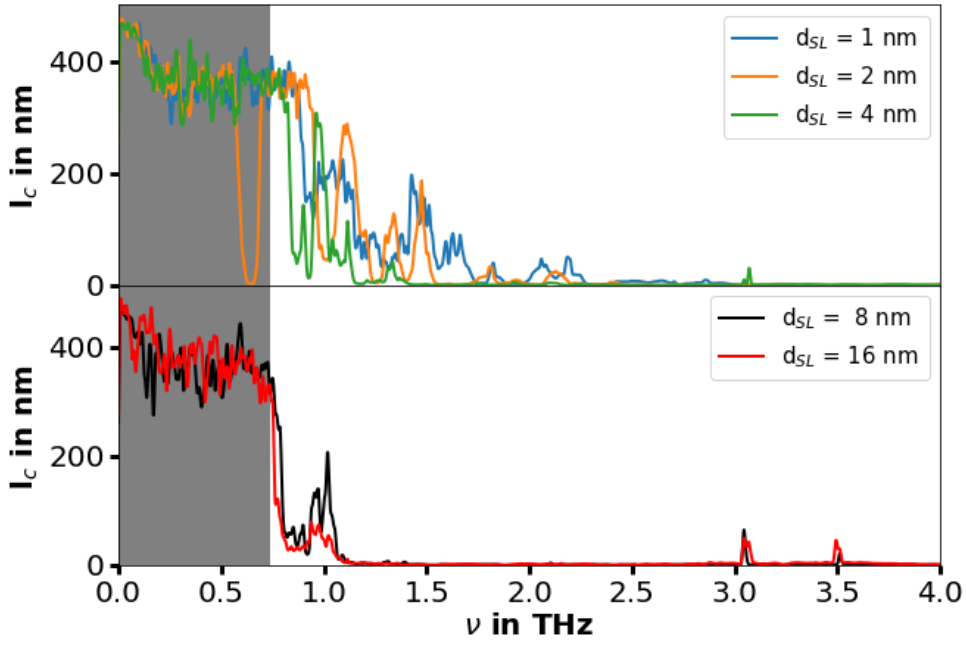

Figure 4.19.: Coherence lengths $l_c(\nu)$ of the LJ-superlattices for different periods d_{SL}. The superlattices with lower period show a higher phonon coherence. (The data of the coherence length was smoothed for better visibility.)

The coherence length for the acoustic phonons is larger than half of the (periodic) simulation box. The plot is shaded in this region up to 0.75 THz, because one cannot be confident in the numerical value. First because the coherence length is limited by the supercell size. Second, because the long wave-length phonon modes are not well described in a MD simulation.

McGaughey and Kaviany stated in their review [51], that when phonons are described as particles, it implies localization. The phonon modes in a crystal, as a result of a plane wave Ansatz (see 2.1), are completely delocalized. A localized wave can be formed as a wave-packet by superimposing modes of similar wavelengths in the near vicinity of the desired phonon mode. To construct a wave packet, the Brillouin-zone must be resolved high enough (to have enough modes close to the desired mode), which requires a large supercell. The wave-packets move around and scatter through various scattering mechanisms, describing the phonons as a phonon gas. In order for the phonon gas model to hold, some conditions need to be satisfied. The extension l of the wave-packet is much greater than the wavelength λ. In the phonon gas model the mean free path Λ should be larger than the extension of the wave packet l, and Λ should be much smaller than the extension of the crystal L to satisfy the condition for diffusive transport. The lowest acoustic modes in the supercell have wavelengths in the range of the simulation box and thus are not described properly by MD.

Above the untrusted region, the superlattices with the smallest period show the highest coherence lengths, while superlattices with larger periods lower phonon coherence. The 1 nm superlattice has coherence lengths up to 100 nm for phonons with frequencies up to 1.5 THz. The superlattices with periods 8 and 16 nm show non negligible coherence lengths only for modes with frequencies shortly above 1 THz. The superlattice with $d_{SL} = 2\,\text{nm}$, has a large drop in the coherence length at 0.65 THz. The DOS of this superlattice shows a large gap in this region (see Figure 4.14), resulting in no modes at this frequency for the mentioned superlattice.
Latour et al [11] studied the same system but with shorter and thicker supercells in the molecular dynamics simulations ($2.5 \times 2.5\,\text{nm}$ compared to $1.6 \times 1.6\,\text{nm}$ in this work). They report as well, that the superlattices with lower period have higher coherence lengths. Their largest system length was 160 nm, while the simulation cell of our system is around 1 µm. They report that the coherence length does not depend on the number of periods (simulation cell length) if the cell is larger than 80 nm, while in the findings of this thesis the coherence length is not saturated for the already large supercell. In the reference, the coherence length is not reported for frequencies below $\approx 0.4\,\text{THz}$. There is no reason mentioned for it, but it is probably due to the fact that the long wavelength modes are not described

well with MD. The supercells in this work are larger and the Brillouin-zone along the superlattice direction is sampled better, allowing to describe modes better down to lower frequency, still the coherence length being limited by the supercell dimension.

To define if the phonons will be transported ballistically or not, the coherence length is compared to the superlattice period. In Figure 4.20, the coherence length over the superlattice period is plotted in a semi-logarithmic plot. For the smallest superlattice period a large range of phonons are coherent, and for the systems with largest superlattice periods only acoustic phonons can be classified as coherent. The coherence length of the superlattice with period $d_{SL} = 1\,\text{nm}$ is larger than the superlattice period up to 3 THz, while for the superlattice with period 2 nm phonons are coherent up to 2.3 THz. For the superlattices with period 8 nm and 16 nm only phonons with frequencies up to 1.1 THz are coherent.

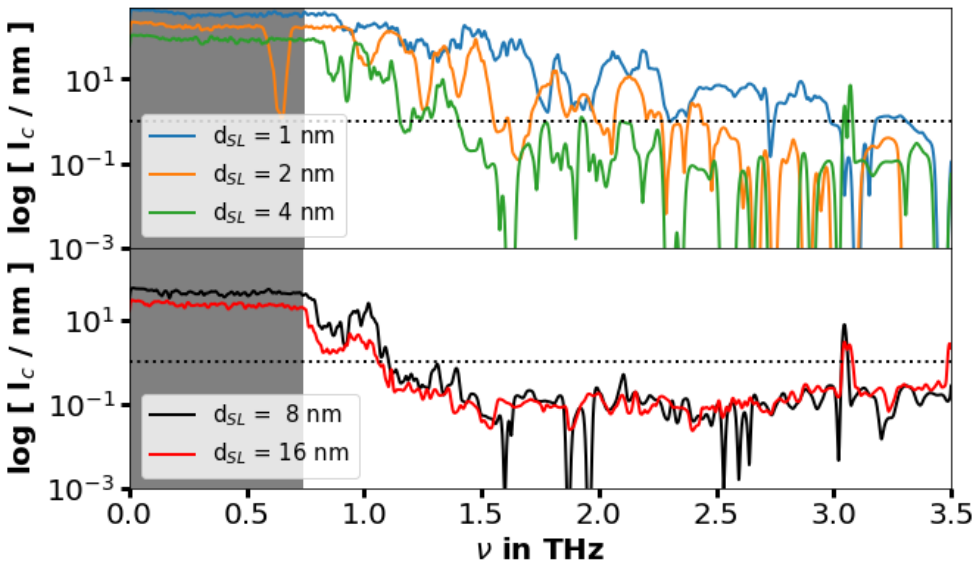

Figure 4.20.: Coherence length $l_c(\nu)$ divided by the superlattice period d_{SL}. If the ratio is larger than 1, the phonon wave packet at this frequency have a spatial extension larger than the superlattice period, and phonons at this frequency will show ballistic transport.

In summary, fitting an attenuated wave to the cross spectral density function is not successful for the three-dimensional Lennard-Jones superlattices. The coherence length for the three-dimensional system is calculated by treating the cross spectral density function as a probability distribution function, and estimating the coherence length as the distance, where 95% of the correlated signal is taken into account. It is found that for modes with frequencies below 0.75 THz, the coherence length is limited by the supercell size, which is already 1 µm large. The superlattice with the lowest period ($d_{SL} = 1\,\mathrm{nm}$ has the longest coherence lengths, while the coherence length gets lower with larger period. This is in contrast to the one-dimensional system, where it was found that the coherence length is mostly independent from the superlattice period.

4.3. Gallium nitride - Indium nitride superlattices

After having studied the microscopic picture of the phonon coherence on two test systems, a more realistic system made of gallium nitride and indium nitride is simulated. Gallium nitride is a widely used material in the semiconductor industry. Gallium nitride (GaN) and indium nitride (InN) show both a wurtzite crystal structure. As both materials have the same crystal structure, coherent superlattices can be formed; at least in a thought experiment, as the lattice mismatch between the materials can introduce dislocations and defects, which destroys the coherent crystal. InGaN heterostructures have applications in optoelectronics for example in light emitting diodes [52].

Wurtzite GaN and InN have a lattice mismatch, as it can be seen in Table 3.1 and 3.2, the ratio between the lattice parameters is roughly 1.1 ($\frac{a_{\mathrm{InN}}}{a_{\mathrm{GaN}}} = 1.103$, $\frac{c_{\mathrm{InN}}}{c_{\mathrm{GaN}}} = 1.099$). This leads to a high strain at the interfaces. The lattice mismatch and the strain at the interfaces can reduce the phonon coherence. However, the strain at the interfaces results in piezoelectric polarization [13], which could be used in possible applications. The piezo-electricity could be used for generating coherent phonons with a light pulse in multiple quantum well (MQW) structures. If the superlattice making the MQW, allows for coherent phonon transport, the coherent phonons can propagate for a certain distance, providing a source for coherent phonons.
It is difficult to grow GaN/InN superlattices due to the different growth temperatures and the high lattice mismatch. The critical thickness for growth of InN on GaN is ≈ 2 monolayers [14], before misfit dislocations appear to lower the stress.

The phonon band structures of GaN and InN can be seen in Figures 3.2 and 3.3, both materials have naturally occurring band gaps in the dispersion relation. GaN is a semiconductor with a high phonon mean free path [53]. The phonon mean free paths (MFP) for GaN and InN were calculated by combining lattice dynamics and molecular dynamics (see Figure A.4). GaN has a MFP up to 1000 nm, while the MFPs of InN are below 10 nm. It is thus expected that thick layers of InN will hinder the phonon coherence.

In the following sections, the results for simulations of GaN/InN super-

lattices with periods of d_{SL} = 1.06, 2.12, 6.36 and 10.6 nm are presented. The simulated supercells have structures of $3 \times 2 \times N$ and $1 \times 1 \times N$, with the latter being the longer supercell. Simulations of structures with InN monolayers in a GaN matrix are also discussed. The last type of structures have been fabricated experimentally [15].

4.3.1. Simulation of superlattices with supercell structure $3 \times 2 \times N$

Superlattices of GaN and InN for the simulations are grown along the c-direction of the wurtzite crystal structure (see Section 2.7). The orthogonal representation of the wurtzite unit cell with 8 atoms in its basis is used for generating the supercell as input of the MD simulations. Symmetric superlattices are simulated, which means that always the same number of GaN cells are stacked on InN cells. Four different superlattices with a stacking of $1-1, 2-2, 6-6, 10-10$, which have a superlattice period of d_{SL} = 1.06, 2.12, 6.36 and 10.6 nm, are simulated. The supercells have a structure of $3 \times 2 \times N$ unit cells. N is chosen such that the total number of atoms in the systems are 24000, or close to it. The supercells have a size of roughly $1.05 \times 1.21 \times 265$ nm. Supercells of pure GaN and InN with the same dimensions are also simulated. This calculations serve as reference for the results obtained for the superlattices.
The temperature is set to 300 K, and the time step of the simulations is d_t = 1 fs. The cells are first relaxed for 0.2 ns in the NVT ensemble and then simulated for 0.5 ns in the NVE. The velocities are sampled every Δt = 10 fs, leading to a maximum frequency of $\nu_{max} = 50$ THz (Eq. 3.3).

The lattice mismatch at the interface between GaN and InN raises the question of what lattice parameter for the InN and GaN unit cells should be used for the NVE simulations of the superlattices. The lengths of the simulation box can be chosen to match the lattice parameters of GaN or InN. GaN is widely used in semiconductor industry and GaN wafers are commercially available. In an experiment, one would probably start from a GaN substrate, and deposit then alternating layers of GaN and InN on it. This constrains the lattice parameter of InN parallel to the interface to the ones of the GaN substrate.

In the NPT simulations, during which the equilibrium volume of the superlattices is calculated, the a-lattice parameter of InN is fixed to GaN, and just the c-lattice parameter in the z-direction is relaxed. Nonetheless, MD simulations using this strategy, have reveled that constraining the a-lattice parameter of InN to GaN, the system is not stable, and dislocations are introduced to the system (using the force field potential from Ref. [38]. Using the a-lattice parameters of InN for both GaN and InN, no dislocations are introduced, and the perfect crystal structure is preserved. Two figures of the stability simulations can be found in the Appendix A.4. Therefore, the equilibrium volume of the GaN/InN superlattices is calculated by stretching the GaN a-lattice parameter to that of InN. An NPT simulation of this superlattice, allowing just relaxations in the z-direction (i.e. the c-lattice parameter), were then performed to calculate the equilibrium volume at 300 K. The fact that the superlattice structures are not stable during the simulation when using the lattice parameter of GaN might reflect that these structures are not stable in reality. In fact, a study showed that during the growth of InN on GaN, dislocations will be introduced after a thickness of $\approx$ 2 monolayers [14].

GaN and InN show phonon frequencies up to 25 THz and 30 THz (Figures 3.2, and 3.3. The superlattices have higher phonon frequencies up to 40 THz (see DOS in Figure 4.21). The modes which show these high frequencies are localized vibrations of the nitrogen atoms at the interfaces. Because of the strain at the interfaces, high forces act on the nitrogen atoms, which leads to rapid oscillations and high frequencies.

The density of states in z-direction, calculated from the velocities obtained during the MD simulation, are displayed in Figure 4.21. Similar to the Lennard-Jones superlattices, the DOS depends on the superlattice period when the superlattice period is small. The DOSs of the superlattices with period of 1 nm and 2 nm are different from those of the superlattices with a period of 6 nm and 10 nm. These DOSs of the latter superlattices are very similar among them, and look more like an average of the DOSs of both materials the superlattices are made of.

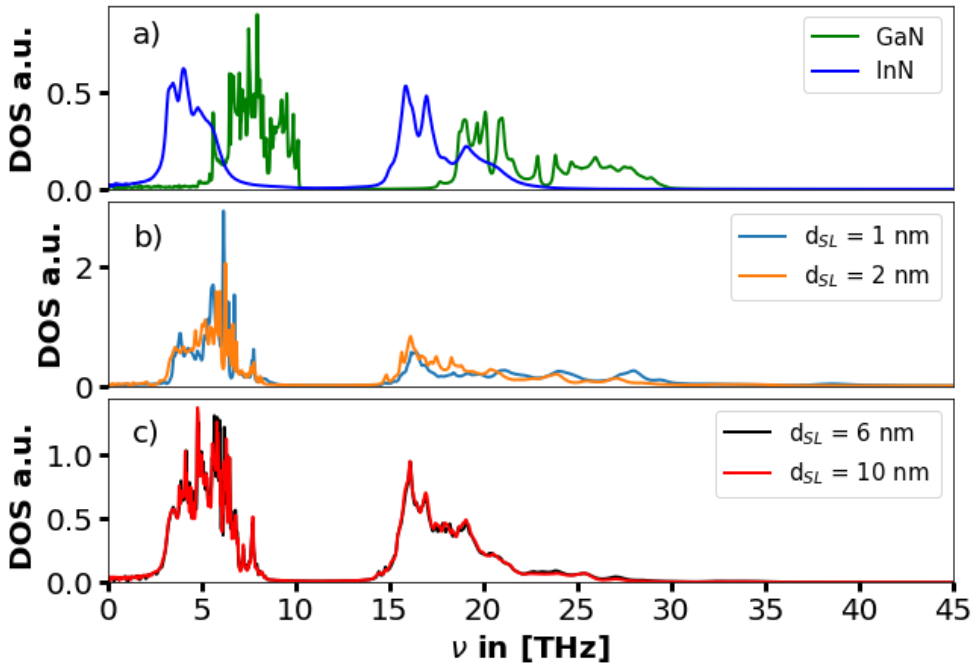

Figure 4.21.: Phonon density of states obtained from MD simulations for (a) GaN, InN and (b,c) GaN-InN superlattices. These calculations were performed using a $3 \times 2 \times N$ supercell.

Calculation of the cross-correlations and coherence lengths

The Gan/InN superlattices are a stacking of unit cells that have different lattice parameters along the superlattice direction. As InN has a larger unit cell than GaN, the InN layer within the superlattice will be longer along the z-direction than a layer of GaN with the same number of atoms. When calculating the cross spectral density function, the correlations of the unit cell at position R_0 and the unit cell at position $R_0 + R$ are calculated. The distance R between unit cells, which are n unit-cells apart, can have different values in the same superlattice, because the unit cells have different lattice parameters. For example two neighboring GaN unit cells are separated by $R = 5.2\,\text{nm}$, while two neighboring InN unit cells are separated by a distance $R = 5.7\,\text{nm}$. To have the cross spectral density still as a function of

discrete, equidistant points in distance R, it is assumed that all the unit cells are separated by integer multiples of the average lattice parameter in the system, when calculating the cross spectral density function.

The calculation of the coherence length by fitting the cross spectral density to equation (2.40) is difficult for the whole frequency spectrum. The same problems discussed for the Lennard-Jones superlattice arise. There is a strong drop in the cross spectral density after $R = 0$, the resolution in R is limited by the lattice parameter, which leads to bad reproducibility of the attenuated wave behavior when the wavelength is small, and if there are two modes at the same frequency. One cannot separate them with our approach.
The approach based on the cumulative distribution function of the cross spectral density function is an alternative tool for calculating the coherence length. It turns out, however, that using this approach, the quantitative result of the coherence length depends strongly on several parameters. For example, the choice to define the coherence length as the distance where the cumulative distribution function (Eq. 4.3) equals 95 %. Although this is a good estimator, it is still rather arbitrarily. It could be chosen to be any other value below 95 %, which would result in lower coherence lengths (or vice versa). In some cases, for instance, lowering the threshold from 95 to 93% leads to a reduction of the coherence length of 50% or more, although the qualitative trends stay the same.

The cross spectral density function $T(\nu_0, R)$ should decay to 0 after some distance R for every frequency ν_0 (e.g. Fig. 4.17). Nonetheless, our data sometimes rises again for large R after falling to zero. Moreover, after falling to zero, there is always small numerical noise for large R in the cross spectral density function. If the function decays to 0 already for small R, the noise in the long tail will have a non-negligible contribution to the cumulative distribution function.

The DOS from molecular dynamics can be smoothed by smoothing the VACF to zero after some time τ (Eq. 4.1, Figure 4.3). The spatial cross spectral density is the Fourier transform of the cross-correlation functions. An attempt to smooth the cross correlations in a similar way as the VACF, to reduce the noise, was made. This would allow to overcome the aforementioned problems to extract the coherence length from these correlations.

Before answering the question of how to possibly smooth the cross correlations, it is important to have look at the cross-correlations. In Figure 4.22, the calculated cross correlations of the atomic velocities for the example of the GaN/InN $1-1$ superlattice are plotted as a two dimensional plot. The color indicates the magnitude of the correlations. On the x-axis is the time τ, and on the y-axis is the distance R. Every horizontal line at an arbitrary R_0 corresponds to the correlation for atoms separated by a distance R_0 (The line at $R_0 = 0$ corresponds to the VACF). Note that all the correlation functions were normalized by the value of the VACF for $\tau = 0$ and have a range between -1 and 1. The cross-correlations for large distances and times are considerably weaker than the auto-correlation function. The range of the color-bar were set to low values to make the weak correlations visible. Because of the low range of the color-bar, strong correlations (for example VACF) are not displayed properly in the plot as their values mostly lie outside of the color range.

The most striking feature in Figure 4.22 is the line starting out from point ($R = 0,\ \tau = 0$), moving with a constant 'speed' towards higher distances and times. This line corresponds to peaks in the correlation functions which appear at the time $\tau_p = R/v$. The 'velocity' v is constant for a superlattice. It coincides well with the group velocity of the low frequency acoustic modes, where the dispersion is linear (compared to v_g from LD calculations). This peak appears due to wave-packets of low frequency acoustic modes, which travel with the group velocity v_g through the crystal. These modes have a large MFP, a large coherence length, and travel a large distance without losing the phase information. It was checked that this line is due to low frequencies, by cutting out the low frequency part in the Fourier transform of the correlations (which is the cross spectral density), and from that calculating the correlation functions again, which leads to a disappearing of the line.

For larger distances, the peak of the low frequency acoustic modes becomes weaker and broader which is a result of the attenuation of these wave packets. As more and more phonons loose coherence, less modes (i.e. frequencies) contribute to the peak. Therefore, the wave packet gets broader.

The simulated supercell is around $L_z = 265\,\text{nm}$ long. The maximum dis-

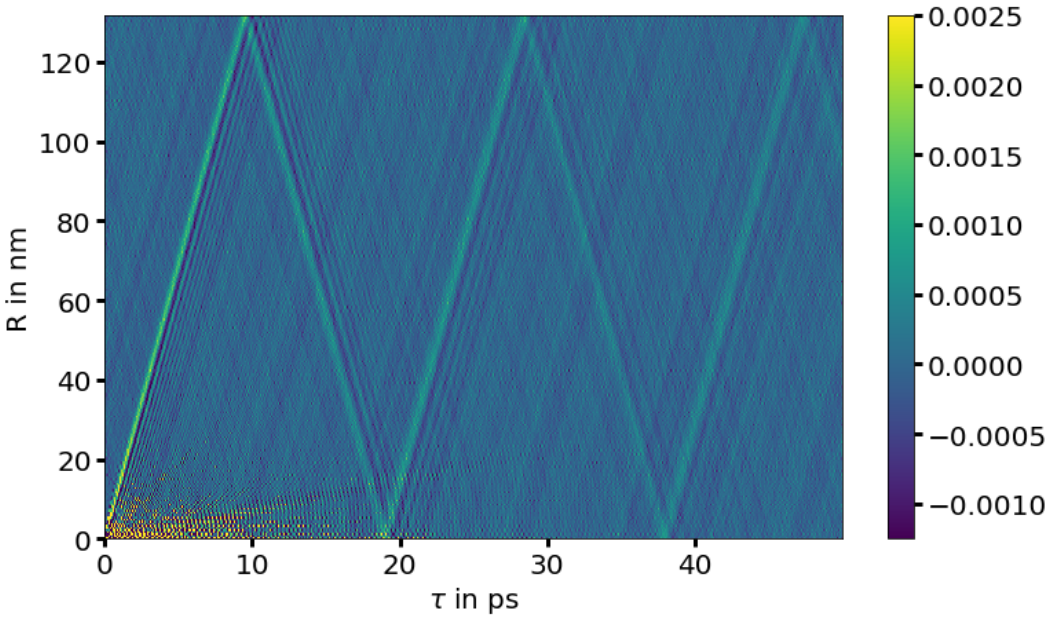

Figure 4.22.: Cross correlation functions of the velocities of atoms separated by a distance R as a function of time τ. The data is obtained from an NVE simulation of a GaN/InN 1-1 superlattice. The data is normalized by the value of the VACF for $\tau = 0$, and the color-bar is set to small values to make the small correlations for larger distances visible. The simulation time was 500 ps, and only correlations up to 50 ps are shown.

tance for which the correlations are calculated is half the simulation box size $R_{max} = 132.5\,\text{nm}$. The box is periodic; therefore, wave-packets will travel in both directions and can arrive again at the position of their origin after some time. If two wave-packet start at some position x in the supercell, and travel in opposite directions, the packet will arrive at the position $x + 50\,\text{nm}$ after time $\tau = 50/v$. The other packet will arrive at the same position, going in the opposite direction, and passing through the periodic boundaries after having traveled a distance of $(L_z - 50\,\text{nm})$. The wave packet will take a time $\tau = 215/v$. In the example of Figure 4.22, a peak for $R = 50\,\text{nm}$ appears at time $\tau_1 \approx 4\,\text{ps}$ and at time $\tau_2 \approx 17\,\text{ps}$ (because of the second packet moving in opposite direction). Because the packets continue to travel further, they arrive at the same place again after having crossed the whole simulation box, and the peak appears again.

Modes with a lower group velocity and a lower coherence length are the source of the correlations at short distance and short times. They do not have such a long MFP to show correlations for larger distances.
In the background of the plot of the correlations, there is noise and weak lines, which are parallel to the line caused by the acoustic modes. As they are weak, it is not possible to track their origin. A possible explanation of this lines is that they are correlations of wave packets which have traveled few times through the whole crystal.

Back to the question on how the smoothing of the cross correlation functions should be done to give a smoother spatial cross correlation function. The first idea would be to smooth all the correlations like the VACF (i.e. to force them to go to 0 after some time τ), with the same time which gives a smooth DOS (Approach A). This would result in correlations which looks like Figure 4.23 a). Of course, this would leave out all the correlations after the point in time at which the correlations have been smoothed to 0, and there might still be some valuable information in this correlations. Another approach is to smooth the correlations with a Gaussian centered at the peaks in the correlations that are due to the coherent acoustic wave-packets [Figure 4.23b)] (Approach B). The third approach is to include all the signal up to the time where the the fastest modes reach a distance half the simulation box length, to avoid any self interactions (Figure 4.23c) (Approach C).

An example for the resulting cross spectral density function (for one frequency $\nu_0 = 0.6\,\mathrm{THz}$) with the different approaches for smoothing the correlation functions can be seen in in Figure 4.24. The different smoothing approaches have different effects on the cross spectral density function. Although these effects are different for different frequencies, a general trend is observed. Smoothing correlations like for the VACF (approach A, Figure 4.23a) leads to a spectral density which decays faster than the original spectral density. Smoothing with approach B (Figure 4.23b), leads to a spatial cross spectral density which rises again after falling. With this approach, the normalized cross spectral density (normalization is done by the value at $R = 0$) can reach even values above unity for distances $R \neq 0$. It is not expected that atoms, which are farther apart, are more correlated than atoms with themselves. Smoothing the correlations using approach C, such

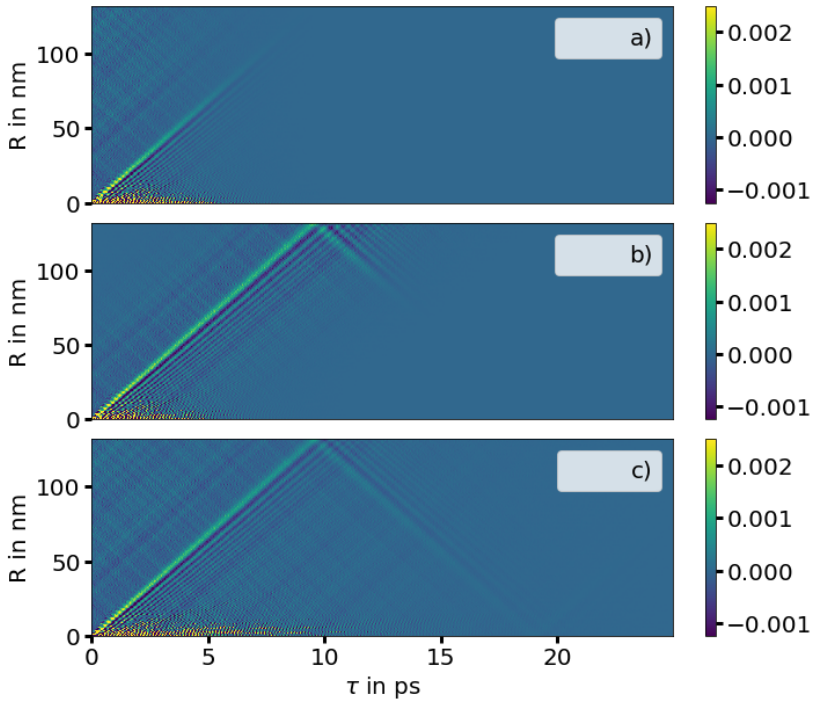

Figure 4.23.: Correlation functions of the GaN/InN 1-1 superlattice. Three different approaches to smooth the correlations to calculate the cross spectral density function, and to reduce the numerical noise are shown. In a) the correlations are smoothed with a Gaussian, following the smoothing approach used for the VACF (in order to obtain the DOS). In b) the correlations are smoothed with a Gaussian centered at the peak coming from the acoustic modes. In the last approach c), the correlations are smoothed starting from the time point, where the acoustic modes have traveled half the simulation box.

that correlations arising from periodic self interactions are neglected (Figure 4.23c), leads to a spectral density that decays with a similar or lower rate than the original one. The raw data often shows an abrupt drop after $R = 0$ as can be seen in the black line in Figure 4.24. Smoothing with the approaches A and C do not show the drop for this example (blue and green curve). But for higher frequencies than $\nu = 0.6\,\mathrm{THz}$, the drop appears again.

To clarify the influence of the smoothing of the cross correlations on the cross spectral density, the original cross spectral density, and the results

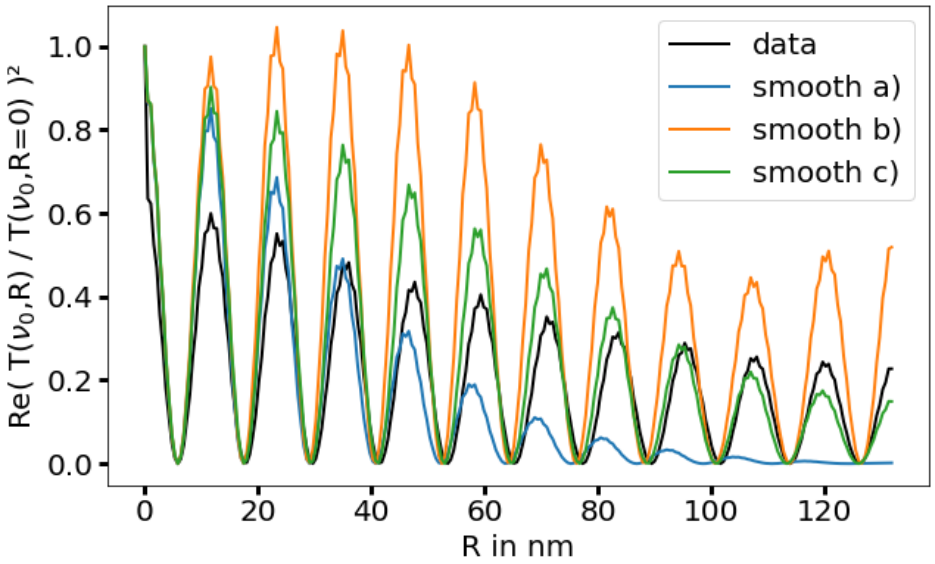

Figure 4.24.: Spatial cross spectral density functions (for one frequency ν_0) calculated from the cross correlations, which have been smoothed in different ways which can be seen in Figure 4.23

from the different smoothing approaches are shown in Figure 4.25 as a 2D-plot. It is seen clearly that only the low frequency modes show a high coherence length. Only for modes below 3 THz the cross spectral density is not almost zero. It also can be seen, that the spectral density obtained with approach A is cut for large R. It falls close to 0 already at $R = 40\,\text{nm}$. The correlations in this approach have been smoothed out starting from relatively low times τ. A wave which would stay coherent for a longer distance is attenuated artificially by the smoothing, leading to vanishing correlations at large distances (see Figure 4.23a).

In order to test the influence of the different smoothing approaches for the cross-correlations on the coherence length, the cumulative distribution function (Eq. 4.3) for the four different cross spectral density functions reported in Figure 4.25 is calculated. The four different spectral densities lead to different values for the coherence lengths as seen in Figure 4.26. Using the raw data leads to an overestimation of the coherence length for

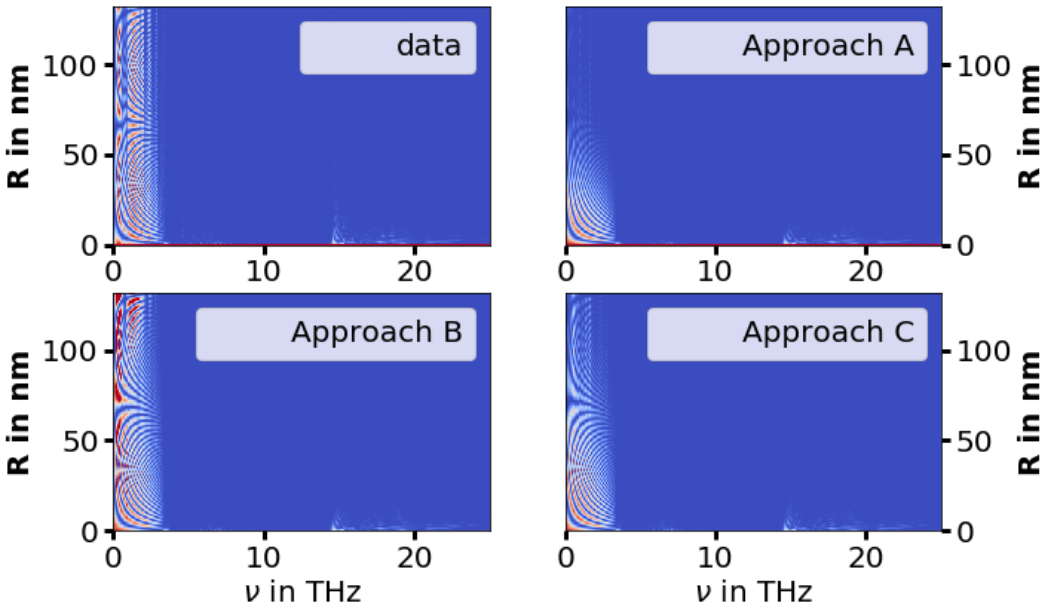

Figure 4.25.: The cross spectral density function $T(\nu, R)$ in a two dimensional representation. The squared real part of $T(\nu, R)$ normalized by the value at $R = 0$ for every frequency ν is plotted. Due to normalization, the values are bounded between 0 (blue) and 1 (red). The simulation was for a GaN/InN 1-1 superlattice. The cross spectral density of the original data is shown in the upper left (data). The other 3 plots (Approaches A-C) show cross spectral densities calculated from differently smoothed correlation functions (see Figure 4.23).

the optical phonons, while all the other three estimators arrive to similar results for this frequency regime. The approach of smoothing the cross correlations like the VACF (Approach A), leads to a clear underestimation of the coherence length for low frequencies, in comparison to the values obtained with the other approaches or with the raw data. Approach C results in a lower coherence length as approach B, but approach B is not reliable, as it sometimes estimates larger correlations for different separated atoms, compared to the auto-correlations. Approach C seems to be the most reliable approach, as it does not cut the low-frequency regime as Approach A and because Approach B is not reliable.

It is important to mention that the quantitative value of the coherence length,

also depends strongly on the parameter σ in Eq. (4.1), when smoothing the correlation functions. σ defines the width in time for the Gaussian function used for the smoothing. Lowering sigma, will take less signal into account. How strongly σ affects the quantitative values depends again on other parameters and the approach.

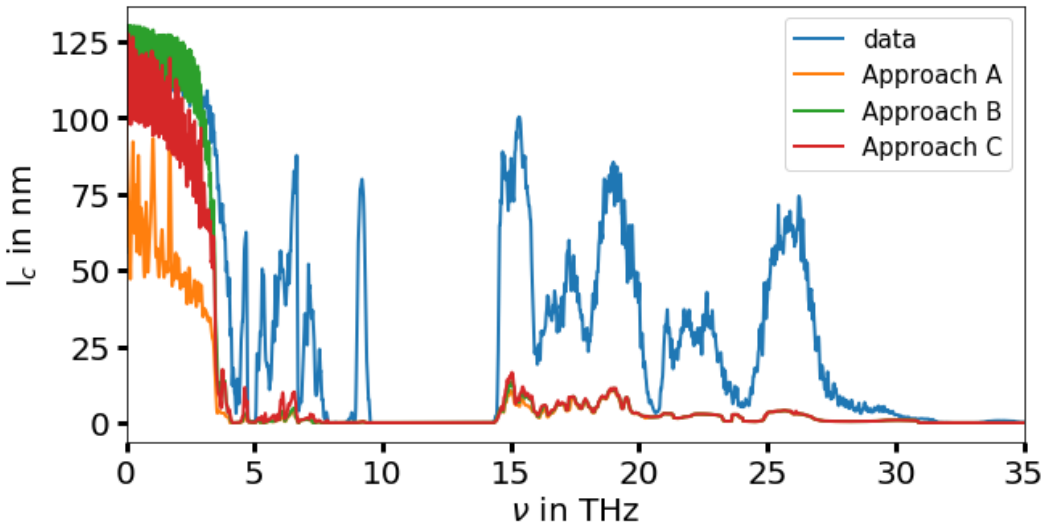

Figure 4.26.: Coherence lengths l_c as a function of frequency ν, for the GaN/InN 1-1 superlattice. The coherence length is calculated from four different cross spectral densities (Figure 4.25) which have been calculated from differently smoothed correlation functions.

Results of the coherence lengths

Based on the discussion above, the coherence length for the GaN/InN superlattices is extracted by smoothing the correlations following approach C (i.e. avoiding periodic self interaction). As expected, the superlattices with lower period show a higher phonon coherence (Figures 4.27 and 4.28). The superlattices with a period larger than 1 nm show significant phonon coherence only in the acoustic region (below 3 THz). The superlattice with a period of 1 nm has large coherence length for phonon frequencies up to 3.5 THz. Indeed, the coherence length is limited by the supercell size for

almost the whole region up to 3 THz, and exceeds 100 nm. Above this frequency the coherence length drops below 25 nm. For the other superlattices the coherence length is limited only up to about 1 THz by the supercell size. In Figs. 4.27 and 4.28), the areas where the value of the coherence length is not trusted is shaded in gray; either because the coherence length is limited by the supercell size ($\frac{L_z}{2} = 133$ nm) or because long wavelength modes with very low frequencies are not represented well in an MD simulation. For the superlattices with period d_{SL} =6 nm and 10 nm the values are trusted above $\nu = 1$ THz, for d_{SL} =2 nm above 1.5 THz, and for d_{SL} =1 nm above 3.2 THz (marked in light gray).

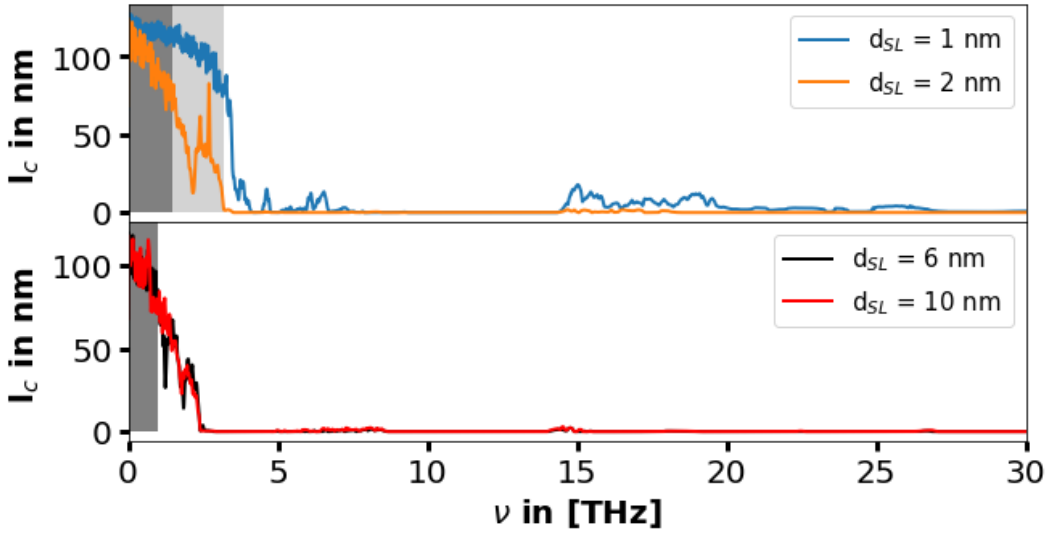

Figure 4.27.: Coherence lengths l_c of the GaN-InN superlattices as a function of the frequency ν. (Longitudinal modes). The gray areas mark the region, where the value of the coherence length is not trusted. For the upper plot the light gray area belongs to $d_{SL} = 1$ nm and the dark gray area to $d_{SL} = 2$ nm.

In the $d_{SL} = 1$ nm superlattice the modes are acoustic up to larger frequencies than in the superlattices with higher period length. This can be seen in the plot of the DOS (Figure 4.21b). The first peak in the DOS of the $d_{SL} = 1$ nm-superlattice appears at higher frequency than for the other superlattices. The first peak in the DOS is located where the acoustic branches start to bend at the Brillouin-zone boundaries. For the $d_{SL} = 1$ nm-superlattice the DOS starts to rise sharply at 3.4 THz, while for $d_{SL} = 2$ nm

at 3.1 THz. For the superlattices with $d_{SL} = 6\,\text{nm}$ and 10 nm the DOS rises at 2.9 THz. Only the superlattice with the smallest period shows a phonon coherence length of few nm for frequencies above the natural band-gap of GaN and InN (located at 10 THz to 17.5 THz for GaN and 7.5 THz to 14 THz for InN.)

As one our main goals is to predict structures that guarantee coherent transport of phonons, it is important to have a closer look at the coherence of the low frequency phonons. These phonons show the highest coherence, and could possibly be excited by optical means. The coherence length of the low frequencies are shown in higher resolution in Figure 4.28. The coherence lengths drops shortly above 2 THz for $d_{SL} = 2\,\text{nm}$, twice between 1 THz and 2 THz for $d_{SL} = 6\,\text{nm}$. For $d_{SL} = 10\,\text{nm}$ it is hard to distinguish any drop. These drops appear due to gaps in the DOS, which have origin in the Brillouin-zone folding. The coherence length for the superlattice with 1 nm period drops sharply after ≈ 3 THz. At this point the region with only acoustic modes ends.

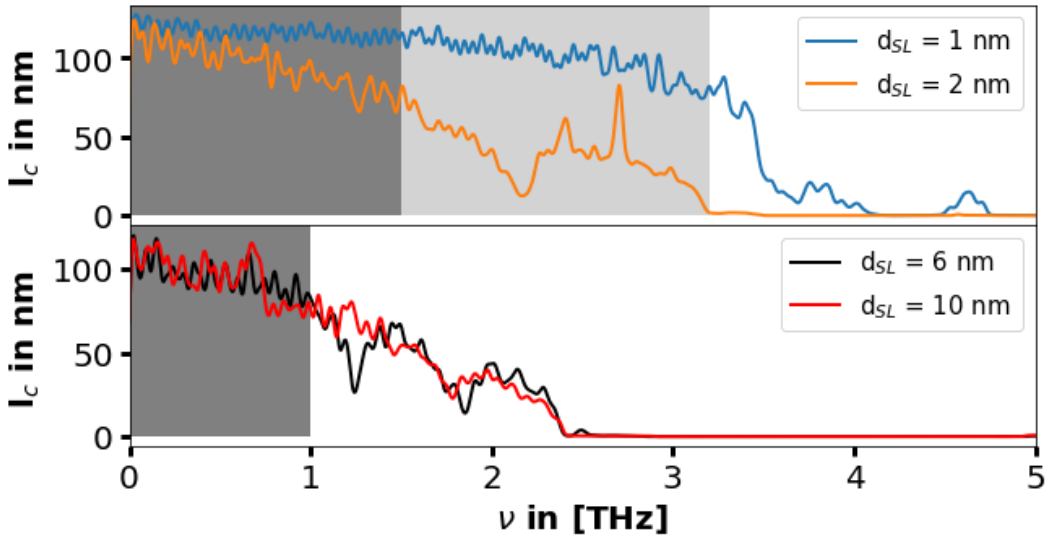

Figure 4.28.: Coherence lengths l_c of the GaN-InN superlattices as a function of the frequency ν only for frequencies up to 5 THz. (Longitudinal modes). The gray areas mark the region, where the value of the coherence length is not trusted. For the upper plot the light gray area belongs to $d_{SL} = 1\,\text{nm}$ and the dark gray area to $d_{SL} = 2\,\text{nm}$.

The coherence length of the superlattice with 1 nm period has some small oscillations below 2 THz. Due to periodic boundaries, only discrete wave-vectors, $\vec{k}$, are allowed in the system, and thus the frequencies are discrete as well. In the acoustic region, the dispersion relation follows (up to the frequency where the band bends) an almost linear behavior $\nu = v_G\vec{k}$ (see for example Figure 2.2). In an MD simulation, the allowed wave-vectors are discrete due to the periodic boundary conditions. The number of the equidistant wave-vector points is determined by the size of the supercell. Due to the relatively large slope of the acoustic branch, the allowed (discrete) frequencies belonging to the discrete wave-vectors have relatively large separations. If the resolution in frequency is high enough (long time series, Eq. 3.4), the discrete frequencies can be resolved in this region. In Figure 4.29 the unsmoothed DOS (a) and the coherence length (b) for the superlattice with $d_{SL} = 1$ nm is shown for a small range of frequencies in the acoustic regime. In a) it can be clearly seen that peaks appear at allowed frequencies, while in between the DOS is zero. Thus, when there are allowed modes, the coherence lengths reaches the maximum value (limited by the supercell size), and falls when the DOS is zero. It is noted that the modes with frequencies close to zero are not described well in the MD simulation, because they have wave-lengths comparable to the supercell size.

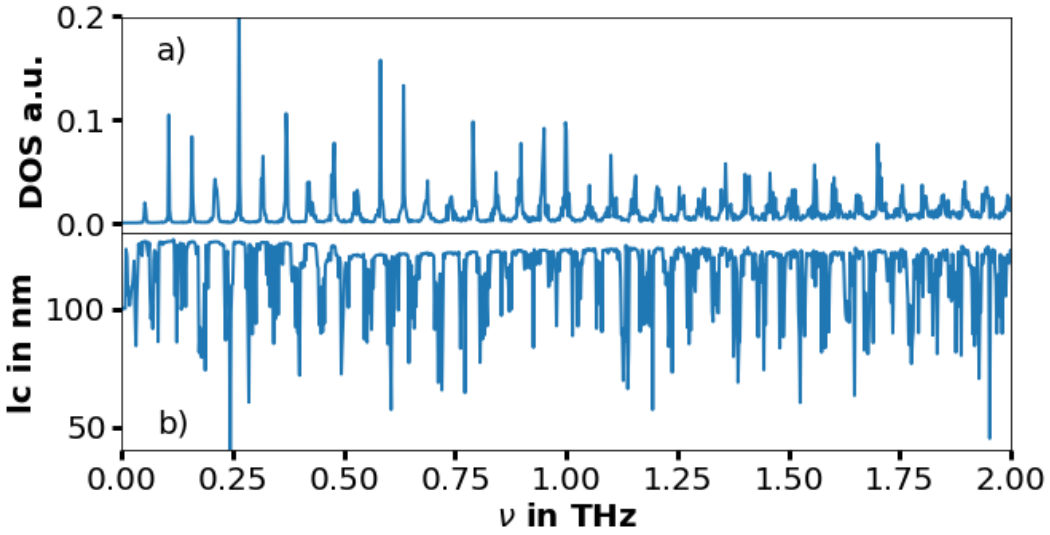

Figure 4.29.: DOS (a) and coherence length (b) of the GaN/InN $1-1$ superlattice for a small range in the acoustic region. Due to periodic boundary conditions the allowed wave vectors and frequencies are discrete. If the resolution in frequency is high enough, the discrete frequencies are resolved in the DOS.

4.3.2. Supercells of structure $1 \times 1 \times N$

The coherence length for the GaN/InN superlattices calculated for supercells of $3 \times 2 \times 1$ structure is limited by the supercell size in the acoustic regime. Because these modes are the ones which show the highest coherence lengths, one wants to get a value of the coherence length which is not affected by the system size. To do this, longer supercells are simulated, which also allows to describe long wavelength modes better. Longer supercells with higher number of unit cells also lead to less spacing between the discrete wave-vectors, and thus less spacing between the discrete phonon mode frequencies.
To limit the computational demand of the MD simulations, superlattices of structure $1 \times 1 \times N$ unit cells are considered. The supercells have dimensions of roughly 0.35 x 0.6 x 1600 nm and have 24000 atoms. The dimensions in x and y are very small, and the behavior of the superlattice in the x-y direction is described poorly. Especially as the periodic images of the atoms in x-y direction are within the potentials cut-off distance of the atoms themselves.

Nonetheless, such structures were simulated, as an increase to a $2 \times 2 \times N$ supercell would result four times computationally more expensive.
The number of allowed values for the wave vectors in x and y direction is limited to one (i.e. Γ point) because only one unit cell in this directions is considered. Phonons propagate only in the superlattice direction, and can not scatter with phonons that are not traveling in this direction (as there are none). This limits the phonon-phonon scattering, because there are less phonons to interact with. It might lead to a longer MFP of the phonons. Although the number of wave-vectors in x and y is one, (were small also for the $3 \times 2 \times N$ supercells), the phonons scattering at the interfaces, or the coherent transport along the superlattice length can be reasonably well described. Superlattices with the same period length used in the previous chapter are used for the $1 \times 1 \times N$ supercell structure. All the other parameters of the simulation are equal.

DOS and cross spectral density function

The DOS obtained from MD calculations is shown in Figure 4.30. The period length dependence of the DOS is in agreement with the results obtained for the $3 \times 2 \times N$ supercells. The DOS of the superlattices with periods 6 nm and 10 nm is very similar, while for lower periods there is a dependence on the period length.

The cross spectral density function of the $1 \times 1 \times N$ supercells does not show a sudden drop at $R = 0$, as it was for the $3 \times 2 \times N$ supercell, in the range of low frequencies (see example in Figure 4.31). There is only one allowed value ($\vec{k} = 0$) for the wave-vector in x-y direction for the $1 \times 1 \times N$ superlattice. So only modes with wave-vector in the superlattice direction contribute to the atoms velocities in z-direction (and modes at the center of the Brillouin-zone, i.e. Γ-point). In the $3 \times 2 \times N$ superlattice, the modes with wave-vectors that are not along the superlattice direction are not coherent, but contribute to the cross spectral density function. The absence of these modes in the $1 \times 1 \times N$ superlattice can be seen as well in the corresponding energy spectral density (Figure 4.32). The $1 \times 1 \times N$ superlattice shows less branches. The additional branches in the spectral energy density of the $3 \times 2 \times N$ superlattice come from modes with wave-vectors that are not

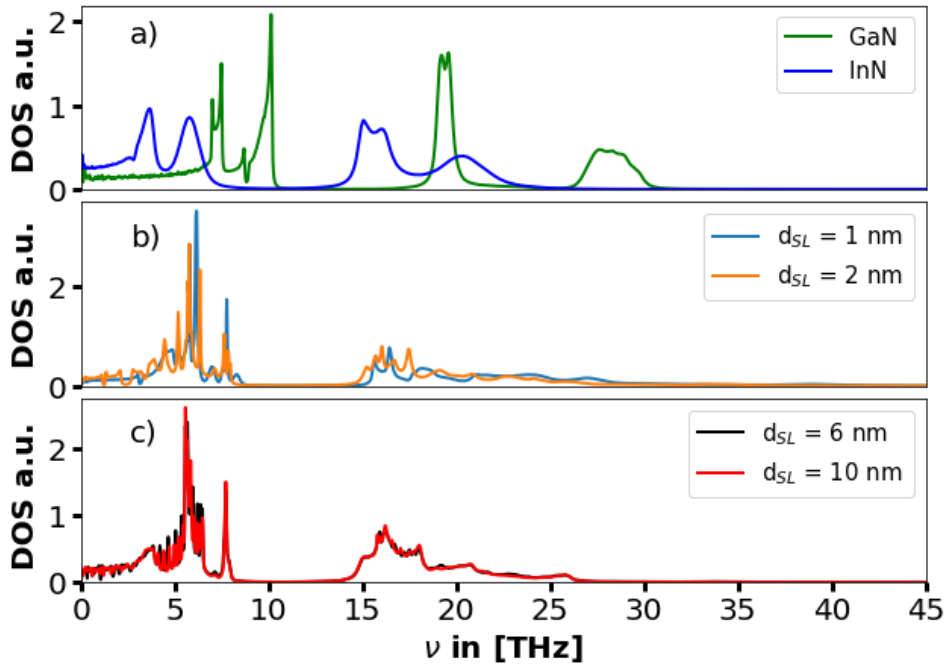

Figure 4.30.: DOS calculated from the VACF (z-component along the superlattice direction) for the superlattices with structure $1 \times 1 \times N$ unit cells.

parallel to the correlation direction. The absence of the fast drop in the cross spectral density function allows to extract the coherence length by fitting it to equation (2.40); at least in the low frequency part, which will be discussed later.

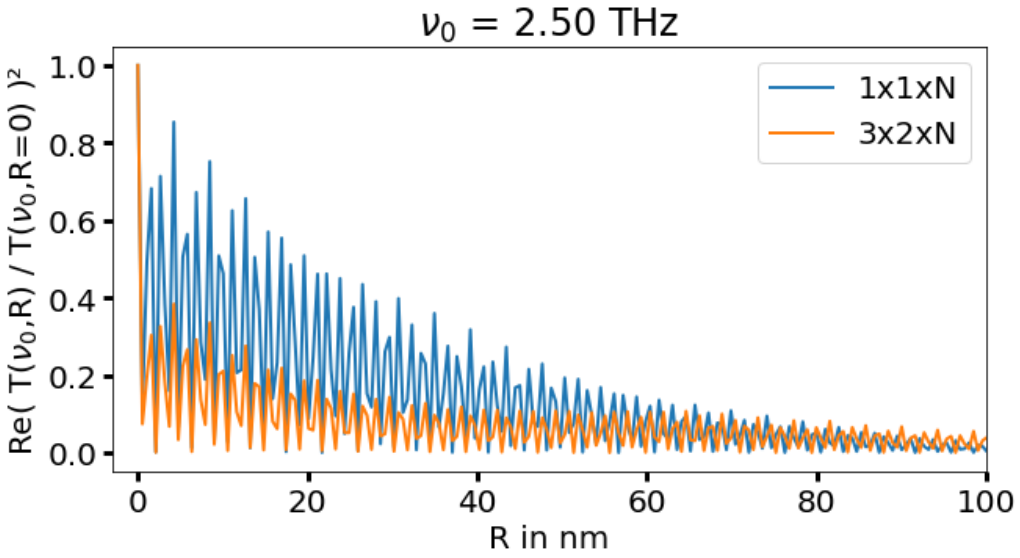

Figure 4.31.: Cross spectral density function for GaN/InN superlattices, obtained for different supercells. The drop in the function is absent for the $1 \times 1 \times N$ supercell.

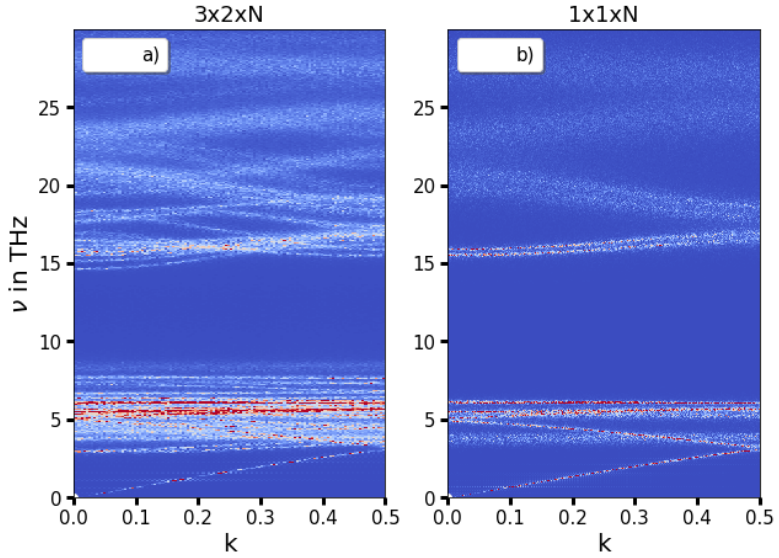

Figure 4.32.: Comparison of spectral energy densities of the z-velocity component for the GaN-InN superlattice. The wave-vector $\vec{k}$ points in the superlattice direction. The $3 \times 2 \times N$ superlattice (a) shows more branches than the $1 \times 1 \times N$ superlattice (b).

4.3.3. Results of coherence lengths

The coherence length for the GaN/InN superlattices is calculated by treating the cross spectral density function like a probability distribution function, and considering the coherence length as the distance where 95% of the correlated signal is account for. The correlation functions are smoothed to avoid any periodic self interactions (Approach C, Sec. 4.3.1). From the smoothed function the cross spectral density is calculated. In Figure 4.33, the coherence lengths are plotted for frequencies up to 27 THz, while in Figure 4.34 for frequencies up to 10 THz (i.e. zooming the low frequency range). The low frequency range is now better described (compared to the $3 \times 2 \times N$ supercell simulations). The coherence lengths are not limited by the supercell size and the values are trusted down to 1 THz. The coherence lengths reach up to 250 nm, suggesting that these phonon modes will be coherent. In agreement with the results for the $3 \times 2 \times N$ supercell, acoustic modes show a higher coherence length, and only the superlattice with the smallest period (1 nm) shows a significant coherence length in the non acoustic region.
For comparison, supercells of pure GaN and InN were simulated and treated as if they were superlattices. GaN shows the largest phonon coherence length for all the simulated systems, while InN (with a phonon MFP by orders of magnitude smaller than GaN) in comparison seems to have a very low phonon coherence. InN is limiting the phonon coherence in the superlattices and already the superlattice with a period of $d_{SL} = 6$ nm has the coherence length going to zero at the same frequency as the InN.
When comparing the coherence length for GaN and InN one needs to keep in mind that acoustic phonons of InN have a lower frequency. The modes of GaN at 5 THz are acoustic while the modes of InN at this frequency are optical. It is noted again here that the quantitative value of the coherence length does depend on the parameters for calculating the coherence length, but the qualitative trends hold. For completeness the coherence lengths of the transverse modes are shown in appendix A.6.1, which show a similar behavior.

As discussed before, the cross spectral density function does not show a fast drop after the first value (R=0). Therefore, although still with a large uncertainty, fitting the cross spectral density to an attenuated wave (equation

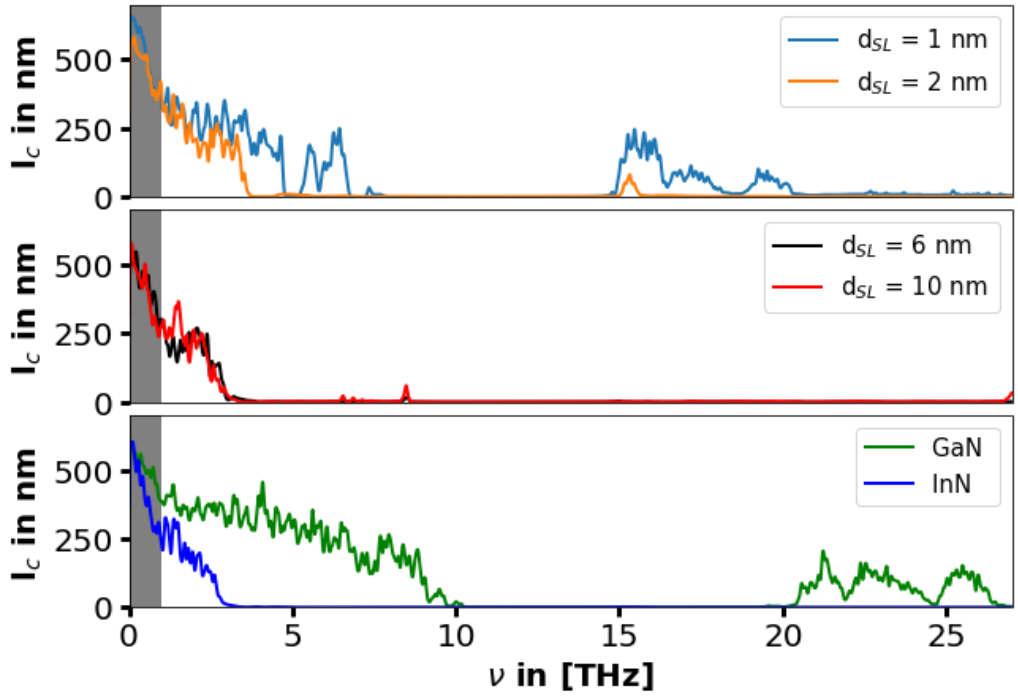

Figure 4.33.: Coherence length of the longitudinal modes for GaN/InN superlattices, obtained from MD simulations of $1 \times 1 \times N$ supercells. For comparison, the 'coherence length' of GaN and InN supercells are plotted as well.

2.40) is more promising. A fit is done for all superlattices. A similar trend in the coherence length, as the one calculated from the cumulative distribution function, can be seen in Figure 4.35. The coherence length calculated by the fitting predicts a lower value, and a faster decrease with frequency. Phonons with low values of coherence lengths ($< 1\,\text{nm}$) are not coherent and the coherence length does not have a physical meaning then. The regime of validity of the coherence lengths goes from approximately 1 THz to the end of the acoustic branch.

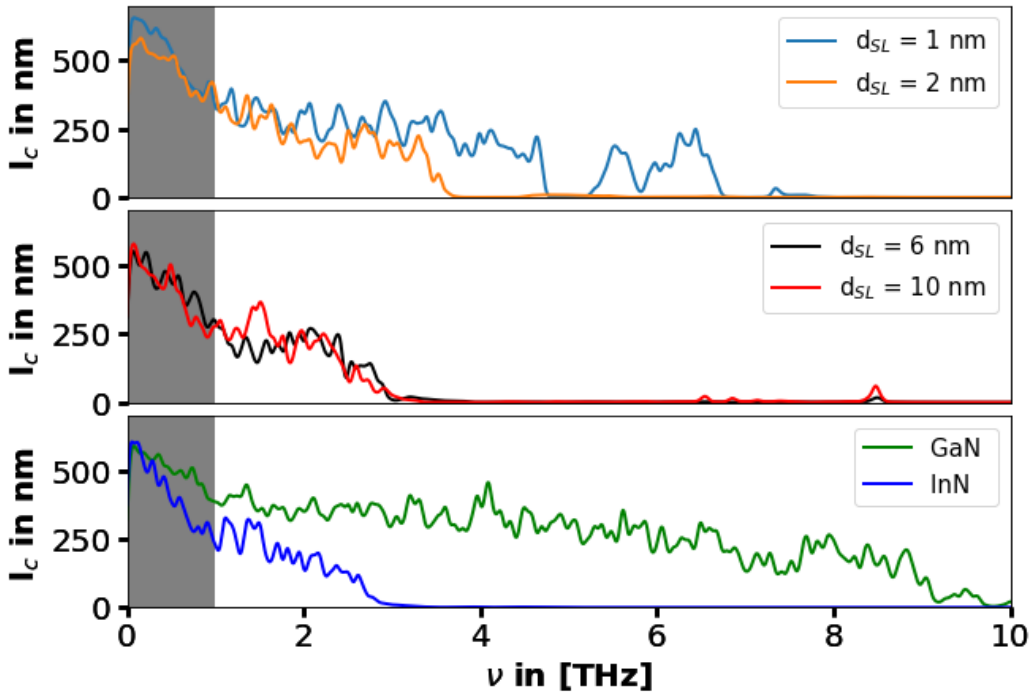

Figure 4.34.: Coherence length of the longitudinal modes of GaN-InN superlattices from the MD simulations of the $1 \times 1 \times N$ structured supercells for frequencies up to 8 THz. For comparison, the 'coherence length' of GaN and InN supercells are plotted as well. The InN seems to limit the phonon coherence of the superlattices and the coherence length of superlattices witch have layer thicknesses of InN a few nm falls to zero at the same frequency as for pure InN.

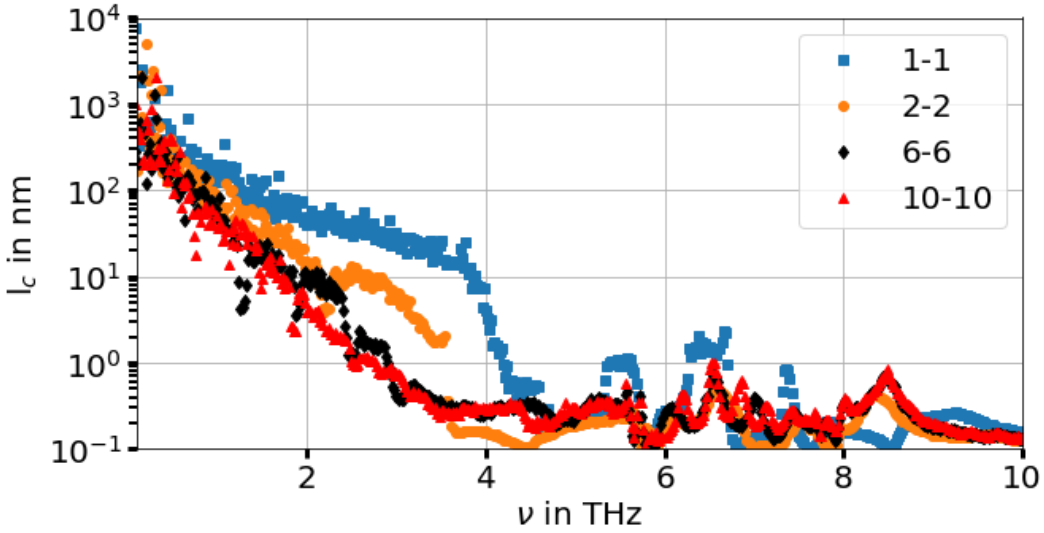

Figure 4.35.: Coherence lengths of the GaN/InN superlattices calculated from fitting an attenuated wave (equation 2.40) to the cross spectral density. The fitting procedure works best for low frequencies but has a large uncertainty.

Summary

The coherence length for GaN/InN superlattices with periods of 1, 2, 6 and 10 nm was calculated. The coherence lengths are estimated by the length, where the cumulative distribution function of the spectral density function takes into account 95% of the signal. The spectral density functions were smoothed before, to avoid periodic self interactions.
The 1 nm superlattice is the only superlattice, which shows non-negligible coherence length outside the acoustic region of the phonon spectrum. All the superlattices show high coherence length in the acoustic region, where the coherence length decreases with phonon frequency. Superlattices with lower superlattice period tend to have longer coherence lengths. For the supercells with structure $3 \times 2 \times N$, it was limited by the supercell size. Therefore, longer supercells are simulated, which also allow to resolve the low acoustic phones better. The superlattices show coherence lengths of 250 nm in the acoustic region.

4.3.4. Monolayers of InN in a GaN matrix

Until now we have presented superlattices of GaN/InN with layers of whole unit cells of GaN and InN, which to our knowledge have not yet been fabricated. Structures with a single monolayer of InN in a GaN matrix have been, however, fabricated [15]. Thus, the phonon coherence length of different structures with a monolayer of InN in a GaN matrix are simulated. The supercells are constructed using the superlattice unit cells shown in Figure 4.36. The monolayer is defined as a layer of GaN or InN, as depicted by the black squares in the figure. Structures with a InN monolayer every 4, 5 and 11 GaN-monolayers are simulated (ML 4-1, ML 5-1, ML 11-1). Moreover, a structure with alternating layers of GaN and InN (ML 1-1) is simulated for comparison. The layers are grown along the z-direction of the wurtzite unit cell. When the number of GaN layer is even, subsequent monolayers of InN will be shifted towards each other in the x-y plane. For example, for the case of ML 4-1 (Figure 4.36), one layer of InN (A) is shifted compared to the next layer of InN (B). The superlattice unit-cell (the smallest repeated unit) of the ML 4-1 is, therefore, larger than for ML 5-1. $1 \times 1 \times N$

supercells have again been considered, with a total number of 24000 atoms. For the monolayer structures, the cell relaxation was allowed in all directions during the NPT simulations, i.e. we have not fix the lattice parameters in x and y to the corresponding lattice parameters of InN (as done before).

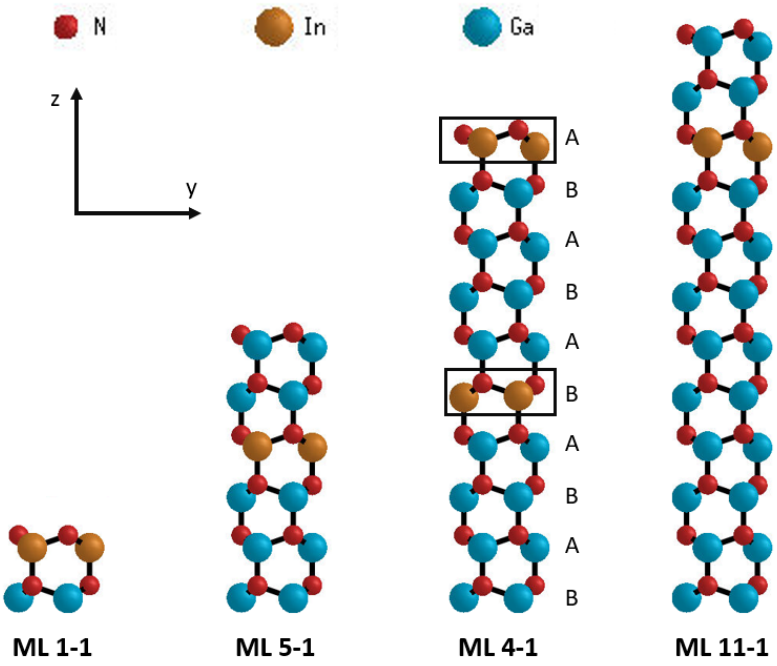

Figure 4.36.: Unit cells used to construct the supercells of monolayers formed by InN in a GaN matrix. The unit cells are stacked in the z direction.

The DOS of the ML structures (in z-direction) is very similar to the DOS of the pure GaN (Figure 4.37), which is expected as the major part of the material is made of GaN, separated by InN monolayers. The GaN DOS, in the range of frequencies between 7 to 10 THz, can be identified in the DOS of all monolayer supercells (except for the ML 1-1). Also, the high frequency part of the DOS of the monolayers, above 19 THz, is similar to that of GaN. The DOS of the monolayers, nonetheless, show more individual peaks and gaps in the low frequency part (4.38). The monolayer introduces a new symmetry to the crystal, which leads to Brillouin-zone folding and, hence, to the creation of band gaps. A high peak appears at 5.3 THz in all ML

structures, which is not present in GaN and InN. These modes are localized oscillations of In atoms in the monolayers. The DOS of the ML 1-1 does not follow the DOS of InN and GaN. Indeed, these DOS are not comparable between them. The ML 1-1 is rather a new material with another unit cell than a wurtzite structure. A lattice dynamics simulations reveled frequency bands from 20 to 60 THz for this material, leading to a low DOS for a large range.

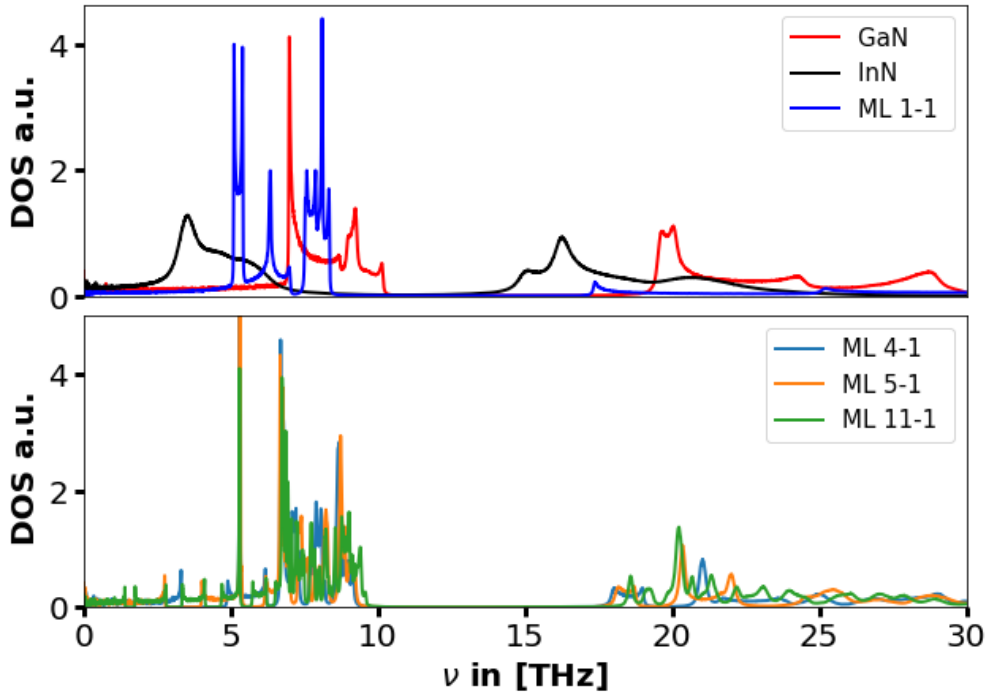

Figure 4.37.: DOS in z-direction of the ML-structures.

The coherence lengths are calculated by using the cumulative distribution function (4.3). The ML structures show a high coherence length (Figure 4.39) for frequencies below the large band gap. The ML 5-1 and ML 4-1 have even higher coherence lengths than GaN for frequencies until 3 THz. The values of the coherence lengths of the ML structures are trusted above 2.5 THz as for lower frequencies the coherence length approaches half the simulation box size.
Overall, the coherence length is high except in the phononic band gaps

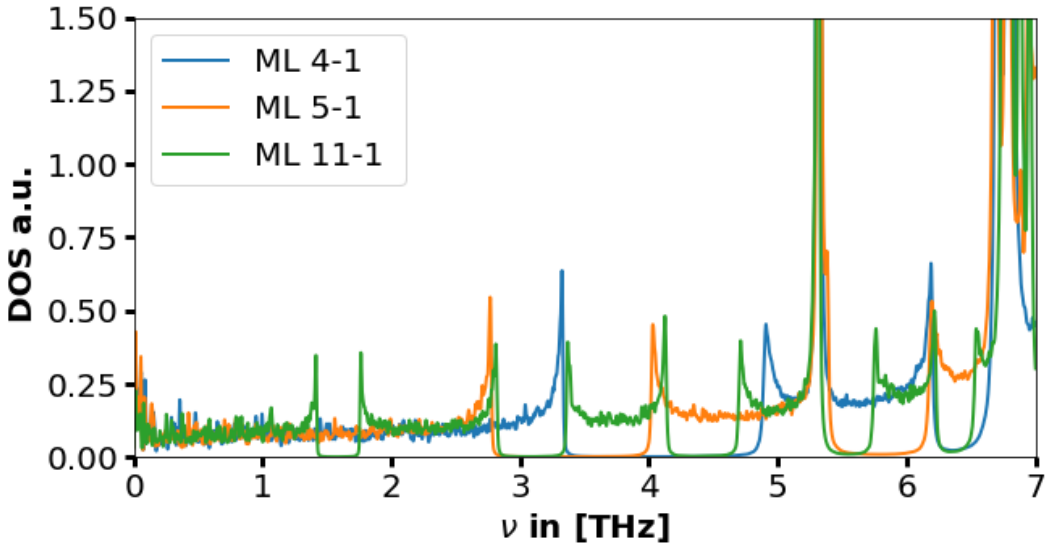

Figure 4.38.: DOS in z-direction of the ML-structures. The InN monolayer introduces a new lateral symmetry to the crystal which leads to Brillouin-folding and the appearance of gaps in the DOS.

(Figure 4.40) where there are no allowed modes (compare to the DOS in Figure 4.38). The ML 1-1 structure seems to have a large phonon coherence length for all its modes. The monolayer of InN in the GaN matrix does not lower the phonon coherence in the ML structures as it does for thicker layers of InN. The monolayer structures show a large phonon coherence length for the longitudinal modes even in the optical modes above the large band gap. In comparison, the transverse optical modes above the band gap do not show a high coherence length (see coherence length for the transverse modes in the appendix A.6.2).

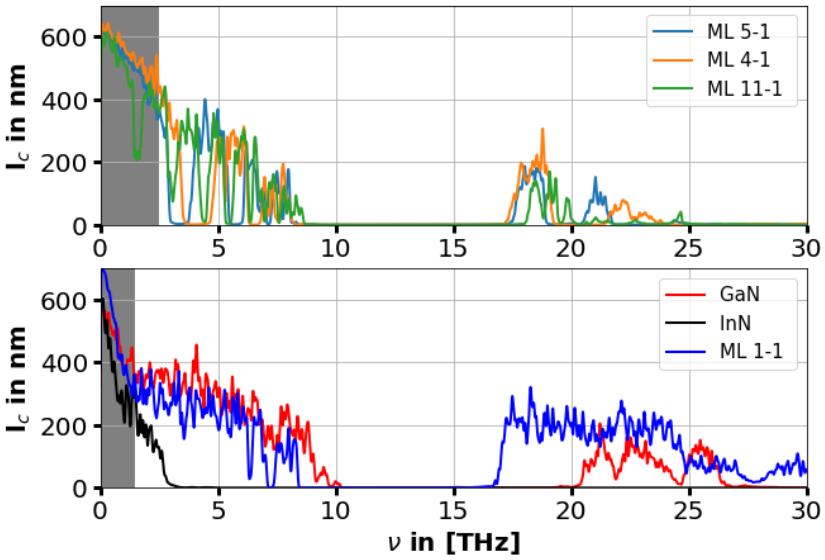

Figure 4.39.: Coherence length of longitudinal modes of the monolayer structures. All the ML structures show high coherence lengths in the acoustic region (below 10 THz) and above the large band gap.

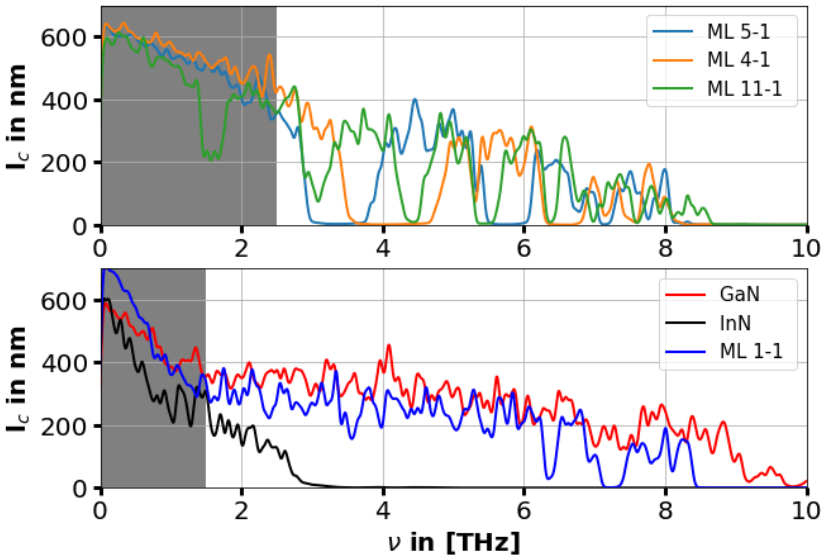

Figure 4.40.: The coherence length in the acoustic regions of the ML structures is high except for the frequencies where the DOS shows a gap. No allowed modes are at the gaps, and the coherence length is zero.

4.3.5. Summary of the results

A program to calculate phonon coherence lengths from molecular dynamics trajectories was developed and tested for a one-dimensional system and a three-dimensional FCC superlattice. For the one-dimensional superlattices, the coherence length was extracted by fitting the cross spectral density function to an attenuated wave. It was found that the frequency dependent coherence length is independent of the superlattice period for the acoustic modes. This is in agreement with previously reported data by Latour and coworker [12]. The quantitative values for the coherence length are, however, 2.5 times higher than the one reported by Latour and coworkers [12].

The fitting of the cross spectral density function to the attenuated wave turned out to be unreliable in a large frequency range for the FCC superlattices, and all other three-dimensional systems. Therefore, the coherence length was extracted by treating the cross spectral density function as a probability density function, calculating the cumulative distribution function from it, and defining the coherence length as the length for which the cumulative distribution function equals 95%.
The FCC-superlattices with the lowest superlattice period show the highest phonon coherence lengths. The DOS of the superlattices shows the appearance of additional band gaps due to Brillouin-zone folding, as with the superlattice period a new transnational symmetry is introduced to the crystal. The coherence length of the low frequency, acoustic phonons is high (up to 400 nm), and limited by the supercell size of the MD simulation.

The DOSs of the GaN/InN superlattices show as well additional gaps due to Brillouin-zone folding. The DOSs of superlattices with periods 1 and 2 nm depends on the superlattice period (fingerprint of phonon coherence), while the DOSs of larger periods (6 and 10 nm) are not affected. It was found that the extraction of the coherence length does depend strongly on several parameters when calculating the coherence length. The quantitative values have a large uncertainty, while trends in the coherence length are mostly independent from the parameters. For the GaN/InN superlattices, mostly only the acoustic modes show a non-negligible coherence length. The superlattice with the smallest superlattice period shows the highest phonon coherence lengths, with coherence lengths of few hundred nm. It is

the only GaN/InN superlattice, which shows some coherence length above the band gap.

Structures made of monolayers of InN in a GaN matrix were also simulated to study phonon coherence. The DOS of this structures is close to that of GaN, with band gaps appearing due to the additional symmetry. The coherence length of the monolayer structures is close to the coherence length of GaN. The acoustic phonons show the highest coherence lengths, but optical modes at high frequencies also show a non-zero coherence length. As the InN-monolayer structures show a high phonon coherence length and because they have been fabricated experimentally [15], they are the most promising candidates out of the systems studied in this thesis for showing high phonon coherence.

5. Discussion, Summary and Outlook

The coherence of phonons can alter the phonon properties; therefore it is interesting to find materials which show coherent phonon transport. Superlattices are periodic crystals of alternating layers of two or more materials and are promising candidates to show high phonon coherence. Because the fabrication of superlattices in the laboratory are often expensive, simulations are used to find possible structures which show high phonon coherence. MD simulations are used to investigate the coherence of phonons in superlattices and to calculate the coherence lengths. The correlations of the atoms velocities in the superlattice are observed throughout the MD simulations, and the coherence lengths are calculated with a methodology adapted from literature [11, 12]. Two test-systems are first investigated, before studying the coherence in GaN/InN superlattices.

As a first test system, one-dimensional superlattices, which interact by means of a Lennard-Jones potential, are simulated for three superlattice periods (1.53, 6.11 and 24.5 nm). The coherence length is estimated by fitting an attenuated wave to the cross spectral density function. Low frequency modes have the higher coherence length. Acoustic modes have low frequencies and show the highest phonon coherence lengths. In the one-dimensional case, it is found that for a given frequency the coherence length does not depend on the superlattice period. To define whether the phonons are transported coherently through the superlattice or not, the coherence length is compared to the superlattice period. As the different superlattices have different periods, the frequency range in which the phonon transport is coherent, is larger for superlattice with lower period-length (see Figure 4.10). In Ref. [12], the same one-dimensional systems are studied. In this work the coherence lengths are found to be a factor of roughly 2.5 higher. The origin

of this deviation could not be tracked, and could possibly be a constant factor in the formal definition of the coherence length.

The second test system was an FCC-superlattice interacting with a Lennard-Jones potential. Five different superlattice periods are simulated (1, 2, 4, 8,16 nm). Compared to the one-dimensional system, it was more difficult to extract the coherence length from the calculated cross spectral density function. As fitting an attenuated wave to the cross spectral density function was not successful, the coherence length is estimated as the length, where 95% of the total correlated signal is taken into account. The coherence length of the acoustic phonon modes is high and goes up to a few 100 nm (Figure 4.19). Indeed, in the large part of the acoustic region, the coherence is limited by the supercell size. The coherence length decreases with increasing phonon frequency, but contrary to the one-dimensional system, the coherence length depends on the superlattice period. Superlattices with lower superlattice period show higher phonon coherence.

As a real system, GaN/InN superlattices are investigated as well as structures with monolayers of InN in a GaN matrix. The latter have been fabricated experimentally [15]. The extraction of the coherence length is done like for the FCC-superlattices, but the numerical values depend on the parameters of the calculation. Different attempts are made to reduce the noise in the cross spectral density function. For the GaN/InN systems the coherence length is calculated by leaving out any signal from periodic self-interactions. Large coherence lengths are found for the acoustic modes in all studied systems. Four different superlattices with periods 1.06, 2.12, 6.36 and 10.6 nm are simulated. The superlattice with the lowest period show the highest phonon coherence length. Because the coherence length in the acoustic region was limited by the supercell size (Figure 4.27), larger supercells are simulated (coherence lengths in Figure 4.33). Again the superlattices with lower periods show longer phonon coherence lengths. up to 250 nm for frequencies up to a few THz.
The monolayer structures (with 4, 5 and 11 monolayers of GaN between 1 monolayer of InN) show as well large coherence lengths in the acoustic region (Figure 4.39), up to 300 nm. There is no big difference in coherence length between the different monolayer-structures.

The most promising candidates for structures with high phonon coherence lengths are the monolayer structures. They show high phonon coherence lengths. Monolayers of InN can be grown on GaN [15], while thicker layers of InN on GaN (for superlattices) are likely not stable without misfit dislocations [14].

Discussion

The quantitative values of the coherence length often depend on several parameters of their calculation. The trends generally hold when varying a parameter, but the quantitative values change. Often, especially in the acoustic region, the values are limited by the supercell size. Sometimes only in a small frequency region the values of the coherence lengths can be trusted. For low frequencies, the supercell size is the limiting factor. For high frequencies the coherence lengths are low and difficult to extract. If the coherence lengths are lower than than the typical structure size, it is not interesting for nano-engineering.

In the following, considerations about the method used in this thesis, and possible improvements are discussed.
The method is based on the statistical fluctuations of the atomic velocities around their equilibrium positions. Several independent simulations of the same system should be done for better statistics. This lowers the noise in the data and improves the reliability of the coherence length. Only one independent run was done for each superlattice in this thesis, while for example in Ref. [11] an average over 10 independent simulations was made for the FCC-superlattices. An average over more simulations should be done for all simulations. Of course, this means a significantly higher computational demand.

The coherence length of acoustic modes are often longer than half of the supercell size, and are limited by it. These modes are the most interesting because they show a high coherence length. To better resolve these coherence lengths, a careful analysis of the dependence on the supercell size needs to be done. By systematically varying the length of the simulation box, one can understand the dependence of the coherence length on it. For a

given frequency (or regime) of interest, the simulation cell size should be increased until the coherence length does not depend anymore on it. This, of course, is computationally demanding as the simulation boxes can become very large.

MD simulations with a few ten thousands of atoms , as well as their post-processing, are computationally expensive. The time-step of the MD simulation cannot be made larger, as this would give erroneous trajectories of the atoms. But the computational demand of the post-processing could be lowered by using a longer sampling step Δt. The sampling step defines the maximum frequency $\nu_{max} = \frac{1}{2\Delta t}$. This can be chosen so that the relevant frequencies (i.e. those of interest) are still captured.

The methodology used in this thesis, allows to calculate the coherence lengths frequency dependent. But it is not possible to distinguish different modes which have the same or similar frequency. Often the calculation of the coherence length is difficult, as the cross spectral density function follows an unexpected behavior, and does not follow an attenuated wave. This might be a consequence of two or more modes at the same frequency. In this case, the resulting cross spectral density is the sum of two or more attenuated waves, which makes the fitting difficult.
A possible way to distinguish two modes with the same frequency is to calculate the energy spectral density. This is done by mapping the MD velocities into the mode eigenvectors of the system. These latter have to be calculated beforehand by using LD. As the eigenvectors [54] (and frequencies) are temperature dependent, thermal expansion should be considered for the LD calculations.

The MD simulations are run with periodic boundary conditions. The structure of the supercells defines the allowed phonon wave-vectors. The more often a unit cell is replicated in one direction for the simulation box, the more allowed wave vectors are in this direction. When calculating the coherence lengths, the supercells are extended many unit cells along the superlattice direction but just one to few in the perpendicular directions. This limits the allowed values of the wave-vector in the perpendicular directions to a few values, and in the case of an extension of one, to the Γ point.
The interaction and scattering of the modes in the superlattice direction with modes that are not in the superlattice direction is limited. This may

have a potential influence on the coherence length.
Longitudinal and transverse modes with wave-vectors not in the superlattice direction have a contribution to the atomic velocities during the simulations. Only modes with wave-vectors in the superlattice direction will be coherent, because they sense the superlattice periodicity. With the methodology used in this thesis, it is not possible to separate the 'coherent' contributions to the velocities from modes in the superlattice direction and the 'non-coherent' contributions from other modes. By calculating the correlations from the velocities, and from that the coherence length, the 'non-coherent' part can lower the coherence length.

The best resolution in frequency that can be achieved for the DOS and the cross spectral density function is defined by the total simulation time $\nu_R = \frac{1}{t_{sim}}$. When the resolution in frequency is smaller than the separation of the allowed modes in a system, the individual modes can be distinguished in the DOS. This requires that the modes have sharp frequencies and are not spread out so that they overlap with neighbouring modes. For example, as can be seen in the example in Figure 4.29, the discrete modes in the acoustic region can be distinguished in the DOS. One could just calculate the coherence lengths for the phonon frequencies, which have been previously identified with LD. This approach would not work for a non-dispersive optical band, as the frequencies would overlap.

Due to the periodic boundary conditions, a coherent wave packet can cross the simulation box several times and stays coherent for this long, if the simulation time is long enough. In Figure 4.22, the correlations of a superlattice is shown as a function of time and distance in a 2D plot, suggesting that the acoustic modes stay coherent for a long time. It might be possible to follow the 'path' of this signal to learn for how long it will stay coherent. However, it is not clear how the wave-packets traveling several times through the simulation box affect the cross spectral density function and, hence, the coherence length. To avoid that a wave packet crosses the simulation box several times during the simulation, one can lower the simulation time or make the simulation size larger so that the modes do not have enough time to cross the whole simulation box more than once.

Another aspect to keep in mind is the resolution in distance of the cross spectral density function. The resolution is limited by the length of the

superlattice unit cell, because only after this length, the same atoms (with the same physical surrounding) appear again. A superlattice with a large period has a poor resolution in distance. Thus, in this thesis the single materials unit cell is taken as the repeat unit for calculating the cross spectral density function, instead of the superlattice unit cell for higher resolution. For the GaN/InN systems, the materials unit cell was used as the repeat unit. GaN and InN have different lattice parameters; strictly speaking, the superlattice-unit cell is the repeat unit with translational symmetry. In future, it should be investigated, if this describes the cross spectral density function correctly. Also if the resolution corresponding to the superlattice period is already enough. The superlattice unit cell-resolution, might be enough to detect coherence lengths in the order of the superlattice period. Smaller coherence lengths are not of interest, as phonon transport is classified as coherent only if the coherence length exceeds the superlattice period.

Last but not least, it is important to comment about the reliability of the force field potential. The potential [38] used to simulate the GaN/InN superlattices does not reproduce the phonon properties of GaN and InN very well. The phonon dispersion relation deviates from DFT data already at the Γ point. While the thermal conductivity of GaN simulated with the potential comes close to reference data from the literature, the thermal conductivity for InN is underestimated by an order of magnitude compared to literature. This suggests that the potential does not properly describe the phonons of InN. The validity of the calculated values for the coherence length depends as well on the capability of the force field to describe the phonons correctly.

Outlook

When one is confident with the simulations and the validity of the coherence length one obtains, further analysis of the coherence lengths is possible, like temperature and pressure dependence and the influence of defects. The methodology can as well be easily adapted to study a different superlattice, if a force-field potential is available. Higher temperature increases the scattering rates and reduces phonon coherence. In an experiment, it is difficult to create perfect structures with no defects. Defects and impurities

in the crystal are disturbing the perfect crystal structure and inter-facial mixing of the materials can occur. The influence of imperfections on the coherence lengths needs to be studied as well as the dependence on the defect-concentration.
Wave-packet dynamics can be done to verify if the wave-packets stays coherent or will decay over time.

List of Figures

Appendix A.

A.1. Wiener-Khinchin- theorem and cross correlation theorem

In this section the Wiener-Khinchin theorem [55] and the cross correlation theorem are presented. The cross correlation theorem is a generalization of the Wiener Khinchin theorem and is widely used in this work to calculate correlation functions efficiently. The Wiener-Khinchin theorem states that the auto-correlation function of a wide-sense stationary random process and the power spectrum of the signal are Fourier-transform pairs. A signal $E(t)$ is wide-sense stationary, when its mean value and auto-correlation function are time invariant. As the system is in equilibrium, and does not change over time, wide-sense stationary is fulfilled for the velocities. As the atoms vibrate around the equilibrium position, the mean of the velocity will be zero (otherwise the system will show a constant drift). Moreover, the VACF is just dependent on the time difference $\tau = t_2 - t_1$. Thus, the conditions for using this theorem are fulfilled for our system.

Let $E(t)$ be a wide-sense stationary random process. The Fourier transform of $E(t)$ is defined by:

$$E(t) = \int E_\omega e^{-it\omega} d\omega. \tag{A.1}$$

The auto-correlation function of $E(t)$ is $C(\tau)$:

$$C(\tau) = \int E^*(t) E(t+\tau) dt. \tag{A.2}$$

The asterisk * denotes the complex conjugate. Inserting equation (A.1) in the auto-correlation function (A.2) results in the following expression:

$$C(\tau) = \int \left[\int E^*_\omega e^{it\omega} d\omega \right] \left[\int E_{\omega'} e^{-i(t+\tau)\omega'} d\omega' \right] dt = \tag{A.3}$$

$$= \int \int \int E^*_\omega E_{\omega'} e^{it(\omega-\omega')} e^{-i\tau\omega'} d\omega d\omega' dt \tag{A.4}$$

Using the identity

$$\int dt e^{it(\omega-\omega')} = \delta(\omega - \omega'), \tag{A.5}$$

one can simplify:

$$C(\tau) = \int E^*_\omega E_\omega e^{-i\tau\omega} d\omega = \int |E_\omega|^2 e^{-i\tau\omega} d\omega. \tag{A.6}$$

The right-hand side is the Fourier transform of the power spectrum of the signal $E(\omega)$. The auto-correlation function can be expressed, then, as the Fourier transform (FT[]) of the power spectrum:

$$C(\tau) = \mathrm{FT}_\omega \left[|E_\omega|^2(\tau) \right] \tag{A.7}$$

The Wiener-Khinchin theorem is a generalization of the cross-correlation theorem. Similarly, one can calculate the cross-correlation using the cross-correlation theorem: Let $x(t)$ and $y(t)$ be two wide-sense stationary random processes. The Fourier-transforms of $x(t)$ and $y(t)$ are:

$$x(t) = \int x(\omega) e^{-i\omega t} d\omega \tag{A.8}$$

$$y(t) = \int y(\omega) e^{-i\omega t} d\omega \tag{A.9}$$

The cross correlation function $\langle x, y \rangle$ of $x(t)$ and $y(t)$ is:

$$\langle x, y \rangle(\tau) = \int x^*(t) y(t+\tau) dt \tag{A.10}$$

Setting equations (A.8) and (A.9) into (A.10)

$$\langle x, y \rangle(\tau) = \int \left[\int x^*(\omega) e^{it\omega} df \int y(\omega') e^{-i\omega'(t+\tau)} d\omega' \right] \tag{A.11}$$

$$= \int \int \int x^*(\omega) y(\omega') e^{it(\omega-\omega')} e^{-i\tau\omega'} dt d\omega d\omega' \tag{A.12}$$

Using the identity (A.5) one obtains:

$$\langle x, y \rangle(\tau) = \int \int x^*(\omega) y(\omega') e^{-i\omega'\tau} \delta(\omega - \omega') d\omega d\omega' = \int x^*(\omega) y(\omega) e^{-i\omega t} d\omega \tag{A.13}$$

The right hand side of this equation is the Fourier transform of the multiplication of the Fourier transformed signals, which is equal to the cross correlation function of those signals.

We use these theorems in order to efficiently calculate the cross-spectral density function (Eq. 2.37). Fast-Fourier-Transform (FFT) is a very fast method to calculate Fourier transforms of discrete signals. It is faster (often more than by one order of magnitude) to calculate the cross- and auto-correlation functions using this theorems. First, calculating the Fourier transforms of the velocities $v(\omega)$, and then from that the power-spectra ($|v(\omega)|^2$) or cross-spectral densities ($v_i^*(\omega) v_j(\omega)$). For the investigation of the coherence length only the cross spectral density functions (Eq. 2.37) are needed. The FFTs towards the cross- and auto-correlations are not needed, although the calculations are faster if one wants to analyze also the correlation functions. As some of the systems have a few 10000 atoms, many correlation functions need to be calculated. Hence, the theorems presented here provide a significant speed up of the post-processing step of the MD simulations.

A.2. Elastic constants

The elastic constants are physical properties that a force-field-potential should reproduce. Table A.1 lists the elastic constants (using Voigt notation) at room temperature calculated with the modified Stillinger-Weber potential. As it can be seen, the values are in reasonably good agreement with the reference data [56, 57]

Table A.1.: Elastic constants of GaN and InN calculated from MD (1) using the modified Stillinger-Weber potential compared to literature values.

	GaN (1)	GaN [56]	InN (1)	InN [57]
C11	427	390	269	190
C22	427	390	269	190
C12	80	145	106	104
C13	88	106	70	121
C33	394	398	173	182
C44	180	104	43	10

A.3. Thermal conductivity of GaN and InN with the modified Stillinger-Weber potential

The Stillinger-Weber force field potential[38], used to simulate superlattices of GaN/In, was parametrized without considering the phonon proprieties. As already remarked, the potential does not perfectly reproduce the ab-initio phonon data (Figure 3.2 and Figure 3.3).

To estimate the impact of the potential limitations to describe phonon related properties, the thermal conductivity of GaN and InN was calculated by two methods: Non-equilibrium molecular dynamics (NEMD) and a combination of lattice dynamics and molecular dynamics (normal mode decomposition).

A.3.1. Non equilibrium molecular dynamics

The calculation of the thermal conductivity, κ, with NEMD is based on the Fourier-law of heat conduction (A.14). In general, the thermal conductivity is a tensor $\kappa_{\alpha\beta}$:

$$\kappa_{\alpha\beta} = -\frac{J_\alpha}{dT/dx_\beta}, \tag{A.14}$$

where J_α is the heat flux in the direction α and dT/dx_β the temperature gradient in the direction β.

In the MD-simulation cell, two areas are defined as the hot and cold regions, where two temperatures are imposed by thermostats. Heat will flow from the warm to the cold bath and a temperature gradient is build up in the not thermostatted region between the hot and the cold bath. The temperature profile, $T(x)$, as a function of distance, x, is calculated from the kinetic energies of the atoms at position x and the heat current can be calculated from the amount of energy the thermostat needs to add/remove from the hot/cold region.
The finite size L of the simulation cell has influence on the thermal conductivity. The hot and cold regions are boundaries for the phonons, limiting their phonon mean free path. The inverse of the thermal conductivity κ_L is a linear function of the system size, and the thermal conductivity of infinite size κ_∞ can be calculated from following equation [58]:

$$\frac{1}{\kappa_L} = \frac{1}{\kappa_\infty} + \frac{K}{L} \tag{A.15}$$

Therefore, several different simulation box sizes have to be simulated to calculate the thermal conductivity. Usually at least three different sizes are simulated, to see if the linear behavior in equation (A.15) is reached. For GaN and InN several different simulation box sizes have been simulated, as it became clear that the first simulation boxes were to small. An example of the temperature profile in the simulation box for GaN is shown in Figure A.1. The temperature profile is calculated by averaging the temperature of a slab of atoms over the simulation time. The temperature gradient is calculated by a simple linear fit.

For GaN simulation cells with lengths $L = 3.7$, 5.6, 7.4, 11.1, 14.9, 23.3, 46.5, 93.1 and 186.1 Å are simulated and for InN cells with lengths 4.1, 6.1, 8.2, 12.3, 16.4, 25.6, 51.2 and 102.3 Å. As one can see in Figure A.2 and Figure A.3 the linear trend of equation (A.15) is not followed. The smallest cells are to small and strongly cut the phonon MFP. For GaN only the values of the two largest cells are used to calculate κ_∞ by a linear regression, while for InN the values of the three largest values are used. For GaN a thermal conductivity of $\kappa = 211\,\mathrm{W\,m^{-1}\,K^{-1}}$ is calculated and for InN a small value of $\kappa == 6.3\,\mathrm{W\,m^{-1}\,K^{-1}}$.

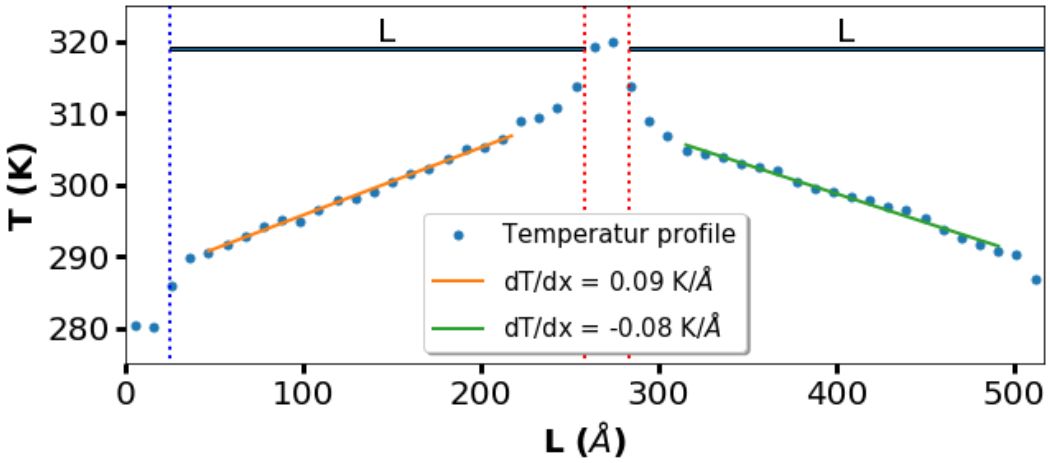

Figure A.1.: Temperature profile in a NEMD calculation of GaN. The temperature gradient is calculated by a fit to the temperature profile. Together with the heat flux calculated from the energy added/removed in the hot and cold regions, the thermal conductivity can be calculated using Fourier's law (Eq. A.14).

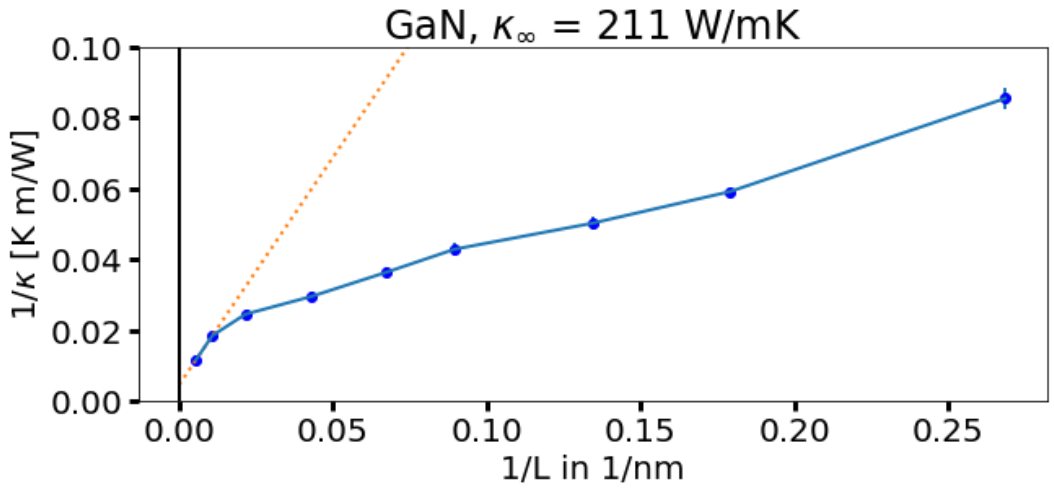

Figure A.2.: Inverse of the thermal conductivity κ as a function of the inverse simulation box length L from NEMD simulations for GaN. Most of the simulation boxes are too small and limit largely the phonon MFP. Only the values of the two largest simulation boxes are taken into account to calculate the thermal conductivity of GaN: $\kappa_\infty = 211\,\mathrm{W\,m^{-1}\,K^{-1}}$

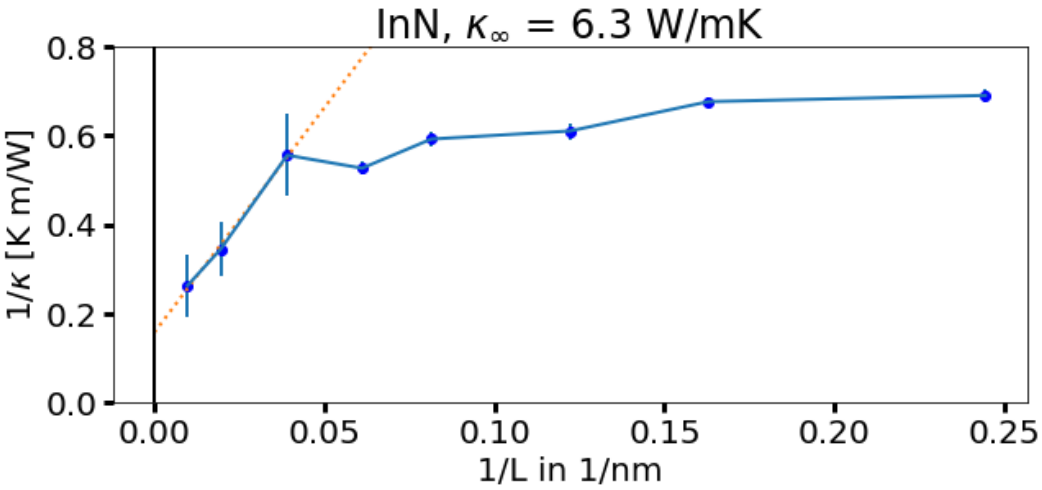

Figure A.3.: Inverse of the thermal conductivity κ as a function of the inverse simulation box length L from NEMD simulations for InN. Only the values of the three largest simulation boxes are taken into account to calculate the thermal conductivity of InN: $\kappa_\infty = 6.3\,\mathrm{W\,m^{-1}\,K^{-1}}$

A.3.2. Normal mode decomposition: LD and MD

The Boltzmann Transport equation under the relaxation time approximation leads to following formula for the thermal conductivity (A.16).

$$\kappa = \sum_{\boldsymbol{k}} \sum_{p} c_{ph}(\boldsymbol{k}, p) v_g^2(\boldsymbol{k}, p) \tau(\boldsymbol{k}, p) \tag{A.16}$$

The sum goes over all wave-vectors $\boldsymbol{k}$ and branches p of the phonon dispersion. The group velocity v_g is calculated from lattice dynamics. c_{ph} is the volumetric phonon specific heat and is a quantum mechanical expression:

$$c_{ph} = \frac{k_B x^2}{V} \frac{e^x}{(e^x - 1)^2} \tag{A.17}$$

Table A.2.: Thermal conductivity of GaN. All the values are in $\mathrm{W\,m^{-1}\,K^{-1}}$

	NEMD	LD and MD	BTE [60]	[53]	[61]	[62]	[63]
κ_a	-	207	235	363	335	$160-220$	230
κ_c	211	232	208	409	316		

$x(\boldsymbol{k}, p)$ is the energy of the mode with frequency $\omega(\boldsymbol{k}, p)$, divided by the thermal energy $k_B T$: $x = \hbar\omega / k_B T$. k_B is the Boltzmann constant, $\hbar$ the reduced Plank constant. The phonon lifetimes $\tau(\boldsymbol{k}, p)$ are calculated by normal mode decomposition using the **Dynaphopy** package. **Dynaphopy** calculates the line widths $\Gamma(\boldsymbol{k}, p)$ of the modes from a normal mode decomposition. The lifetimes are the inverse of the line widths : $\tau = \frac{1}{2\Gamma}$. The thermal conductivity of GaN and InN is anisotropic. For GaN $\kappa_a = 207\,\mathrm{W\,m^{-1}\,K^{-1}}$ and $\kappa_c = 232\,\mathrm{W\,m^{-1}\,K^{-1}}$ is obtained at 300 K. κ_c is comparable to the value obtained from NEMD simulations. Using the Boltzmann Transport solver **ShengBTE** [59] with ab initio input from a database [60], thermal conductivity of $\kappa_a = 235\,\mathrm{W\,m^{-1}\,K^{-1}}$ and $\kappa_c = 208\,\mathrm{W\,m^{-1}\,K^{-1}}$ is calculated. The values are comparable but the reference has a lower thermal conductivity in c-direction than in a-direction. Other theoretical studies show a higher thermal conductivity up to $400\,\mathrm{W\,m^{-1}\,K}$, while experimental studies report thermal conductivity in the range of $160\,\mathrm{W\,m^{-1}\,K}$ to $230\,\mathrm{W\,m^{-1}\,K}$. The values are presented in table A.2.

For InN thermal conductivities of $\kappa_a = 5.2\,\mathrm{W\,m^{-1}\,K^{-1}}$ and $\kappa_c = 10.1\,\mathrm{W\,m^{-1}\,K^{-1}}$ are calculated (with LD and MD). The thermal conductivity in c-direction is higher than the result of the NEMD simulations ($6.3\,\mathrm{W\,m^{-1}\,K^{-1}}$). Values for the thermal conductivity of InN in literature are rare but all predict a significantly higher thermal conductivity. An early study [64] reported an experimental value of $45\,\mathrm{W\,m^{-1}\,K^{-1}}$ and predicted for an ideal lattice $\kappa = 176\,\mathrm{W\,m^{-1}\,K^{-1}}$. An experimental study [65] reported a thermal conductivity of $120\,\mathrm{W\,m^{-1}\,K^{-1}}$, while a study [42] from first principles reports a thermal conductivity of $\kappa_a = 130\,\mathrm{W\,m^{-1}\,K^{-1}}$ and $\kappa_b = 145\,\mathrm{W\,m^{-1}\,K^{-1}}$.

From the NEMD and the normal mode decomposition simulations similar results for the thermal conductivities for the same system are calculated. The results for the thermal conductivity of GaN are comparable to literature al-

though other theoretical studies report a higher thermal conductivity. Using the modified Stillinger Weber potential [38], the thermal conductivity of InN results in a low value for both methods. The Stillinger-Weber potential [38] underestimates the thermal conductivity of InN by an order of magnitude compared to values from literature.

A.3.3. Phonon mean free path

From the lifetimes τ of the phonon modes and the group velocities v_g the phonon mean free path Λ is calculated by $\Lambda = \tau v_g$. In Figure A.4 the phonon mean free path spectra of GaN and InN are shown. It can be seen that with the Stillinger-Weber potential [38] significantly higher mean free paths are predicted for GaN than for InN. For InN only few phonon modes have mean free paths above 10^1 nm, while many modes of GaN have a mean free path lying between 10^2 nm and 10^3 nm. The mean free paths of GaN are predicted about an order of magnitude larger than for InN.

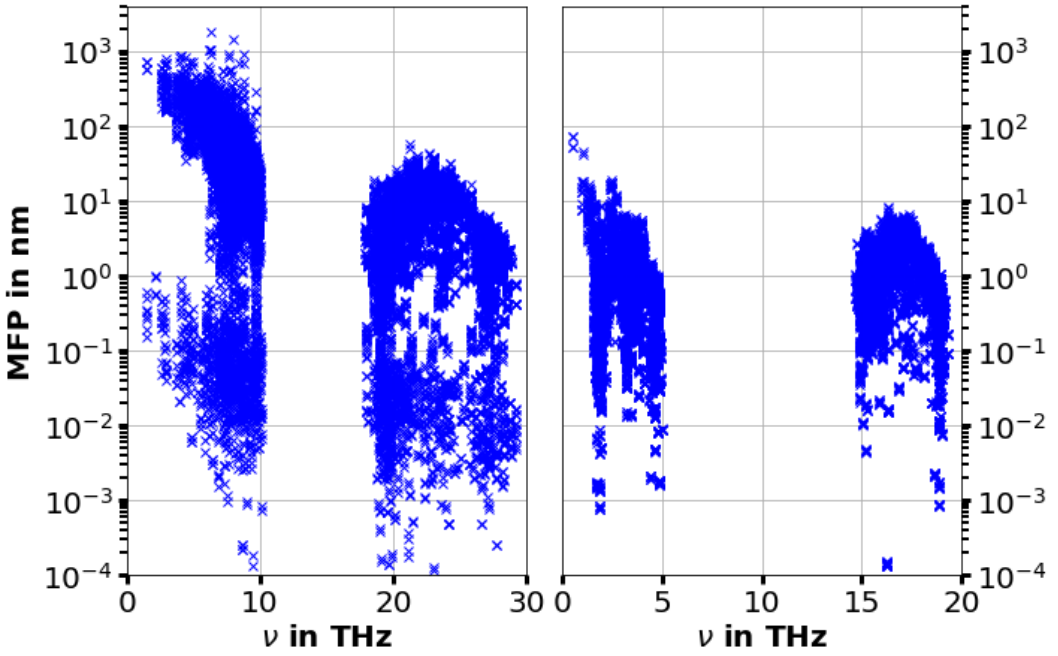

Figure A.4.: Phonon mean free path spectra of GaN (left) and InN (right) calculated using the Stillinger-Weber potential [38].

A.4. Stability of GaN/InN superlattices with the modified Stillinger Weber potential

In a short investigation, before the start of the thesis, the stability of the superlattices of GaN/InN was tested with the Stillinger-Weber potential from literature [38]. Here the results are shortly presented to motivate the constriction of the a-lattice parameter of GaN/InN superlattices to InN when doing MD simulations. When fixing the a-lattice parameter to GaN, the coherent crystal structure becomes disordered while relaxing the c-parameter as can be seen in Figure A.5. When fixing the a-parameter to InN the crystal structure is preserved (Figure A.6). When an average lattice parameter was chosen, the structure was stable as well. Still the lattice parameter of InN was used for the simulations.

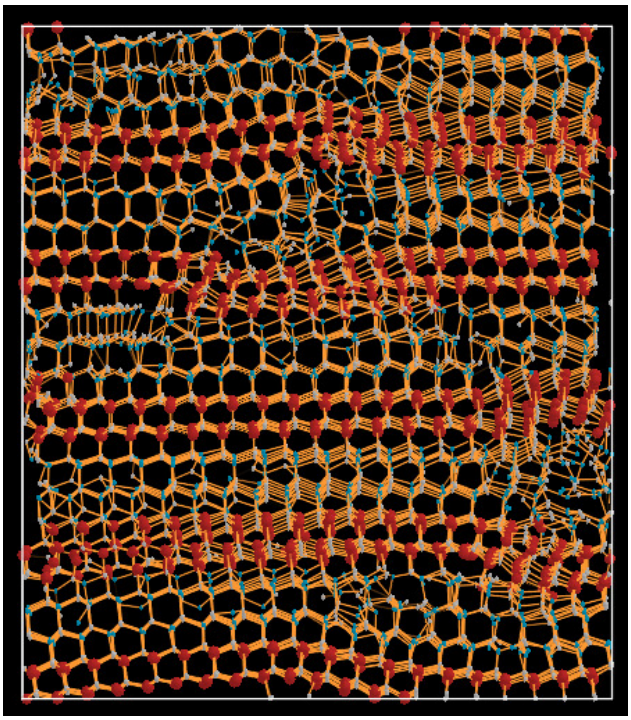

Figure A.5.: Disordered superlattice after relaxation of the structure in superlattice direction, while keeping the lattice parameter perpendicular to the superlattice direction fixed to GaN.

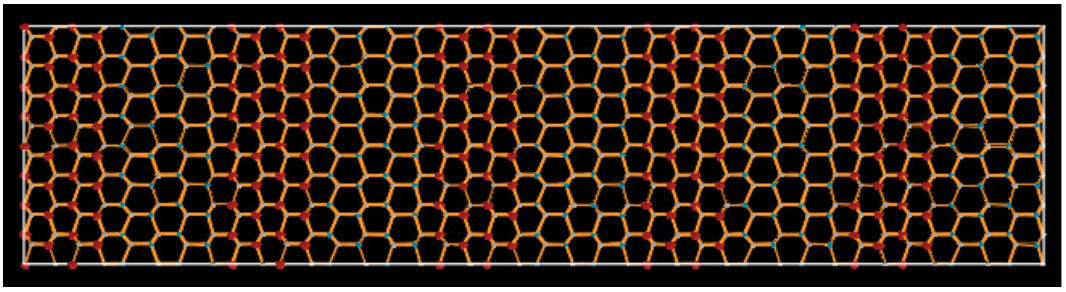

Figure A.6.: Crystal structure is stable, when keeping lattice parameter perpendicular to the superlattice direction fixed to InN.

A.5. Unit cell and Brillouin-zone of the LJ-superlattice

The unit cell of the Lennard-Jones superlattice with period $d_{SL} = 1\,\text{nm}$ is shown in Figure A.7, which was used to calculate the phonon dispersion relation (Figure 4.12). The Brillouin zone is shown in figure A.8. This figure was obtained with the online-tool of **SeeK-path** [66, 67]. The superlattice direction is along Γ to Z.

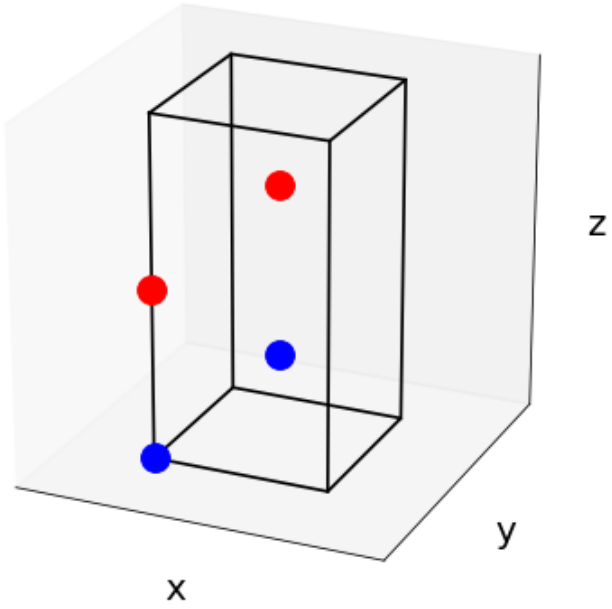

Figure A.7.: Unit cell of the LJ-superlattice with period $d_{SL} = 1\,\text{nm}$.

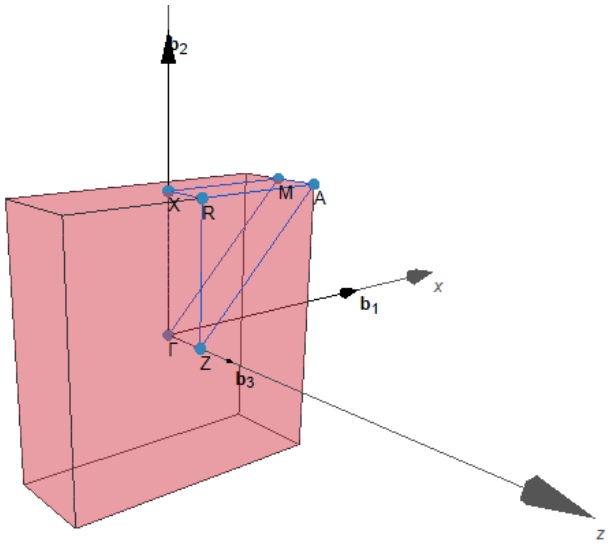

Figure A.8.: Brillouin zone of the unit cell of Figure A.7.This figure was obtained with the online-tool of **SeeK-path** [66, 67].

A.6. Coherence length of the transverse modes

In the main part, the coherence lengths of the longitudinal modes are presented. Here the coherence lengths of the transverse modes of the GaN/InN systems are presented (for supercells with structures $1 \times 1 \times N$).

A.6.1. GaN/InN superlattices

The coherence length of the transverse modes for the GaN/InN superlattices are plotted in Figure A.10 (v_x) and Figure A.10 (v_y). The two transverse directions are different as the velocity v_x is parallel to the $A1$ lattice vector (Eq. 2.43) and v_y is perpendicular to $A1$. The wurtzite crystal looks different in the two directions.

The transverse modes show a similar behavior in the coherence length. The superlattice with the smallest superlattice period has the highest coher-

ence length. The superlattices with period of 6 nm and 10 nm have similar coherence lengths than the InN.

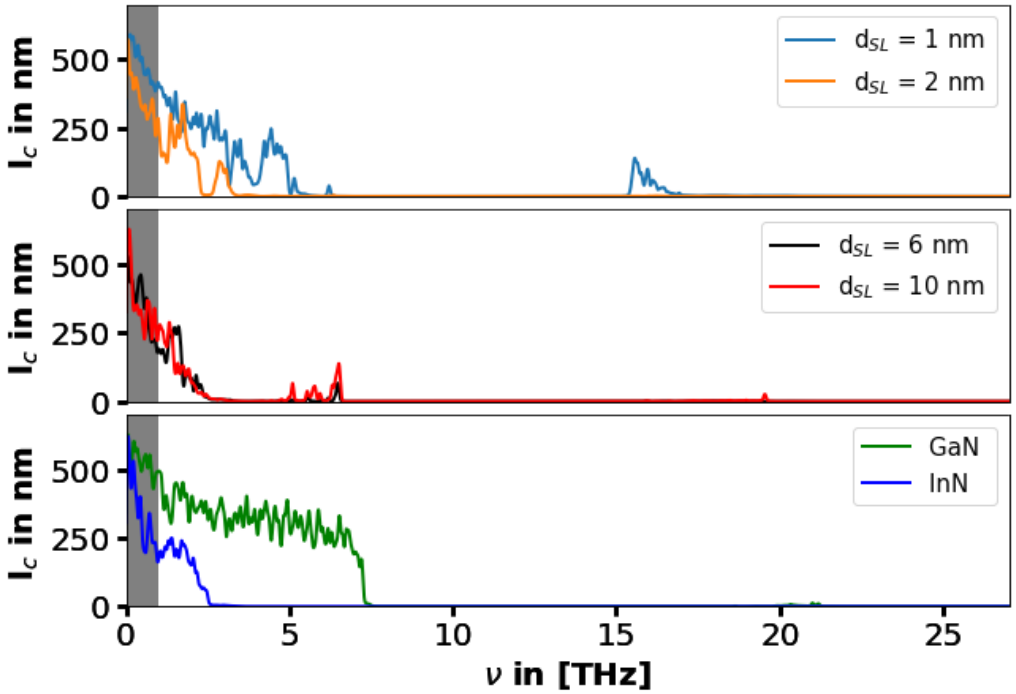

Figure A.9.: Coherence length of the transverse modes (v_x) of GaN-InN superlattices from the MD simulations of the 1x1xN structured supercells. For comparison the coherence length of GaN and InN supercells are plotted as well.

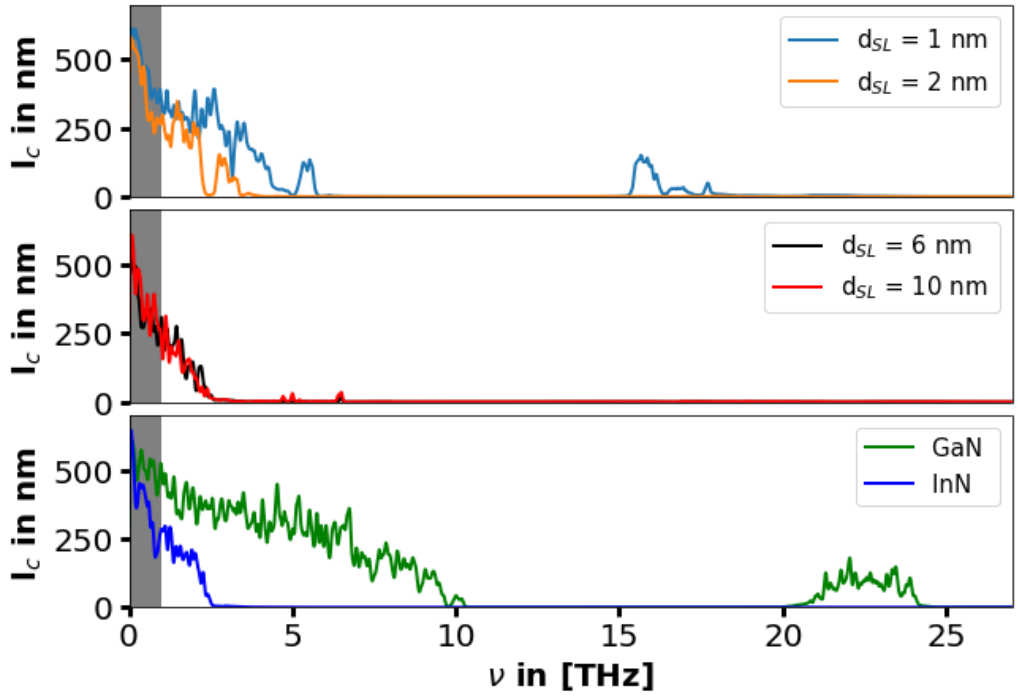

Figure A.10.: Coherence length of the transverse modes (v_y) of GaN-InN superlattices from the MD simulations of the 1x1xN structured supercells. For comparison the coherence length of GaN and InN supercells are plotted as well.

A.6.2. InN monolayers in GaN matrix

The coherence lengths for the transverse modes of the structures with a monolayer of InN in a GaN matrix is plotted in Figure A.11 (v_x) and Figure A.12 (v_y). All the simulated monolayer structures show a large coherence length in the acoustic region. The transverse optical modes above the band gap are not coherent, in contrast to the longitudinal modes in this region (compare Figure 4.39).

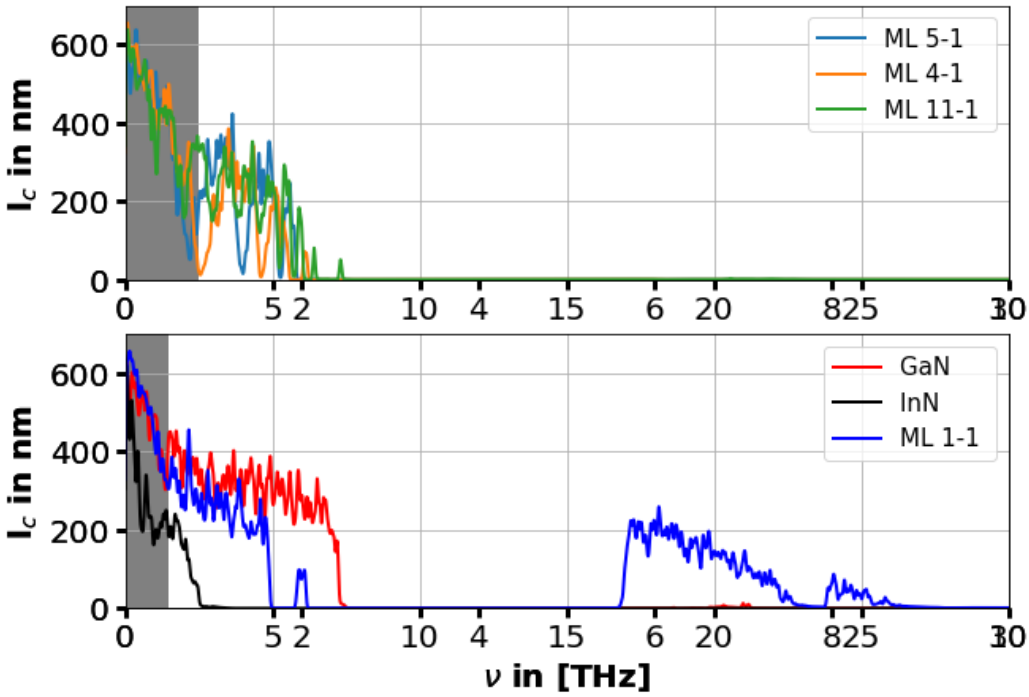

Figure A.11.: Coherence length of transverse modes (v_x) modes of the monolayer structures. All the ML structures show high coherence lengths in the acoustic region (below 10 THz).

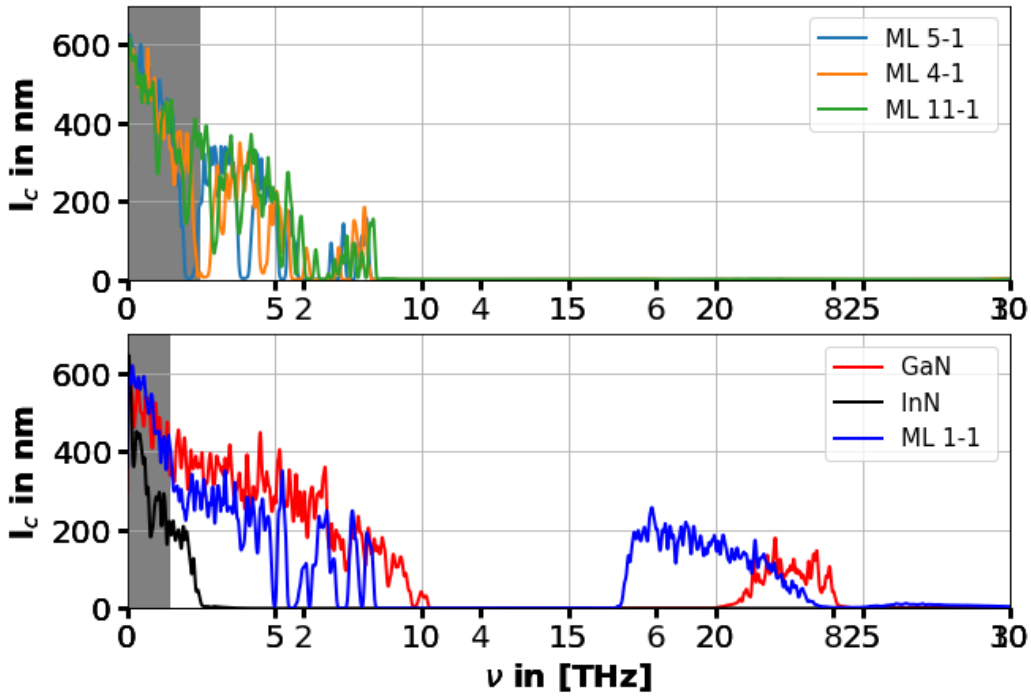

Figure A.12.: Coherence length of longitudinal modes (v_y) of the monolayer structures. All the ML structures show high coherence lengths in the acoustic region (below 10 THz).

Appendix B.

B.1. Python code for post-processing

In this Appendix, the **python** code for the post-processing of the MD simulations is presented. The script `scsdf_calculation.py` calculates the cross spectral density function, while `scsdf_analysis.py` is used to calculate the coherence length from the cross spectral density function and to do further analysis. The modules `functions_latour.py`, `functions_cells.py` and `functions_postprocess.py` contain functions which are used by the two scripts.

scsdf_calculation.py

Script for post-processing the MD simulations. Calculates the spatial cross correlation function from the velocities of the MD simulations:

```
#!/usr/bin/env python3
# -*- coding: utf-8 -*-
"""
--------------------------------------------------------------------------------
description:
Script for calculating the spatial cross spectral density (T(w,R)) as definded
in the of Latour  et al. (10.1103/PhysRevB.95.214310)

--------------------------------------------------------------------------------

required modules and/or scripts:
functions_latour.py
functions_cells.py

--------------------------------------------------------------------------------
"""

import numpy as np
import matplotlib.pyplot as plt
import functions_latour as fl
import functions_cells as cl
import time
import os
import sys



directory = '/path/to/simulation/'


''' READING THE PARAMETERS OF THE SIMULATION from the parameter file '''
N_configs,md,simulation_step,n_species,teq,T,ensemble_length = \
    fl.read_parameter(directory+'param_file')

N_ensembles = int((N_configs-teq)/ensemble_length) #Number of ensembles


#Reading infromtation of the initial positions from start.dump file
dump = open(directory+'start.dump','r')
for i in range(3):
    dump.readline() # Skip hte first three lines
N_atoms = int(dump.readline())
placeholder = dump.readline()
#Reading simulation box sizes
words = dump.readline().split()
sizex = float(words[1])-float(words[0])# Size of the simulaiton box
words = dump.readline().split()
sizey = float(words[1])-float(words[0])
words = dump.readline().split()
sizez = float(words[1])-float(words[0])
placeholder = dump.readline()

#Reading the masses of the atoms
mass_of_each_atom = np.zeros([N_atoms])
for i in range(N_atoms):
    words = dump.readline().split()
    mass_of_each_atom[i] = float(words[1])
dump.close()
```

```
'''
Reading the unitcell of the material in the simulation
file in xsf format with FRACTIONAL coordinates --> repeated_unitcell
Example of a unitcell:
    - a cubic fcc for Argon
    - an orthorhombic representation of the wurtzite structure wiht 8 atoms for
      the InN/GaN system
'''

cell_filename = directory+'repeated_unitcell'
#lenght in x,y,z,
l_unitvec_a,l_unitvec_b,l_unitvec_c,Nc,atoms_frac =  \
    cl.load_unit_cell(cell_filename)

#Position of the atoms of the unit cell in cartesian coordinates
atoms = atoms_frac*np.array([l_unitvec_a,l_unitvec_b,l_unitvec_c])

# How often the unit cell is replicated in each direction. Either with Lammps
# or with atomsk.
N_cellsx = int(np.round(sizex/l_unitvec_a))
N_cellsy = int(np.round(sizey/l_unitvec_b))
N_cellsz = int(np.round(sizez/l_unitvec_c))

N_cells = N_cellsx*N_cellsy*N_cellsz
N_atoms = Nc*N_cells #total number of atoms in the simulation

print('Resolution in distanc for the cohernce length: %6.4f Angstrom'%l_unitvec_c)

'''Creating dictionaries for the skeleton'''
cell_dict,string_cells_dict,points_on_skeleton = \
    cl.create_dictionaries_skeleton(N_cellsx,N_cellsy,N_cellsz\
        ,Nc,l_unitvec_a,l_unitvec_b,l_unitvec_c,atoms)

#%%

'''
In LAMMPS each atom has a specific atom-id (some integer number from 1 to N)
When dumping the velocites, the velocities are ordered according to the atom
ids.

Now we need to find out to which cell (cells are labeled in cell_dict) an atom
with an atom-id belongs. We know that a cell has some lattice-points,
whos coordinates are well defined.

So we compare the coordinates of the atom with atom-id in LAMMPS to the
coordinates of the lattice points to find out to
WHICH LATTICE-POINT the atom with the LAMMPS-atom-id belongs.

'''

# Read the first configuration from the dump output 'start.dump'
# to assign each atom to a position
config1 = open(directory+'start.dump','r')
for i in range(9): #skip some lines
    config1.readline()

#In the following array the positions of the starting configuration of the
# atoms in Lammps are stored. The position of the atom with id K will be
```

```
# stored in the Kth row
positions_in_lammps = np.zeros([N_atoms,3])
for K in range(N_atoms):
    words = config1.readline().split()
    positions_in_lammps[K,:] = \
        np.array([float(words[2]),float(words[3]),float(words[4])])


# Now we will identify which atom sits in which lattice-point, by sorting
    # If done brute force in will be 1/2*N_atoms^2 operations.

#If the Sorting has already been done once before, no need to redo it as
# it takes some time. Load the result of prevoius run.
if os.path.isfile(directory+'in_pos_sits_atom.npy'):
    print('Sorting of atoms to the skeleton has already been done.')
    print('Loading in_pos_sits_atom.npy')
    in_point_sits_atomid = np.load(directory+'in_pos_sits_atom.npy')

else: #if not done already, sort!
    in_point_sits_atomid,dummy = \
        cl.order_atomid_on_skeleton(points_on_skeleton,positions_in_lammps)

    if dummy == False:
        np.save(directory+'in_pos_sits_atom.npy_F',in_point_sits_atomid)
        sys.exit()
    else:
        np.save(directory+'in_pos_sits_atom.npy',in_point_sits_atomid)

# in point_sits_atom_id:
# 'lattice' point | atom_id
#        1           2
#        2           4
#        3           xy

#With the gained knowledge where each atom, with the LAMMPS atom-id k, sits on the
# skeleton, we can now rewrite the the cell dictionary to contain the
# LAMMPS atom IDs and no longer the 'lattice-'-point ids

cell_dict_LAMMPS_ids = {}
for key in cell_dict.keys():
    cell_dict_LAMMPS_ids[key] = in_point_sits_atomid[cell_dict[key],1]


#%%
'''Reading the velocites from the LAMMPS simulation and storing them in an
array: velocities'''

useall = 'xyz' # Which velocity components to load and use
velocity_list = fl.get_velocities(N_atoms,teq,N_configs,\
                                  ensemble_length,N_ensembles,directory,useall)

velocities = (velocity_list[0])
np.save(directory+'velocities.npy',velocities)

#%%

#Define of which velocity components you want to calculate the cohrenece.
#Save it in a list. 0 = vx, 1 = vy, 2 = vz
#[0,2] means thus correlation between vx and vz
```

```
ABs = [[0,0],[1,1],[2,2]]
ABs.sort()
ab = (len(ABs),)
# Printing some output that one understands what correlations are calculated
fl.print_correlation_pairs(ABs)


# FOR FFT of VELOCITIES
pad = 1  #How much the velocites get padded. Not more than two. And not less than 1!

#Calculate the discrete fruequencies, at which the time Fourier transform of
# the velocites will be calculated with numpy.fft
try:
    n_fourier = velocities.shape[1]*pad #Lenght of the input for the FFT
except:
    n_fourier = ensemble_length*pad
omega_val = (np.fft.rfftfreq(n_fourier)/(md*simulation_step))
n_omegas = len(omega_val)  # Number of frequency points up to omega max
#%%

NORM = 'ortho' # Values divided by square root of number of points of the FFT
NORM = None

#Calculating the discrete Fouriertransform of the velocities
def caluculateFFTofvel():
    fft_velocities =  np.complex64(np.zeros([N_atoms,n_omegas,ab[0]]))
    for i in range(N_atoms):
        vel = velocities[i,:,:]
        for component in range(ab[0]):
             fft_velocities[i,:,component] = \
             np.fft.rfft(vel[:,component],n_fourier,norm = NORM)[:n_omegas]
fft_velocities = caluculateFFTofvel()

#%%
"""Calculating the spatial cross spectral density function T(w,R)!

It is done seperately for Argon and GaN/InN systems, as for GaN/InN systems,
the correlations for N and Ga/In atoms are calculated seperately. This was done
to understand things better.
"""



""" FOR ARGON SYSTEM ONLY"""
if 'ArgonSL' in directory:
    print('Argon SL')
    if ab[0] == 1: #chooses right components even if only one pair is wanted
        ABs = [[0,0],[1,1],[2,2]]
    t0 = time.time()

    #Doing the spatial cross correlation to get T(w,R)
    #Periodic boundary conditions are applied to the simulation. Therefore:
    max_distance = int(N_cellsz-1)/2

    #Doing it first for all the strings seperately and then summing it up
    T_R = np.complex128(np.zeros([int(max_distance+1),n_omegas,ab[0]]))

    for dist in range(int(max_distance+1)): #looping over all distances R
        too = time.time()
```

```
            T_dist = np.complex128(np.zeros([n_omegas,ab[0]]))

            for i in range(N_cellsz): #looping over all origins R0s
               #forwards
                r0_1 = i  # The cell at the origin r0_i (origins numbered by i)
                r0_2 = i + dist
                if r0_2 > N_cellsz-1:  # Due to periodic boundary conditions
                    r0_2 -= N_cellsz # Number of second plane


                W_r1_r2 = np.complex128(np.zeros([n_omegas,ab[0]]))

                # Going over all strings of atoms
                for string_cells_key in string_cells_dict.keys():
                    # Getting the cells in the current string
                    cell_ids = string_cells_dict[string_cells_key]

                    atoms1 = cell_dict_LAMMPS_ids[cell_ids[r0_1]]
                    atoms2 = cell_dict_LAMMPS_ids[cell_ids[r0_2]]

                    #Looping over the corresponfing atom pairs which have to
                    #be correlated
                    for a1,a2 in zip(atoms1,atoms2):
                        fft_v1 = fft_velocities[a1,:,:]
                        fft_v2 = fft_velocities[a2,:,:]
                        mass_factor = np.sqrt(mass_of_each_atom[a1]*\
                                              mass_of_each_atom[a2])

                        for [alpha,beta],pair_index in zip(ABs,range(ab[0])):
                            W_r1_r2[:,pair_index] += np.conjugate(fft_v1[:,alpha])\
                            *fft_v2[:,beta]*mass_factor/2

                T_dist += W_r1_r2

            T_R[dist,:,:] = T_dist
            if dist==0:
                print('Expected duration = %5.2f min'%((time.time()-too)/60*int\
                                                       (max_distance+1)))

        print(time.time()-t0)

        #Dividing by number of summations
        T_R/=len(string_cells_dict.keys())#*Nc*N_cellsz #== /N_atoms

        #Saving the calculated spatial cross spectral density function
        np.save(directory+'T_R.npy',T_R)

    ##########################################################################
    ##########################################################################
    ##########################################################################
        """ For GaN InN"""
    elif 'SL-GaN-InN' in directory:
        print('GaN-InN')

        if ab[0] == 1: #chooses right components even if only one pair is wanted
            ABs = [[0,0],[1,1],[2,2]]

        t0 = time.time()
        #Periodic boundary conditions are applied to the simulation. Therefore:
```

```
max_distance = int(N_cellsz-1)/2

T_GaIn = np.complex128(np.zeros([int(max_distance+1),n_omegas,ab[0]]))
T_N    = np.complex128(np.zeros([int(max_distance+1),n_omegas,ab[0]]))
mGaIn = np.array([69.723,114.818])

for dist in range(int(max_distance+1)): #looping over all distances R

    too = time.time()

    for i in range(N_cellsz): #looping over all origins R0s
        r0_1 = i  # The cell at the origin r0_i (origins numbered by i)
        r0_2 = i + dist
        if r0_2 > N_cellsz-1:  # Due to periodic boundary conditions
            r0_2 -= N_cellsz # Number of second plane

        W_r1_r2 = np.complex128(np.zeros([n_omegas,ab[0]]))

        # Going over all strings of atoms
        for string_cells_key in string_cells_dict.keys():
            # Getting the cells in the current string:
            cell_ids = string_cells_dict[string_cells_key]

            atoms1 = cell_dict_LAMMPS_ids[cell_ids[r0_1]]
            atoms2 = cell_dict_LAMMPS_ids[cell_ids[r0_2]]

            #Looping over the corresponfing atom pairs which have to be
            #correlated
            for a1,a2 in zip(atoms1,atoms2):
                fft_v1 = fft_velocities[a1,:,:]
                fft_v2 = fft_velocities[a2,:,:]
                m1 = mass_of_each_atom[a1]; m2 = mass_of_each_atom[a2]
                mass_factor = np.sqrt(m1*m2)
                W_a1_a2 = np.complex128(np.zeros([n_omegas,ab[0]]))

                for [alpha,beta],pair_index in zip(ABs,range(ab[0])):
                    W_a1_a2[:,pair_index] = np.conjugate(fft_v1[:,alpha])\
                    *fft_v2[:,beta]*mass_factor/2

                W_r1_r2 += W_a1_a2
                #element wise only
                if m1 == m2 and m1 == 14.007: #N
                    T_N[dist,:,:]   += W_a1_a2
                elif m1 in mGaIn and m2 in mGaIn:
                    T_GaIn[dist,:,:]+= W_a1_a2
                else:
                    print('Something went wrong!!!'); sys.exit()


    #esimating the necessary time
    if dist==0:
        print('Expected duration = %5.2f min'%((time.time()-too)/\
                                                60*int(max_distance+1)))
print(time.time()-t0)

T_N/=N_atoms/2 #half of the atoms are always Nitrogen
T_GaIn/=N_atoms/2 #half of the atoms are always In or Ga
T_R = T_GaIn+T_N
np.save(directory+'T_N.npy',T_N)
```

```
    np.save(directory+'T_GaIn.npy',T_GaIn)

    #Saving the calculated spatial cross spectral density function
    np.save(directory+'T_R.npy',T_R)

# Cleaning RAM:
del fft_v1
del fft_v2
del fft_velocities
```

scsdf_analysis.py

Script for post-processing the MD simulations. Calculates the coherence lengths from the spatial cross correlation function and does further analysis:

```
#!/usr/bin/env python3
# -*- coding: utf-8 -*-
"""
--------------------------------------------------------------------------------
description:
Script for analyzing the spatial cross spectral density (T(w,R)) and
calculating the coherence length
--------------------------------------------------------------------------------

required modules and/or scripts:
functions_latour.py
functions_cells.py
functions_postprocess.py

--------------------------------------------------------------------------------
last changes:
1.0 2020.01.13,     Script created by Tobias Spitaler

"""

import numpy as np
import matplotlib.pyplot as plt
import functions_latour as fl
import functions_cells as cl
import functions_postprocess as fun
import scipy.optimize as optim
from matplotlib import cm


def find_f_point(freq):
    '''Finds the index in omega_val of the element which is closest to a
    desired frequency freq'''
    return np.argmin(np.abs(freq-omega_val))

directory = '/path/to/simulation/'

directory = '/home/t.spitaler/correlation_length/SL-GaN-InN/NVE/GaN/tersoff/'


''' READING THE PARAMETERS OF THE SIMULATION from the parameter file '''
N_configs,md,simulation_step,n_species,teq,T,ensemble_length = \
fl.read_parameter(directory+'param_file')
#Number of ensembles to average over
N_ensembles = int((N_configs-teq)/ensemble_length)
# The discrete time points of the simulation
times = np.arange(ensemble_length)*md*simulation_step #in ps


dump = open(directory+'start.dump','r')
for i in range(3):
    dump.readline() # Skip hte first three lines
N_atoms = int(dump.readline())
placeholder = dump.readline()
#Reading simulation box sizes
words = dump.readline().split()
sizex = float(words[1])-float(words[0])# Size of the simulaiton box
words = dump.readline().split()
sizey = float(words[1])-float(words[0])
words = dump.readline().split()
```

```
sizez = float(words[1])-float(words[0])
placeholder = dump.readline()

dump.close()


'''
Reading the unitcell of the material in the simulation
file in xsf format with FRACTIONAL coordinates --> repeated_unitcell
Example of a unitcell:
    - a cubic fcc for Argon
    - an orthorhombic representation of the wurtzite structure wiht 8 atoms for
      the InN/GaN system
'''
cell_filename = directory+'repeated_unitcell'

#lenght in x,y,z,
l_unitvec_a,l_unitvec_b,l_unitvec_c,Nc,atoms_frac = \
 cl.load_unit_cell(cell_filename)

# How often the unit cell is replicated in each direction. Either with Lammps
# or with atomsk.
N_cellsx = int(np.round(sizex/l_unitvec_a))
N_cellsy = int(np.round(sizey/l_unitvec_b))
N_cellsz = int(np.round(sizez/l_unitvec_c))

N_cells = N_cellsx*N_cellsy*N_cellsz
N_atoms = Nc*N_cells #total number of atoms in the simulation

print('Resolution in distance for the coherence length: %6.4f Angstrom'%l_unitvec_c )


#Calculate the discrete fruequencies, at which the time Fourier transform of
# the velocites will be calculated with numpy.fft

# FOR FFT of VELOCITIES
pad = 1  #How much the velocites get padded. Not more than two. And not less than 1!
n_fourier = ensemble_length*pad
omega_val = (np.fft.rfftfreq(n_fourier)/(md*simulation_step))
n_omegas = len(omega_val)  # Number of frequency points up to omega max


#Loading the cross spectral density function
T_R = np.load(directory+'T_R.npy')


max_distance = int(N_cellsz-1)/2
#The discrete distances for which the cross sepctral density function
#was calculated
R_values = np.arange(int(max_distance+1))*sizez/N_cellsz/10 #nm

#Calculating the cross_correlations for different distances between the atoms
#from the LDOS (discrete fouriertransform from time to frequency domain)
corr_R = np.fft.irfft(T_R[:,:,:],axis = 1)

#%%


#Plotting the LDOS
```

```
LDOS = np.real(T_R[0,:,:])
plt.figure()
plt.plot(omega_val,(LDOS)[:,0],label = 'x')
plt.plot(omega_val,(LDOS)[:,1],label = 'y')
plt.plot(omega_val,(LDOS)[:,2],label = 'z')
plt.legend()
plt.xlabel('w in THz')
plt.ylabel('LDOS')

#%%

#Calculating the smoothed T_R by smooting the corr_R and backcalculating T_R
# (Approach A)

sigma = 3/(md*simulation_step) #  the number  gives the desired value in ps
T_Rsmooth = np.zeros_like(T_R)
corr_Rsmooth = np.zeros_like(corr_R)
for i in range(T_R.shape[0]):
    foo = fun.smooth_corr(corr_R[i,:,:],sigma)
    corr_Rsmooth[i,:,:] = foo
    T_Rsmooth[i,:,:] = np.fft.rfft(foo,axis = 0)

#%%
#Calcualaing the T_R by a smoothed corr_R with a Gaussian coverage on top of
# the  peaks (Appraoch B)

# -> need to find the velocity of the peaks
#(in terms of indexes od positions and times)
# the user needs to check with the figure if the procedure finished correctly
peak_pos = np.argmax(corr_R[:,:int(corr_R.shape[1]/2),:],axis = 1)
plt.figure()
plt.plot(peak_pos)
plt.title('finding vg of the peaks')
plt.xlabel('distance R (index)')
plt.ylabel('time of maximum (index)')
il = 45; ih = 360#580

# by a linear fit to the lines of maxima. requires no data off the line
v_group  = np.zeros(3)
for xyz in range(3):
    fit = np.polyfit(np.arange(il,ih),peak_pos[il:ih,xyz],1)
    plt.plot(np.arange(peak_pos.shape[0]),np.arange(peak_pos.shape[0])\
             *fit[0]+fit[1],'k:')
    v_group[xyz] = fit[0]**-1

plt.plot([ih,ih,ih],peak_pos[ih],'rx')
plt.plot([il,il,il],peak_pos[il],'rx')
plt.show()


T_Rsmooth_gauss = np.zeros_like(T_R)
corr_Rsmooth_gauss = np.zeros_like(corr_R)
for i in range(T_R.shape[0]):
    for j in range(3):
        t0=  i/v_group[j]
        foo= fun.smooth_corr_gauss(corr_R[i,:,j],sigma,t0)
        corr_Rsmooth_gauss[i,:,j] = foo
        T_Rsmooth_gauss[i,:,j] = np.fft.rfft(foo,axis = 0)
```

```
#%%
##   SMOOTHING TO THE POINT the accousitc waves made half the cell ##

#Calculating the smoothed T_R by smooting the corr_R and backcalculating T_R
T_Rsmooth_long = np.zeros_like(T_R)
corr_Rsmooth_long = np.zeros_like(corr_R)
for xyz in range(3):
    for i in range(T_R.shape[0]):
        sigma = corr_R.shape[0]/v_group[xyz]
        foo = fun.smooth_corr(corr_R[i,:,xyz],sigma)
        corr_Rsmooth_long[i,:,xyz] = foo

T_Rsmooth_long[:,:,:] = np.fft.rfft(corr_Rsmooth_long,axis = 1)

#%%

#Plotting the cross_correlation as a heatmap

for xyz in range(2,3): #choose the dimension vx,vy,or bz or all
    R_min = 0;   R_max = 33333  #! Indices
    t_min = 0;   t_max = int(len(times)/2)

    x = R_values[R_min:R_max]
    y = times[t_min:t_max]
    X,Y = np.meshgrid(y,x)
    Z = corr_R[R_min:R_max,t_min:t_max,xyz]/(corr_R[0,0,xyz])
    # (normalized by the value of corr_R[0,0,xyz])

    plt.figure(figsize=[12,7])
    plt.pcolormesh(X,Y,Z[:-1,:-1],vmin = -1/2/400,vmax = 1/400)
    plt.colorbar()
    plt.ylabel('R in nm')
    plt.xlabel('$\\tau$ in ps')
    plt.title('Correlations')


#%%
#Plotting the cross spectral density (T(R)) as a heatmap

for xyz in range(2,3):
    R_min = 0;   R_max = 2000  #Indices!!!
    f_min = 0;   f_max = len(omega_val)

    x = R_values[R_min:R_max]
    y = omega_val[f_min:f_max]
    X,Y = np.meshgrid(y,x)
    T = T_R
    Z = (np.real(T[:,:,xyz]/T[0,:,xyz])**2)
    #Z = (np.real(C_spatial[R_min:R_max,f_min:f_max,2])**2)

    plt.figure()
    plt.pcolormesh(X,Y,Z[:-1,:-1],vmin = 0,vmax = 1,cmap = cm.coolwarm)
    plt.colorbar()
    plt.ylabel('R in nm')
    plt.xlabel('$\\nu$ in THz')
    #plt.xlim([0,4]) #THz
    #plt.ylim([0,100]) #R
    plt.title('np.real(T_R(R,$\\nu$))**2'+', xyz = %g'%xyz)
```

```
#%%
# Plotting the spectral energy density T(k,w)
# Calculating the T_k(w) from the T_R(w) and plotting the 'bands'
T_kw = np.fft.irfft((T_R[::2,:,:]),axis = 0)


for xyz in range(2,3):
    #Plotting the T_R as a heatmap
    k_min = 0;    k_max = T_kw.shape[0]//2  #Indices!!!
    f_min = 0;    f_max = find_f_point(30)#len(omega_val)

    y = np.arange(T_kw.shape[0])[0:k_max]
    x = omega_val[f_min:f_max]
    X,Y = np.meshgrid(y,x)
    Z = np.swapaxes(np.real(T_kw[0:k_max,f_min:f_max,xyz])\
                    /np.max(np.real(T_kw[0:k_max,f_min:f_max,xyz])),0,1)
    ##Doing a heatmap instead of a 3d plot:
    plt.figure(figsize= [10,10])
    plt.pcolormesh(X,Y,Z[:-1,:-1],vmin = -0.0,vmax = 0.005,cmap = cm.coolwarm)

    plt.colorbar()
    plt.xlabel('k')
    plt.ylabel('f in THz')
    plt.title('T(k,$\\nu$)'+', xyz = %g'%xyz)



#%%

""" Calculation of the coherence length by treating the cross spectral density
as a cumulative distribution function """


# Write in the list the type of cross spectral density function you want to use
# to calculate the coherence length
list_scsdf = ['T_R','T_Rsmooth','T_Rsmooth_gauss','T_Rsmooth_long']


plt.figure()

# Possible to define a list of thresholds:
#->the coherence length is the distance at which the cumulatice distributin
#function equals the threshold. e.g 95%
threshold_list = [0.95]


# define the list of the dimensions (0 = x, 1 = y, 2 = z) of the velocity the
# cohernce length should be calculated off
dimensions = [2]

for scsdf in list_scsdf:

    #calcualte the cumulative distribution function
    F_cumulative = fun.get_F_cumulative(eval(scsdf),mode = 'real')

    # Initalizing array for cohernece length
    coherence_lengths = np.zeros([n_omegas,eval(scsdf).shape[2]])
```

```
    for dim in dimensions: #loop over number of correlation pairs

        for threshold in threshold_list: # loop over possible thresholds

            for w in range(n_omegas): #looping over frequency points

                #Finding where the F is equal to 0 and doing a linear
                #interpolation to find that distance
                index2 = np.argmax(F_cumulative[:,w,dim]>=threshold)

                if index2 ==0:
                    coherence_lengths[w]=0
                else:
                    index1 = index2-1
                    #the following index is a float now, nor an integer,
                    #as it gives the place between two indexes
                    index = (threshold-F_cumulative[index1,w,dim])\
                        /((F_cumulative[index2,w,dim] \
                           - F_cumulative[index1,w,dim])\
                            /(index2-index1))+index1
                    lc = index*R_values[1]
                    coherence_lengths[w,dim] = lc


            ''' Plot COHERENCE LENGTH '''

            plt.plot(omega_val,coherence_lengths[:,2],'-', \
                     label = '%s;  '%scsdf+str(threshold)+'%  dim= '+str(dim))


        plt.xlabel('$\\nu$ in THz ')
        plt.ylabel('$l_c$')

plt.legend()
plt.xlim([0,30])
plt.show()


#%%###

""" Fittingthe data to an attenuated wave (funct1) to the calculated cross
 spectral density function, to extract the cohernece lenght.
It does not work well for the 3D systems!
"""

T_fit = T_R # Choosing the cross spectral density function to fit

# Counting the failed fits! Not really representative as some fits are
#considered successfull by the fitting routine but are acutally not
# reproducing the date well.
fail1 = 0
fail2 = 0


def funct1(R,l,lc):
    '''Fitfunction for tht T_R[R,w0]
    lc: coherence length
    l : wavlengtk (=pi/k)
    '''
```

```
    return np.cos(2*np.pi*R/l)**2 * np.exp(-R/lc)

frequenies = omega_val[:] #define some freqeuncy range I want to have a look at

#Initalizing the coherenece lengths and wave-lengths for the attenuated wave
coh_len = np.zeros([len(frequenies),3])
labds  = np.zeros_like(coh_len)



for i in range(len(frequenies)): #looping over freuqencies

    #Find the index (in omega_val) of the current frequency
    ind = find_f_point(frequenies[i])
    x = R_values[:] # in nm

    for xyz in range(2,3): #for which pairs to fit the cohrence lengths

        y = (np.abs(np.real((T_fit[:,ind,xyz]/T_fit[0,ind,xyz])))**2)[:]


        ''' Inital guess for the cl and lambda:
            An eduacated guess for lambda often helps to get better fit
            results, but it is a bit a playing around
            Different dimensions need different inital guesses as well
        '''
        if xyz ==0:
            const_lam_guess = 5
            #const_lam_guess = v_group[xyz]/2*times[1]/R_values[1]*100 #for argon
            const_lam_guess = v_group[xyz]/2*times[1]/R_values[1]*1e4 #for GaN/InN

        elif xyz == 1:
            const_lam_guess = 5.3
            #const_lam_guess = v_group[xyz]/2*times[1]/R_values[1]*100 #for argon
            const_lam_guess = v_group[xyz]/2*times[1]/R_values[1]*1e4 #for GaN/InN

        elif xyz == 2:
            #const_lam_guess = v_group[xyz]/2*times[1]/R_values[1]*100 #for argon
            const_lam_guess = v_group[xyz]/2*times[1]/R_values[1]*1e4 #for GaN/InN
        #inital guess of the parameters
        x0 = np.array([const_lam_guess/omega_val[ind],200])

#         #Sometimes it also helps to use the fitresults of neighbouring
#         #frequencies
#         if i > 5:
#             x0 = [labds[i-1,xyz],coh_len[i-1,xyz]*4]


        try:
            x_opt,cov = optim.curve_fit(funct1,x,y,x0)
        except(RuntimeError):
            fail1 +=1
            continue



##############
# Running a second fit using the outcome of the first one to decide how long
```

```
# the signal taken into account should be can improve the fitting results

coh_len2 = np.zeros_like(coh_len)
labds2 = np.zeros_like(coh_len)

for i in range(0,len(frequenies)):
    ind = find_f_point(frequenies[i])

    for xyz in range(2,3):

        lc_old = coh_len[i,xyz]

        take_up_to = np.argmin(np.abs(lc_old*3.5-R_values))
        if take_up_to > T_fit.shape[0]:
            take_up_to == T_fit.shape[0]

        if take_up_to < 20:
            take_up_to = 20
            lc_old = lc #taking the value of the previous frequency as a guess

        y = (np.abs(np.real((T_fit[:,ind,xyz]/T_fit[0,ind,xyz])))\
             **2)[0:take_up_to]
        x = R_values[0:take_up_to] # in nm

        #using the wavelength from the first fitting round and the cohernece
        #length of the neighbouring frequency as an inital guess
        x0 = np.array([labds[i,xyz],lc_old*1.3])


        try:
            x_opt,cov = optim.curve_fit(funct1,x,y,x0)
        except(RuntimeError):
            fail2 += 1
            continue


        lam = x_opt[0]
        lc = x_opt[1]

        coh_len2[i,xyz] = x_opt[1]
        labds2[i,xyz] = x_opt[0]
```

functions_latour.py

Module containing functions used by `scsdf_calculation.py` and `scsdf_analysis.py`:

```
#!/usr/bin/env python3
# -*- coding: utf-8 -*-
#####################################################
#####################################################
"""
--------------------------------------------------------------------------------

description:
This module contains  functions which are needed for calculating the spatial
cross spectral density function and to calculate the phonon coherence length
of superlattices.

--------------------------------------------------------------------------------

required modules and/or scripts:

--------------------------------------------------------------------------------
"""
#############################################################
#############################################################

#modul import
import numpy as np
import time
import math as mat

#%%

#function read_parameter(filename):
#
#last change: 2019.09.10 Tobias Spitaler

def read_parameter(filename):
    '''Reads the paramter file of the simulation out of filename

    return([N_configs,md,simulation_step,n_species,teq,T,ensemble_size])
    N_configs : Number of sampling points
    md: The simulation has sampled the configuration each md step
    simulation_step: Actual simulationstep in ps
    n_species : Number of different atom species in simulation
    teq: Number of configurations to skip at the beginning
    T: Temperature of simulation
    ensemble_size: number of simulation steps to consider
    '''

    params = open(filename,'r')
    # Number of configurations saved in the dump file
    N_configs = int(params.readline())

    words = params.readline().split()
    md = int(words[0])                    # Sampling step
    simulation_step = float(words[1])     # Actual simulationstep in ps
    ensemble_size = int(words[3])

    # Number of different atom species in simulation
    n_species = int(params.readline())

    # Number of configurations to skip at the beginning
    teq = int(params.readline())
```

```
    # The starting configuration is always left out, so teq >=1
    if teq < 1:
        teq = 1

    T = float(params.readline())        # Temperature of simulation

    params.close()
    return([N_configs,md,simulation_step,n_species,teq,T,ensemble_size])


#%%

#function get_velocities:
#
#last change: 2019.09.10 Tobias Spitaler, reading velocities of more ensembles

def get_velocities(N_atoms,teq,N_configs,ensemble_lenght,N_ensembles,\
                   directory = './',useall= 'xyz'):
    ''' Reading the velocites from the dump-file (custom) and storing them
    in an array:

    velocites is matrix of N_atoms*(ensemble_length)*3
    atom_id | timestep | velocity_component (x,y,z)
    '''
    t0 = time.time()
    print('\nStarting extracting the velocities from the dump file')
    velocity_list = []

    dump = open(directory+'dump.txt','r')


    #Skip the configurations we do not want to use
    lines_to_skip = teq*(N_atoms+9) #+9 for the header lines
    for i in range(lines_to_skip):
        dump.readline()

    for N in range(N_ensembles):

        #Initializing the velocity array
        velocities = np.zeros([N_atoms,ensemble_lenght,len(useall)])

        #Looping over all samplings in an ensemble
        for i in range(ensemble_lenght):
            #Skip the headerlines
            for oo in range(9):
                dump.readline()
            #Looping over all atoms
            for n in range(N_atoms):
                words = dump.readline().split()
                atom_id = int(words[0])

                if useall == 'xyz':
                    vx = float(words[5])
                    vy = float(words[6])
                    vz = float(words[7])
                    velocities[atom_id-1][i][0]= vx
                    velocities[atom_id-1][i][1]= vy
                    velocities[atom_id-1][i][2]= vz
                elif useall == 'x':
```

```
                    vx = float(words[5])
                    velocities[atom_id-1][i][0]= vx
                elif useall == 'y':
                    vy = float(words[6])
                    velocities[atom_id-1][i][0]= vy
                elif useall == 'z':
                    vz = float(words[7])
                    velocities[atom_id-1][i][0]= vz
                elif useall == 'xy':
                    vx = float(words[5])
                    vy = float(words[6])
                    velocities[atom_id-1][i][0]= vx
                    velocities[atom_id-1][i][1]= vy
                elif useall == 'xz':
                    vx = float(words[5])
                    vz = float(words[7])
                    velocities[atom_id-1][i][0]= vx
                    velocities[atom_id-1][i][1]= vz
                elif useall == 'yz':
                    vy = float(words[6])
                    vz = float(words[7])
                    velocities[atom_id-1][i][0]= vy
                    velocities[atom_id-1][i][1]= vz

            if not(i%int(N_configs/10)):
                print(str(i//int(N_configs/10)*10)+'% done after ',\
                      '%6.0g'%(time.time()-t0),' seconds')

        velocity_list.append(velocities)
    t1 = time.time()
    print('All velocities are extracted in %g s'%(t1-t0))
    dump.close()
    return velocity_list



#%%

def print_correlation_pairs(ABs):
    ''' Help function which prints which pairs of veloity components are
    correlated (the pairs are storded in ABs) '''

    names = ['vx','vy','vz']
    num = len(ABs)
    print('\nThe correlations between %g pairs of velocity components is calculated.'%
    print('The pairs are stored in gamma as follows:')
    for i in range(num):
        AB = ABs[i]
        s = '('+names[AB[0]]+','+names[AB[1]]+\
            ') is stored in gamma [:,:,:,'+str(i)+']'
        print(s)
```

functions_cells.py

Module containing functions used by `scsdf_calculation.py` and `scsdf_analysis.py`:

```
#!/usr/bin/env python3
# -*- coding: utf-8 -*-
"""
Created on Tue Oct 22 10:38:41 2019


File contains functions which are needed for different other scripts for the
calulation of the correlation length, when the knowledge of the unit cell,
which is replicated, is used to identify the positions of the atoms with a
specific atom id in LAMMPS


@author: t.spitaler
"""

import numpy as np
import time
import sys
#%%

def load_unit_cell(cell_filename):
    '''This function loads the xsf file in fractional coordinates of the unit
    cell, which has been repilicated to construct the simulaiton box.
    Function calculates the size of the unit cell and extraxts the positions
    of the atoms within the unit cell.

    Returns the dimensions of the unitcell and the positions of the atoms in
    the unitcell in fractional coordinates.

    Restrictions: orthogonal unitcell
    '''

    cell = open(cell_filename,'r')

    #Skip header lines
    for i in range(3):
        cell.readline()
    #Read dimensions of unit cell
    len_a = float(cell.readline().split()[0])
    len_b = float(cell.readline().split()[1])
    len_c = float(cell.readline().split()[2])

    for i in range(6): #skip some rows
        cell.readline()

    atompos_frac= []
    line = cell.readline()
    while line:
        words = line.split()
        pos = [float(words[1]),float(words[2]),float(words[3])]
        atompos_frac.append(pos)

        line= cell.readline()

    Nc = len(atompos_frac)

    atoms_frac = np.array(atompos_frac) # In fractional coordinates

    if np.max(atoms_frac) > 1:
```

```
        print("'repeted_unitcell' not in fractional coordinates!")
        sys.exit()


    return [len_a,len_b,len_c,Nc,atoms_frac]

#%%
def create_dictionaries_skeleton(N_cellsx,N_cellsy,N_cellsz,Nc,unitvec_a,\
                                 unitvec_b,unitvec_c,atoms):
    ''' This function creates some dictionaries which are needed for calculting
    the cross specral densitiy function.

    The atoms of one unitcell are correlated with the atoms of the other unit-
    cells. Therefore one needs to know to which unitcell an atom belongs.

    First we find the coordinates of the lattice-points on the supercell. They
    are labeld just by rising integers 0 to N_atoms -1. Coordinates are
    stored in:
        points_on_skeleton

    Then we label the cells by ascending integers. For each cell, the
    corresponding labels of the SC-lattice-points are stored in a dictionary:
        cell_dict

    The correlations are done in one direction (line/string). Creating a
    dictionary which contains the labels of all cells along a certain string:
        string_cells_dict

    '''

    N_cells = N_cellsx*N_cellsy*N_cellsz
    N_atoms = N_cells*Nc

    #Defining the points of the atomic positions in the SC, starting from the
    #positions of the atoms of the simple unitcell which is repeated over
    #the simulation box
    points_on_skeleton = np.zeros([N_atoms,3])
    i = 0 # Position index
    for z in range(N_cellsz):
        for y in range(N_cellsy):
            for x in range(N_cellsx):
                unit_cell_position = \
                    np.array([x*unitvec_a,y*unitvec_b,z*unitvec_c])
                for atom in range(Nc):
                    points_on_skeleton[i,:] = unit_cell_position+atoms[atom]
                    i+=1

    #Creating a cell dictionary for the skeleton.
    cell_dict = {}
    cell_id = 0
    for z in range(N_cellsz):
        for y in range(N_cellsy):
            for x in range(N_cellsx):
                cell_dict[cell_id] = np.arange(Nc)+(cell_id*Nc)
                cell_id+=1

    # Make the lists of the cells which are on the same string along the
    #correlation direction for the skeleton (assumed to be in z)
    string_cells_dict = {}
```

```
    n_cells_plane = N_cellsx*N_cellsy
    for i in range(n_cells_plane):
        string_cells_dict[i] = \
            np.arange(i,n_cells_plane*(N_cellsz),n_cells_plane)

    return [cell_dict,string_cells_dict,points_on_skeleton]


#%%
#Added on 2019.11.05 by Tobias Spitaler
def order_atomid_on_skeleton(positions_atoms_on_skeleton,positions_in_lammps):

    print(' ')
    print('Start ordering the atoms in LAMMPS onto their points on the skeleton.')
    print('the structure file for the skeleton needs to be in fractional coordinates!'
    print('Might take some time ...')

    t0 = time.time()

    N_atoms = positions_atoms_on_skeleton.shape[0]
    in_point_sits_atomid = np.zeros([N_atoms,2],dtype = int)
    in_point_sits_atomid[:,0] = np.arange(N_atoms)

    delta_roundoff = 0.3 # The search is critical to this parameter. It must
    #not be to big or to small.

    for i in range(N_atoms): # Looping over all atoms in Lammps
        pos_lammps = positions_in_lammps[i]

        #Now finding the corresponding position in the skeleton
        for j in range(N_atoms):
            pos_skeleton = positions_atoms_on_skeleton[j]

            dist = (np.linalg.norm(pos_lammps-pos_skeleton)) ###

            if dist < delta_roundoff:
                in_point_sits_atomid[j,1]  = i

                break

    t1 = time.time()

    #Doing a silent test if each atom has only be assigned once:
    test = np.sort(in_point_sits_atomid[:,1])
    if not(test == np.arange(N_atoms)).all():
        print('THE sorting failed. Some atoms assigned more times or not at all')
        print('The ordering of the atoms on their positions took: ',t1-t0,' seconds')
        return [in_point_sits_atomid,False]

    print('The ordering of the atoms on their positions took: ',t1-t0,' seconds')

    return [in_point_sits_atomid,True]
```

functions_postprocess.py

Module containing functions used by `scsdf_calculation.py` and `scsdf_analysis.py`:

```
#!/usr/bin/env python3
# -*- coding: utf-8 -*-

#########################################################
#########################################################
"""
--------------------------------------------------------------------------------

description:
This module contains  functions which are needed for calculating the spatial
cross spectral density function and to calculate the phonon cohenerence length
of superlattices.

--------------------------------------------------------------------------------

required modules and/or scripts:

--------------------------------------------------------------------------------
"""
#########################################################
#########################################################


import numpy as np

#%%

def get_F_cumulative(C_spatial,mode = 'abs'):
    ''' Calculating the cumulative distribution function F[n,nu,xyz]

    C_spatial[distance,omega,xyz]

    '''

    if mode =='abs':
        C_spatial = np.abs(C_spatial)**2
    if mode == 'real':
        C_spatial = np.real(C_spatial)**2

    F_cumulative = np.cumsum(C_spatial,axis = 0)
    F_cumulative/= F_cumulative[-1,:,:]
    return F_cumulative


#%%

def smooth_corr(corr,sigma):
    ''' Functions for smoothing the correlation functions to get a different
    cross spectral density function. [Approach A and Approach C (higher sigma)]

    The higher sigma, the more of the correlatios (up to higher tau) is taken
    into account. The corr contains positive and negative times. '''

    if len(corr.shape) ==2:
        '''Havinf x,y,z differently'''
        length = corr.shape[0]
        dummy1 = np.arange(int(length/2)) +1
        dummy2 = np.arange(int(length)-len(dummy1))+1
        s1 = np.exp(-dummy1**2/(2*sigma**2))
```

```
        s2 = np.exp(-dummy2**2/(2*sigma**2))
        s = np.zeros(corr.shape)
        s[0:int(length/2),:] = s1[:,np.newaxis]
        s[int(length/2):,:]  = s2[-1::-1,np.newaxis]
        return corr*s

    elif len(corr.shape) == 1:
        length = corr.shape[0]
        dummy1 = np.arange(int(length/2)) +1
        dummy2 = np.arange(int(length)-len(dummy1))+1
        s1 = np.exp(-dummy1**2/(2*sigma**2))
        s2 = np.exp(-dummy2**2/(2*sigma**2))
        s = np.zeros(corr.shape)
        s[0:int(length/2)] = s1[:]
        s[int(length/2):]  = s2[-1::-1]
        return corr*s


def smooth_corr_gauss(corr,sigma,x0):
    '''  Functions for smoothing the correlation functions to get a different
    cross spectral density function. (Approach B)

    Smoothing the correlation function, by putting a gaussian over the
    signal with the Gaussian centered at x0'''
    length = corr.shape[0] #length in time
    dummy1 = np.arange(int(length/2)) +1
    #both dummy1 and 2 needed in case length is odd
    dummy2 = np.arange(int(length)-len(dummy1))+1
    s1 = np.exp(-(dummy1-x0)**2/(2*sigma**2))
    s2 = np.exp(-(dummy2-x0)**2/(2*sigma**2))
    s = np.zeros(corr.shape)
    s[0:int(length/2)] = s1[:]
    s[int(length/2):]  = s2[-1::-1]
    return corr*s


def smooth_corr_long(corr_shape,sigma,v_group):
    ''' Functions for smoothing the correlation functions to get a different
    cross spectral density function. (Approach C)

    Smoothing the correlation function, by smoothing after the accousitc modes
    rach half the cell length.

    requieres the group velocity v_group of the long wavelength accousitc modes
    '''
    length = corr_shape[1] # length in time
    s = np.zeros([corr_shape[1],corr_shape[2]])#

    for xyz in range(3):#
        x0 = corr_shape[0]/v_group[xyz]

        dummy1 = np.arange(int(length/2)) +1
        #both dummy1 and 2 needed in case length is odd
        dummy2 = np.arange(int(length)-len(dummy1))+1

        s1 = np.exp(-(dummy1-x0)**2/(2*sigma**2))
        s1[:int(x0)] = 1
        s2 = np.exp(-(dummy2-x0)**2/(2*sigma**2))
        s2[:int(x0)] = 1
```

```
        s[0:int(length/2),xyz] = s1[:]
        s[int(length/2):,xyz]  = s2[-1::-1]

    return s
```

Bibliography

[1] Martin Maldovan. "Sound and heat revolutions in phononics." In: *Nature* 503.7475 (2013), pp. 209–217 (cit. on p. 1).

[2] Martin Maldovan. "Phonon wave interference and thermal bandgap materials." In: *Nature materials* 14.7 (2015), pp. 667–674 (cit. on pp. 1, 2).

[3] Sebastian Volz et al. "Nanophononics: state of the art and perspectives." In: *The European Physical Journal B* 89.1 (2016), p. 15 (cit. on p. 1).

[4] Ali Shakouri. "Recent developments in semiconductor thermoelectric physics and materials." In: *Annual review of materials research* 41 (2011) (cit. on pp. 1, 2).

[5] David G Cahill et al. "Nanoscale thermal transport." In: *Journal of applied physics* 93.2 (2003), pp. 793–818 (cit. on p. 1).

[6] David G Cahill et al. "Nanoscale thermal transport. II. 2003–2012." In: *Applied physics reviews* 1.1 (2014), p. 011305 (cit. on p. 1).

[7] Guofeng Xie, Ding Ding, and Gang Zhang. "Phonon coherence and its effect on thermal conductivity of nanostructures." In: *Advances in Physics: X* 3.1 (2018), p. 1480417 (cit. on p. 1).

[8] Jayakanth Ravichandran et al. "Crossover from incoherent to coherent phonon scattering in epitaxial oxide superlattices." In: *Nature materials* 13.2 (2014), pp. 168–172 (cit. on pp. 1, 2, 11).

[9] Feng He, Wenzhi Wu, and Yaguo Wang. "Direct measurement of coherent thermal phonons in Bi 2 Te 3/Sb 2 Te 3 superlattice." In: *Applied Physics A* 122.8 (2016), p. 777 (cit. on pp. 1, 11).

[10] Maria N Luckyanova et al. "Coherent phonon heat conduction in superlattices." In: *Science* 338.6109 (2012), pp. 936–939 (cit. on pp. 1, 11).

[11] Benoit Latour, Sebastian Volz, and Yann Chalopin. "Microscopic description of thermal-phonon coherence: From coherent transport to diffuse interface scattering in superlattices." In: *Physical Review B* 90.1 (2014), p. 014307 (cit. on pp. 2, 5, 17, 40, 52, 60, 64, 97, 99).

[12] Benoit Latour and Yann Chalopin. "Distinguishing between spatial coherence and temporal coherence of phonons." In: *Physical Review B* 95.21 (2017), p. 214310 (cit. on pp. 2, 5, 17, 20, 40, 41, 45, 47–50, 95, 97).

[13] O Ambacher et al. "Pyroelectric properties of Al (In) GaN/GaN hetero- and quantum well structures." In: *Journal of physics: condensed matter* 14.13 (2002), p. 3399 (cit. on pp. 2, 67).

[14] David Holec et al. "Equilibrium critical thickness for misfit dislocations in III-nitrides." In: *Journal of Applied Physics* 104.12 (2008), p. 123514 (cit. on pp. 3, 67, 69, 99).

[15] A Yoshikawa et al. "Fabrication and characterization of novel monolayer InN quantum wells in a GaN matrix." In: *Journal of Vacuum Science & Technology B: Microelectronics and Nanometer Structures Processing, Measurement, and Phenomena* 26.4 (2008), pp. 1551–1559 (cit. on pp. 3, 39, 68, 90, 96, 98, 99).

[16] MT Dove. "Introduction to the theory of lattice dynamics." In: *École thématique de la Société Française de la Neutronique* 12 (2011), pp. 123–159 (cit. on p. 5).

[17] Younès Ezzahri et al. "Coherent phonons in Si/ Si Ge superlattices." In: *Physical Review B* 75.19 (2007), p. 195309 (cit. on p. 11).

[18] K Mizoguchi et al. "Observation of coherent folded acoustic phonons propagating in a GaAs/AlAs superlattice by two-color pump-probe spectroscopy." In: *Physical Review B* 60.11 (1999), p. 8262 (cit. on p. 11).

[19] GD Sanders, CJ Stanton, and Chang Sub Kim. "Theory of coherent acoustic phonons in In x Ga 1- x N/GaN multiple quantum wells." In: *Physical Review B* 64.23 (2001), p. 235316 (cit. on p. 11).

[20] Albrecht Bartels et al. "Coherent zone-folded longitudinal acoustic phonons in semiconductor superlattices: excitation and detection." In: *Physical review letters* 82.5 (1999), p. 1044 (cit. on p. 11).

[21] MV Simkin and GD Mahan. "Minimum thermal conductivity of superlattices." In: *Physical Review Letters* 84.5 (2000), p. 927 (cit. on p. 11).

[22] Yunfei Chen et al. "Minimum superlattice thermal conductivity from molecular dynamics." In: *Physical Review B* 72.17 (2005), p. 174302 (cit. on p. 11).

[23] Brian C Daly et al. "Molecular dynamics calculation of the thermal conductivity of superlattices." In: *Physical review B* 66.2 (2002), p. 024301 (cit. on p. 11).

[24] S Chakraborty et al. "Thermal conductivity in strain symmetrized Si/Ge superlattices on Si (111)." In: *Applied Physics Letters* 83.20 (2003), pp. 4184–4186 (cit. on p. 11).

[25] Erika Ye and Austin J Minnich. "Ab initio based investigation of thermal transport in superlattices using the Boltzmann equation: Assessing the role of phonon coherence." In: *Journal of Applied Physics* 125.5 (2019), p. 055107 (cit. on p. 11).

[26] M Hijazi and M Kazan. "Phonon heat transport in superlattices: Case of Si/SiGe and SiGe/SiGe superlattices." In: *AIP Advances* 6.6 (2016), p. 065024 (cit. on p. 11).

[27] Jos Thijssen. "Molecular dynamics simulations." In: *Computational Physics*. 2nd ed. Cambridge University Press, 2007, pp. 197–262. DOI: 10.1017/CBO9781139171397.010 (cit. on p. 12).

[28] Dennis C Rapaport. *The art of molecular dynamics simulation*. eng. Cambridge university press, 1998 (cit. on p. 12).

[29] SV Meshkov. "Low-frequency dynamics of Lennard-Jones glasses." In: *Physical Review B* 55.18 (1997), p. 12113 (cit. on pp. 13, 16).

[30] Changyol Lee et al. "Ab initio studies on the structural and dynamical properties of ice." In: *Physical Review B* 47.9 (1993), p. 4863 (cit. on pp. 13, 16).

[31] Leonard Mandel and Emil Wolf. *Optical coherence and quantum optics*. Cambridge university press, 1995 (cit. on p. 17).

[32] Rémi Carminati and Jean-Jacques Greffet. "Near-field effects in spatial coherence of thermal sources." In: *Physical Review Letters* 82.8 (1999), p. 1660 (cit. on p. 17).

[33] Sonja Franke-Arnold, Guillaume Huyet, and Stephen M Barnett. "Measures of coherence for trapped matter waves." In: *Journal of Physics B: Atomic, Molecular and Optical Physics* 34.5 (2001), p. 945 (cit. on p. 17).

[34] URL: http://link.aps.org/supplemental/10.1103/PhysRevB.95.214310 (cit. on p. 20).

[35] Yoyo Hinuma et al. "Choice of basis vectors for conventional unit cells revisited." In: *arXiv preprint arXiv:1506.01455* (2015) (cit. on pp. 22, 24).

[36] Frank H Stillinger and Thomas A Weber. "Computer simulation of local order in condensed phases of silicon." In: *Physical review B* 31.8 (1985), p. 5262 (cit. on p. 27).

[37] Jerry Tersoff. "New empirical approach for the structure and energy of covalent systems." In: *Physical Review B* 37.12 (1988), p. 6991 (cit. on p. 27).

[38] Xiaowang W Zhou, Reese E Jones, and Kevin Chu. "Polymorphic improvement of Stillinger-Weber potential for InGaN." In: *Journal of Applied Physics* 122.23 (2017), p. 235703 (cit. on pp. 28, 29, 69, 102, 112, 117, 118).

[39] Heinz Schulz and KH Thiemann. "Crystal structure refinement of AlN and GaN." In: *Solid State Communications* 23.11 (1977), pp. 815–819 (cit. on p. 28).

[40] Jorge Serrano et al. "InN thin film lattice dynamics by grazing incidence inelastic X-ray scattering." In: *Physical review letters* 106.20 (2011), p. 205501 (cit. on p. 29).

[41] URL: http://www.almabte.eu/index.php/database/ (cit. on pp. 28, 29).

[42] Jinlong Ma, Wu Li, and Xiaobing Luo. "Intrinsic thermal conductivity and its anisotropy of wurtzite InN." In: *Applied Physics Letters* 105.8 (2014), p. 082103 (cit. on pp. 29–31, 116).

[43] Abel Carreras, Atsushi Togo, and Isao Tanaka. "DynaPhoPy: A code for extracting phonon quasiparticles from molecular dynamics simulations." In: *Computer Physics Communications* 221 (2017), pp. 221–234 (cit. on pp. 30, 32).

[44] URL: `https://phonolammps.readthedocs.io/en/master/` (cit. on p. 31).

[45] A Togo and I Tanaka. "First principles phonon calculations in materials science." In: *Scr. Mater.* 108 (Nov. 2015), pp. 1–5 (cit. on p. 31).

[46] Steve Plimpton. *Fast parallel algorithms for short-range molecular dynamics*. Tech. rep. Sandia National Labs., Albuquerque, NM (United States), 1993. URL: `http://lammps.sandia.gov` (cit. on p. 32).

[47] URL: `http://lammps.sandia.gov` (cit. on pp. 32, 33).

[48] William C Swope et al. "A computer simulation method for the calculation of equilibrium constants for the formation of physical clusters of molecules: Application to small water clusters." In: *The Journal of Chemical Physics* 76.1 (1982), pp. 637–649 (cit. on p. 33).

[49] T Schneider and E Stoll. "Molecular-dynamics study of a three-dimensional one-component model for distortive phase transitions." In: *Physical Review B* 17.3 (1978), p. 1302 (cit. on p. 33).

[50] William G Hoover. "Canonical dynamics: Equilibrium phase-space distributions." In: *Physical review A* 31.3 (1985), p. 1695 (cit. on p. 33).

[51] Alan JH McGaughey and M Kaviany. "Phonon transport in molecular dynamics simulations: formulation and thermal conductivity prediction." In: *Advances in heat transfer* 39 (2006), pp. 169–255 (cit. on p. 64).

[52] D Doppalapudi et al. "Phase separation and ordering in InGaN alloys grown by molecular beam epitaxy." In: *Journal of Applied Physics* 84.3 (1998), pp. 1389–1395 (cit. on p. 67).

[53] Yongqiang Jiang et al. "Phonon transport properties of bulk and monolayer GaN from first-principles calculations." In: *Computational Materials Science* 138 (2017), pp. 419–425 (cit. on pp. 67, 116).

[54] Tianli Feng, Bo Qiu, and Xiulin Ruan. "Anharmonicity and necessity of phonon eigenvectors in the phonon normal mode analysis." In: *Journal of Applied Physics* 117.19 (2015), p. 195102 (cit. on p. 100).

[55] Alexander Khintchine. "Korrelationstheorie der stationären stochastischen Prozesse." In: *Mathematische Annalen* 109.1 (1934), pp. 604–615 (cit. on p. 109).

[56] URL: http://www.ioffe.ru/SVA/NSM/Semicond/GaN/mechanic.html (cit. on pp. 111, 112).

[57] URL: http://www.ioffe.ru/SVA/NSM/Semicond/InN/mechanic.html (cit. on pp. 111, 112).

[58] Stephen Stackhouse, Lars Stixrude, and Bijaya B Karki. "Thermal conductivity of periclase (MgO) from first principles." In: *Physical review letters* 104.20 (2010), p. 208501 (cit. on p. 113).

[59] Wu Li et al. "ShengBTE: a solver of the Boltzmann transport equation for phonons." In: *Comp. Phys. Commun.* 185 (2014), pp. 1747–1758. DOI: 10.1016/j.cpc.2014.02.015 (cit. on p. 116).

[60] Jesus Carrete et al. "almaBTE: A solver of the space–time dependent Boltzmann transport equation for phonons in structured materials." In: *Computer Physics Communications* 220 (2017), pp. 351–362 (cit. on p. 116).

[61] Kunpeng Yuan et al. "Anomalous pressure effect on the thermal conductivity of ZnO, GaN, and AlN from first-principles calculations." In: *Physical Review B* 98.14 (2018), p. 144303 (cit. on p. 116).

[62] A Jeżowski et al. "Thermal conductivity of GaN crystals in 4.2–300 K range." In: *Solid state communications* 128.2-3 (2003), pp. 69–73 (cit. on p. 116).

[63] C Mion et al. "Accurate dependence of gallium nitride thermal conductivity on dislocation density." In: *Applied physics letters* 89.9 (2006), p. 092123 (cit. on p. 116).

[64] S Krukowski et al. "Thermal properties of indium nitride." In: *Journal of Physics and Chemistry of Solids* 59.3 (1998), pp. 289–295 (cit. on p. 116).

[65] AX Levander et al. "Effects of point defects on thermal and thermoelectric properties of InN." In: *Applied Physics Letters* 98.1 (2011), p. 012108 (cit. on p. 116).

[66] URL: https://www.materialscloud.org/work/tools/seekpath (cit. on pp. 120, 121).

[67] Yoyo Hinuma et al. "Band structure diagram paths based on crystallography." In: *Computational Materials Science* 128 (2017), pp. 140–184 (cit. on pp. 120, 121).